

AFIT/DS/ENY/96-7

OPTIMAL CONTINUOUS-THRUST ORBIT TRANSFERS

DISSERTATION

James Dana Thorne
Major, USAF

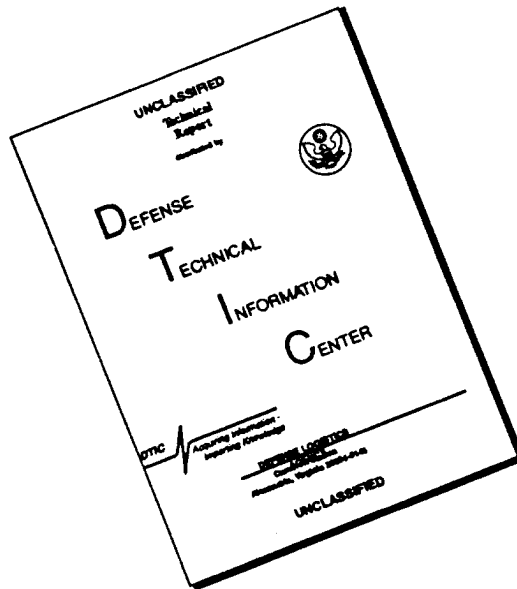
AFIT/DS/ENY/96-7

DTIC QUALITY INSPECTED 3

Approved for public release; distribution unlimited

19960718 122

DISCLAIMER NOTICE



THIS DOCUMENT IS BEST QUALITY AVAILABLE. THE COPY FURNISHED TO DTIC CONTAINED A SIGNIFICANT NUMBER OF PAGES WHICH DO NOT REPRODUCE LEGIBLY.

The views expressed in this dissertation are those of the author and do not reflect the official policy or position of the Department of Defense or the U. S. Government.

AFIT/DS/ENY/96-7

OPTIMAL CONTINUOUS-THRUST ORBIT TRANSFERS

DISSERTATION

Presented to the Faculty of the Graduate School of Engineering
of the Air Force Institute of Technology

Air University

In Partial Fulfillment of the
Requirements for the Degree of
Doctor of Philosophy

James Dana Thorne, B.S., M.S.

Major, USAF

June, 1996

Approved for public release; distribution unlimited

OPTIMAL CONTINUOUS THRUST ORBIT TRANSFERS

James Dana Thorne, B.S., M.S.

Major, USAF

Approved:

Christopher D. Hall May 20, 1996
Christopher D. Hall, Research Advisor
Assistant Professor of Aerospace and Systems Engineering
Department of Aeronautics and Astronautics

William E. Wiesel May 20, 1996
William E. Wiesel
Professor of Astronautical Engineering
Department of Aeronautics and Astronautics

Peter S. Maybeck May 20, 1996
Peter S. Maybeck
Professor of Electrical Engineering
Department of Electrical and Computer Engineering

Mark E. Oxley May 20, 1996
Mark E. Oxley
Associate Professor of Mathematics
Department of Mathematics and Statistics

Accepted:

Robert A. Calico, Jr.
Robert A. Calico, Jr.
Dean, Graduate School of Engineering

Acknowledgments

Many generous people provided their assistance and support in the preparation of this dissertation. A special note of thanks goes to my advisor, who is also my long-time friend and colleague, Dr. Christopher D. Hall. Dr. Hall consistently provided me with stimulating technical discussions, very sound academic advice, and a sharp editor's eye. I look forward to continuing our personal and professional association.

I would also like to thank Dr. William E. Wiesel of my research committee for his suggestion to consider the zero-gravity case. This idea led to the fundamental analytical results presented here. Dr. Wiesel also provided many enlightening technical discussions and helped to clarify the various subtleties of Euler-Lagrange theory.

My sincere gratitude goes to Dr. Peter S. Maybeck, also of my research committee, who agreed to help me with this project when the need arose for a representative from another department. Also, Dr. Maybeck showed great patience when I repeatedly discussed the calculus of variations during his course sequence, which is nominally on the subject of stochastic estimation and control.

This work could not have been completed without the love and support of my wife, Andrea D. Thorne, who also helped me with technical advice on computer programming.

Finally, I would like to dedicate this work to my parents, Dr. James Dale Thorne and Mrs. Doris Jean Thorne, whom I believe are my biggest fans. I'll make sure to always "keep my eye on the sky."

James Dana Thorne

Table of Contents

	Page
Acknowledgments	ii
List of Figures	vi
List of Tables	viii
List of Symbols	ix
Abstract	xi
I. Introduction	1-1
1.1 Background	1-1
1.2 Problem Statement	1-2
1.3 Research Goal	1-2
1.4 Thesis Outline	1-3
II. Literature Review	2-1
2.1 Optimal Impulsive Maneuvers	2-1
2.2 Optimal Continuous Thrust Maneuvers	2-1
2.3 Summary	2-4
III. Continuous-Thrust Spacecraft Dynamics	3-1
3.1 Equations of Motion in Three Dimensions	3-1
3.2 Equations of Motion in Two Dimensions	3-3
3.3 Equations of Motion under the KS Transformation	3-4
3.4 Summary	3-6

	Page
IV. Optimal Control Formulations and Solutions	4-1
4.1 Optimal Control in Three Dimensions	4-5
4.2 Optimal Control in Two Dimensions	4-9
4.2.1 Comparison of Cartesian and Polar Hamiltonians	4-13
4.3 Optimal Control under the Kustaanheimo-Stiefel (KS) Transformation	4-15
4.4 Solution of the Optimal Control Problem	4-17
4.4.1 The Shooting Method	4-17
4.4.2 Dynamic Step Limiter	4-21
4.5 Summary	4-23
V. Optimal Initial Costate Locus	5-1
5.1 Parabolic Region	5-5
5.1.1 Equations of Motion with Zero Gravity	5-7
5.1.2 Rectilinear Case	5-8
5.2 Elliptic and Spiral Regions	5-14
5.3 Convergence Sensitivity	5-17
5.4 Optimal Initial Costate Locus under the KS Transformation	5-19
5.5 Summary	5-20
VI. Numerical Examples	6-1
6.1 Two-Dimensional Problems	6-2
6.1.1 Circle-to-Circle	6-2
6.1.2 KS Transformation	6-7
6.1.3 Circle-to-Hyperbola	6-10
6.2 Three-Dimensional Problems	6-13
6.2.1 Time per Revolution	6-19
6.2.2 Minimum Time vs. Ascending Node	6-21
6.3 Summary	6-22

	Page
VII. Summary and Conclusions	7-1
7.1 Summary	7-1
7.2 Conclusions	7-1
Appendix A. Numerical Solution and the Shooting Method	A-1
Bibliography	BIB-1
Vita	VITA-1

List of Figures

Figure	Page
3.1. Problem Geometry in Three Dimensions	3-1
3.2. Problem Geometry in Two Dimensions	3-3
4.1. Iteration History for Modified vs. Unmodified Quasi-Newton Method .	4-23
5.1. Optimal Initial Costate Locus for $R = 2, \dot{m} = 0$	5-3
5.2. Optimal Initial Costate Locus for $R = 2, 1-12$ Revolutions	5-3
5.3. Optimal Initial Costate Locus for $R = 2, \dot{m} = -0.01, -0.1$	5-4
5.4. Optimal Initial Costate Loci	5-6
5.5. Comparison Costate Solutions to Exact Cases	5-11
5.6. Final R vs. Orbital Revolutions	5-14
5.7. Elliptic Region Angles for $R = 1.1, 5, 100$	5-15
5.8. Elliptic Fit for $R = 1.525, 100$	5-16
5.9. Convergence Sensitivity to Initial Costate Model	5-18
5.10. Optimal Initial Costate Locus under the KS Transformation	5-20
6.1. Iterative Search History for ASAT Avoidance Example	6-3
6.2. Control Angle History for ASAT Avoidance Example	6-4
6.3. Optimal Trajectory for ASAT Avoidance Example	6-4
6.4. Iterative Search History for Bryson and Ho Example	6-6
6.5. Control Angle History for Bryson and Ho Example	6-6
6.6. Optimal Trajectory for Bryson and Ho Example	6-7
6.7. Iterative Search History for Bryson and Ho KS Example	6-9
6.8. Iterative Search History for Hyperbolic Example	6-11
6.9. Control Angle History for Hyperbolic Example	6-12
6.10. Optimal Trajectory for Hyperbolic Example	6-13

Figure	Page
6.11. Flight Path for Two-Dimensional Example	6-14
6.12. Flight Path for Three-Dimensional Example	6-14
6.13. Flight Path for Polar-Elliptical Example	6-15
6.14. Iterative Search History for Two-Dimensional Example	6-16
6.15. Iterative Search History for Three-Dimensional Example	6-17
6.16. Iterative Search History for Polar-Elliptical Example	6-17
6.17. Control Angle Histories for 2D and 3D Examples	6-18
6.18. Control Angle Histories for Polar-Elliptical Example	6-19
6.19. Time Per Revolution, Circle-to-Circle	6-20
6.20. Time for One Revolution, Circle-to-Circle	6-20
6.21. Time of Flight to Various Ascending Nodes	6-22
A.1. Flowchart for the Shooting Method	A-2

List of Tables

Table	Page
4.1. Initialization for 3D Problem	4-9
4.2. Initialization for 2D Problem	4-11
4.3. Initialization for Polar Coordinate Problem	4-13
4.4. Initialization for KS Problem	4-17
4.5. Comparison of Search Methods for $R = 2.2$, $A = 0.01$	4-24
6.1. ASAT Avoidance Example	6-2
6.2. Bryson and Ho Example	6-5
6.3. Bryson and Ho Example under KS Transformation	6-8
6.4. Hyperbolic Example	6-11
6.5. Planar vs. Non-Coplanar Example	6-16

List of Symbols

Symbol	Page
A ... Thrust Acceleration of Spacecraft	3-1
μ ... Gravitational Parameter	3-1
r ... Position Vector Magnitude	3-1
R ... Desired Final Orbit Radius	3-1
m_0 ... Initial Mass of Spacecraft	3-1
\dot{m} ... Mass Flow Rate	3-1
DU ... Canonical Distance Unit	3-1
TU ... Canonical Time Unit	3-1
MU ... Canonical Mass Unit	3-1
x ... Cartesian X-Coordinate	3-1
y ... Cartesian Y-Coordinate	3-1
z ... Cartesian Z-Coordinate	3-1
α ... Inertial Thrust Angle in X-Y Plane	3-1
β ... Inertial Thrust Angle Perpendicular to X-Y Plane	3-2
$\Sigma \vec{F}_{ext}$... Sum of External Forces	3-2
\vec{V}_e ... Propellant Exhaust Velocity	3-2
\vec{r} ... Position Vector	3-2
T ... Constant Thrust Magnitude	3-2
t ... Time	3-2
u ... Radial Velocity Component	3-3
v ... Tangential Velocity Component	3-3
ϕ ... Thrust Angle in Polar Coordinates	3-3
u_1 ... KS First Position Coordinate	3-4
u_2 ... KS Second Position Coordinate	3-4
s ... Fictitious Time	3-4

Symbol	Page
γ ... Simplified Thrust Angle under KS Transformation	3-5
\mathcal{J} ... Cost Functional	4-2
t_f ... Final Time	4-2
\mathcal{L} ... Lagrangian	4-2
\vec{x} ... State Vector	4-2
\vec{f} ... Equations of Motion	4-2
$\vec{\lambda}$... Lagrange Multiplier Vector	4-2
\vec{u} ... Control Vector	4-2
\mathcal{H} ... Hamiltonian	4-2
\vec{h} ... Angular Momentum Vector	4-7
J ... Jacobian Matrix	4-21
S ... Rectilinear Semi-Flight Time	5-10

Abstract

In this dissertation, we investigate the minimum-time orbital transfer problem for spacecraft with steerable, continuous thrust of constant magnitude. The optimal control problem is developed using Euler-Lagrange theory, which leads to the optimal control law in terms of the Lagrange multipliers or costates, and provides the differential equations governing these costates. Determination of the costates as functions of time through numerical solution of the differential equations requires initial values for the costates which determine the initial steering angle of the thruster. It is well known that finding the initial values of the costates is the most difficult part of solving optimal control problems of this type. The standard solution technique is to use the shooting method to solve a boundary value problem in which the initial and final values of the states are specified, but the initial and final values of the costates are unknown. This iterative procedure is sensitively dependent on the initial conditions provided for the costates. This research has developed reliable approximate models for the initial values of the costates, such that the shooting method will always converge over a given range of problem parameters. Employing a combination of analytical and empirical results, the optimal initial costates are modeled as functions of the problem parameters which are the initial thrust acceleration, A , and the final orbit radius, R , in canonical units. For circle-to-circle, coplanar orbit transfers, these approximate initial costate models lead to convergence in the shooting method for all practical values of A and R . In addition, the models lead to convergence for a wide range of other problems, including circle-to-hyperbola transfers and non-coplanar transfers. To counter the extreme sensitivity to small changes in the initial costate conditions, a dynamic step limiter is introduced which improves convergence properties. The minimum-time problem is also modeled using the Kustaanheimo-Stiefel (KS) transformation, and the optimal initial costates are shown for comparison. Several numerical examples are provided for coplanar and non-coplanar orbital transfers with various end conditions.

OPTIMAL CONTINUOUS-THRUST ORBIT TRANSFERS

I. Introduction

1.1 Background

The fascinating possibilities of space flight in fact and fiction have inspired many people to pursue careers in the astronautical sciences. As a result, continual advances are being made in the science of spacecraft design. Propulsion systems in particular have improved dramatically since the first black powder rockets of antiquity. Robert Goddard, also inspired by the potential of space flight, is considered the father of modern rocketry for his successful experiments using liquid fuels. Today, propulsion research continues with the development of high efficiency non-chemical thrust devices. Thus, there are three common approaches to space propulsion: solid fuel, liquid fuel, and non-chemical.

Goddard [13] recognized that to launch his rockets in the most fuel-efficient manner possible, he would need to solve the optimal control problem using the calculus of variations. For Goddard's experiments, an approximation to the optimal control law was used instead. Since the boost phase of a chemical rocket is typically of short duration, an approximation is usually considered to be good enough. However, a full-scale booster rocket has a much longer thrusting phase than Goddard's experiments. Also, the thrust duration of a non-chemical propulsion system can become quite lengthy. In either case, the need for optimal control solutions becomes much greater as the duration of the thrusting phase grows large compared to the total flight time, since the usual approximations become less valid.

Normally, the goal of the optimization problem is to minimize either the fuel used or the time taken to complete a mission. The problem has been solved [13] for both quantities if one considers the velocity changes to occur instantaneously. However, there is still no closed form solution available for the finite duration thrust case. Numerical methods are typically used to determine an optimal thrust program to meet boundary conditions for position and velocity.

Non-chemical thrust devices are appealing because they typically have high propulsive efficiencies, measured by the specific impulse. A highly efficient propulsive system is very desirable for an orbiting spacecraft, simply because there is rarely, if ever, an opportunity to refuel on orbit. Although finite thrust devices such as electrical arcjets use less fuel than chemical thrusters for a given change in spacecraft velocity, they normally produce very small thrust levels. For this reason, finite thrust propulsion systems need to operate continuously for extended periods to accomplish orbital maneuvers.

1.2 Problem Statement

When a spacecraft is being accelerated by a thruster for significant portions of the planned trajectory, the effect can not be considered instantaneous, or "impulsive." Thus, the orbital path will not be Keplerian. The optimal magnitude and direction of the thrust must then be found as a function of time to meet mission objectives. It is possible to find this function, the optimal control law, by using Euler-Lagrange theory, which will be discussed in Chapter 4. However, knowledge of the optimal control law is not sufficient to solve the problem of meeting desired end conditions, because Euler-Lagrange theory introduces adjoint variables which must be initialized. These variables, also known as Lagrange multipliers or costates, are difficult to initialize because there is insufficient information from the boundary conditions to specify their initial values. Without this information, it is not possible to propagate the differential equations that govern the behavior of the states and costates. Typically, the initial values of the costates are guessed, then an attempt is made to solve the boundary value problem by refining the guesses in some automated way. Due to the sensitivity of the costates to errors in the initial conditions, poor guesses may preclude any hope of convergence to the desired end conditions. Thus, the problem is to find the initial values of the costates that will lead to the desired final orbital conditions, in the minimum time.

1.3 Research Goal

The goal of this research is to provide insight into the selection of initial values for the Lagrange multipliers, leading to reasonable certainty of convergence for the boundary

value problem of a spacecraft under continuous thrust with fixed end conditions. To gain this insight, both analytical and empirical means will be used to model the optimal initial costates as functions of the problem parameters.

1.4 Thesis Outline

Chapter 2 provides a literature review related to the problem of optimal control for impulsive and continuous-thrust orbital maneuvers. In Chapter 3, the equations of motion for a spacecraft influenced by gravity and continuous thrust are derived in several coordinate systems. Chapter 4 starts with a presentation of Euler-Lagrange theory, which is then used to develop the optimal control law and costate equations in each of the coordinate systems. The shooting method is also discussed in Chapter 4. Chapter 5 contains an analysis of the optimal initial costate locus, which is used to initialize the shooting method. Numerical examples of optimal continuous-thrust transfers using the costate locus analysis are presented in Chapter 6. Finally, a summary of this research is presented and conclusions are discussed in Chapter 7.

II. Literature Review

There are hundreds, if not thousands, of papers to be found in the literature on optimal space maneuvers. For example, Bell [5] cites 160 articles in his survey of published work on optimal space trajectories. The two most commonly addressed issues are minimum-fuel transfers and minimum-time transfers. For a spacecraft under continuous thrust with no throttling, the resulting solutions will be the same. Without throttling, the mass flow rate of propellant is constant, so if time is minimized then the fuel consumed will be minimized as well.

Depending on the design of the propulsion system, the velocity change may occur in a very short time, or in a very long time compared to the period of the desired final orbit. Short thrusts are treated as *impulsive*, and long thrusts are modeled as *continuous* effects for finite durations.

2.1 Optimal Impulsive Maneuvers

One of the earliest definitive works on optimized impulsive maneuvers is by Lawden [13]. He posed the minimum-fuel space trajectory as a Mayer problem [13], and sought solutions using variational calculus methods and Lagrange multipliers. Lawden treated the Lagrange multipliers as components of a vector, which he called the "primer vector." The behavior of the primer vector gave the optimal directions for impulsive maneuvers, and thus solved the optimization problem for impulsive thrust. This work also verified Hohmann's result for a minimum-fuel impulsive orbital transfer. Lawden's book is commonly referenced in contemporary literature and serves as a starting point for much of the work that follows.

2.2 Optimal Continuous Thrust Maneuvers

Although the optimization of impulsive transfers yielded a direct solution [13], none has been found for the continuous-thrust case. This problem may be solved numerically, and many examples of this are to be found in the literature [5]. Optimization of a continuous-thrust trajectory involves the simultaneous solution of an optimal control

problem and a boundary value problem. The initial and final states are normally given, but there is usually no information available for the initial values of the Lagrange multipliers. This presents quite a problem, since the optimal control law is often a function of the Lagrange multipliers which must be initialized for numerical integration. The usual approach is to make an educated guess for the initial values, then update them by solving the boundary value problem. Prussing [17], Broucke [6] and others have recast the boundary value problem in terms of other variables, but the initial values of these must be guessed and refined as well. Prussing [17] incorporates the second derivative of the primer vector into a fourth order dynamics equation, thus eliminating the control variables. Once this is accomplished, four constants of integration must be iterated to find the correct optimal trajectory. Broucke [6] expresses the Lagrange multipliers as functions of new auxiliary variables, and graphically examines the behavior of the new variables. Pines [15] and Redding and Breakwell [18] have suggested using the results of optimal impulsive maneuvers to serve as an initial guess for the continuous-thrust case. However, this method produces poor results for small values of continuous thrust, particularly if there are no coasting arcs used. Thus, there are no models or techniques in the literature to provide good estimates for the initial Lagrange multiplier values for the continuous-thrust, minimum-time orbit transfer problem.

Closed form non-optimal solutions have been found for spacecraft trajectories where special assumptions are made about the control law. If the thrust vector is directed either radially from the attracting center or tangentially to the orbital path, it is possible to integrate the equations of motion analytically. Battin [4] (section 8.8) presents results for the time to reach escape velocity and the number of revolutions for both thrust assumptions.

Assumptions about the thrust magnitude will also allow closed form non-optimal solutions through the method of averaging [1, 26]. If the thrust level is small enough, there is only a small change in semi-major axis or eccentricity for a single orbital revolution. Then, a correction is made to the semi-major axis at the completion of each revolution. These approximations are reasonable for orbital transfers that require roughly ten or more revolutions to complete [1, 26]. Using these assumptions, it is possible to solve for the

trajectory analytically. The thrust is directed tangentially, which is also perpendicular to the orbit radius since the eccentricity is assumed to be zero for individual revolutions.

In another approach [11], finite difference equations are used in place of the exact differential equations of motion. Then, a choice must be made for a step or mesh size in the search space. By refining the mesh, the solution *may* approach the optimal trajectory. A method known as "differential inclusion" [19, 8] also uses finite difference equations. These methods can be very efficient. However, it is difficult to guarantee that the converged solution is the desired optimal path since the differential equations governing the costates are not used. These methods have gained in popularity because of their inherent robustness and the increasing power of digital computers.

Another numerical method that has been used with success for the minimum-fuel problem is hybrid non-linear programming, or HNLP [27]. In this case, the cost function is evaluated directly while the transversality conditions are satisfied implicitly. HNLP combines the advantages of using costate equations and the simplicity of directly evaluating the cost function. This method can be made more robust than propagating the exact state and costate equations, but the performance depends on an optimal choice of additional variables and constraints.

For circle-to-circle coplanar orbital transfers, the minimum time of flight may be derived from the accumulated velocity change on the trajectory [2]. It is possible to display the optimal accumulated velocity change in graphical form as a function of constant thrust level, ratio of final to initial orbit radius, and mass propellant fraction [2]. In this way, a wide range of possible cases may be represented through the use of universal variables. To produce the graphical results, many different cases must be solved numerically to allow for interpolation. Although linear interpolation from a graph will not provide great precision, it does show general trends for mission design. In particular, a graph of the number of revolutions for the optimal path versus the logarithm of thrust magnitude shows a distinct change in trajectory characteristics at integer values of revolutions [2].

2.3 Summary

Many different approaches have been used to solve the optimal continuous-thrust orbit transfer problem. While methods that propagate the exact equations of the states and costates will guarantee optimality, they are not robust due to sensitivity to initial conditions. Direct methods that simply evaluate the cost function with approximate finite difference equations are typically robust, but are not optimal. Finally, exact solutions to approximations of the equations of motion or control law also sacrifice optimality. An ideal solution technique would have both guaranteed optimality and robustness, but none exists in the literature for a wide range of spacecraft design parameters and orbital boundary conditions. In particular, there are no models or techniques in the literature to provide good estimates for the initial Lagrange multiplier values for the continuous-thrust, minimum-time orbit transfer problem, based on problem parameters.

III. Continuous-Thrust Spacecraft Dynamics

In this chapter, the equations of motion for a spacecraft under the influence of gravity and continuous thrust are derived for a variety of coordinate systems. The resulting differential equations will be used for the optimal control formulations of Chapter 4. The acceleration due to constant, non-throttleable thrust is A , the gravitational parameter is μ . The length of the position vector is r , and the final desired value of r will be given by R . The spacecraft's initial mass is m_0 , and the mass flow rate is \dot{m} . The thrust acceleration A may or may not be a function of time, depending on the value of \dot{m} , as will be shown in the next section. In canonical units [3], the gravitational constant μ is unity regardless of the system under consideration as long as the initial radius is defined to be one distance unit, (DU), and the initial circular velocity at that radius is one distance unit per time unit, (DU/TU). Also, the initial spacecraft mass is one mass unit (MU).

3.1 Equations of Motion in Three Dimensions

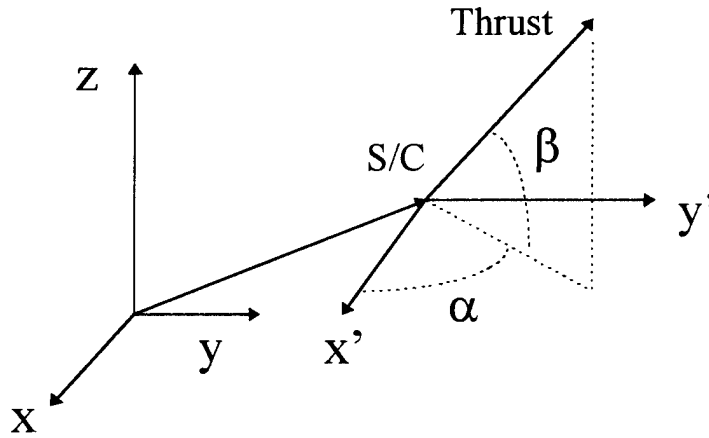


Figure 3.1 Problem Geometry in Three Dimensions

The equations of motion are most easily expressed using an inertially fixed, right-handed Cartesian system of x , y , and z coordinates as shown in Figure 3.1. The x' and y' axes shown in Figure 3.1 are parallel to the x and y axes, respectively. The initial circular orbit lies in the x, y plane, and the initial position is at $x = 1, y = 0, z = 0$. The thrust direction must be defined with (at least) two angles. The angle α lies in the x, y plane,

and is measured from the x axis in the positive direction. The angle β is measured “up” from the x, y plane, and lies in the plane containing the thrust vector and the z axis. The magnitude of the position vector is $r = \sqrt{x^2 + y^2 + z^2}$.

The equation of motion for a rocket [25] is as follows:

$$\Sigma \vec{F}_{ext} + \dot{m} \vec{V}_e = m \ddot{\vec{r}} \quad (3.1)$$

where $\Sigma \vec{F}_{ext}$ is the sum of the external forces acting on the spacecraft, \vec{V}_e is the exhaust velocity of the propellant, \vec{r} is the position vector, and $\ddot{\vec{r}}$ is the spacecraft total acceleration. The second term of Equation (3.1) represents the thrust, and the magnitude of the thrust acceleration is $A = T/(m_0 + \dot{m}t)$ where T is the constant thrust magnitude of the propulsion system, and t is the time. If $\dot{m} = 0$, then A is equal to a constant. The only external force we will consider is that of gravity from a single point source, and Newton’s Law of Gravitation may be used to express this as follows:

$$\vec{F}_g = -\frac{\mu}{r^3} \vec{r} \quad (3.2)$$

The two-body assumption is used to simplify the equations of motion enough to allow closed form solutions which are presented in Chapter 5. Other gravitational models may be considered, but the majority of missions of interest are primarily influenced by two-body effects and thrust. Therefore, any results obtained with the two-body assumption may be used as a starting point for a great number of more complex orbital problems. It may even be possible to approach the restricted three-body problem by treating the mass of the third body as a parameter, and using two-body results as initial estimates for small values of the mass parameter. However, that subject is beyond the scope of this research. The equations of motion are as follows, where the thrust terms are the components of $\dot{m} \vec{V}_e$:

$$\ddot{x} = -(\mu/r^3)x + A \cos \beta \cos \alpha \quad (3.3)$$

$$\ddot{y} = -(\mu/r^3)y + A \cos \beta \sin \alpha \quad (3.4)$$

$$\ddot{z} = -(\mu/r^3)z + A \sin \beta \quad (3.5)$$

3.2 Equations of Motion in Two Dimensions

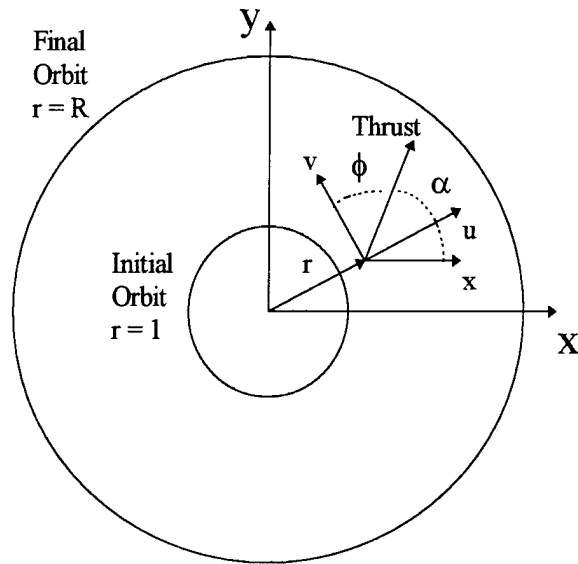


Figure 3.2 Problem Geometry in Two Dimensions

For the case where the motion remains in the initial orbital plane, the geometry simplifies to that of Figure 3.2. Since $\beta = 0 = z$, Equations (3.4)-(3.5) reduce to:

$$\ddot{x} = -(\mu/r^3)x + A \cos \alpha \quad (3.6)$$

$$\ddot{y} = -(\mu/r^3)y + A \sin \alpha \quad (3.7)$$

The two-dimensional equations of motion may also be expressed in polar coordinates which include r as the scalar distance from the attracting center, u as the time rate of change of r , and v as the velocity component perpendicular to u directed along the spacecraft horizon. The polar thrust angle, ϕ , is measured clockwise ("up") from the spacecraft local horizontal, as shown in Figure 3.2. This results in the following differential equations:

$$\dot{r} = u \quad (3.8)$$

$$\dot{u} = \frac{v^2}{r} - \frac{\mu}{r^2} + A \sin \phi \quad (3.9)$$

$$\dot{v} = -\frac{uv}{r} + A \cos \phi \quad (3.10)$$

3.3 Equations of Motion under the KS Transformation

The Kustaanheimo-Stiefel (KS) transformation is intended to regularize the equations of motion in the problem of two bodies [21]. The purpose of the regularization is to reduce numerical integration difficulties when r is small, by placing the inverse of r into a term that represents the constant angular momentum magnitude of a two-body orbit. This term premultiplies the state variables u_1 and u_2 in Equations (3.15) and (3.16), but it will not remain constant with the influence of thrust. When this transformation is used in conjunction with a change of independent variable, the equation of motion in two dimensions has the form of a harmonic oscillator [20]. This allows for simple analytical solutions, which may be perturbed by other forces such as a third body or a propulsion system. In Chapter 4, we will apply Euler-Lagrange theory to the two-dimensional regularized equations of motion to solve the minimum-time problem for a coplanar orbital transfer under continuous thrust. The purpose of this development is to compare the costate behavior with the Cartesian case in Chapters 5 and 6.

The equations of motion for a two-dimensional orbit are as follows:

$$\ddot{x} = -\frac{\mu}{r^3}x \quad (3.11)$$

$$\ddot{y} = -\frac{\mu}{r^3}y \quad (3.12)$$

Using the KS transformation for two dimensions, the coordinates x and y are replaced by u_1 and u_2 through the following relationship:

$$(u_1 + iu_2)^2 = x + iy \quad (3.13)$$

The independent variable t is replaced by the fictitious time s with the following differential equation:

$$\frac{dt}{ds} = r \quad (3.14)$$

These transformations lead to the regularized equations of motion [20]:

$$u_1'' = \left[\frac{2(\vec{u}'^T \vec{u}') - \mu}{2r} \right] u_1 \quad (3.15)$$

$$u_2'' = \left[\frac{2(\vec{u}'^T \vec{u}') - \mu}{2r} \right] u_2 \quad (3.16)$$

The primes indicate differentiation with respect to s , $\vec{u} = (u_1, u_2)$, and $r = u_1^2 + u_2^2$. The symbol $(\vec{u}'^T \vec{u}')$ indicates an inner product. A thrust model may be added as follows:

$$u_1'' = \left[\frac{2(\vec{u}'^T \vec{u}') - \mu}{2r} \right] u_1 + \frac{1}{2} A r^{3/2} \cos \gamma \quad (3.17)$$

$$u_2'' = \left[\frac{2(\vec{u}'^T \vec{u}') - \mu}{2r} \right] u_2 + \frac{1}{2} A r^{3/2} \sin \gamma \quad (3.18)$$

where A is the magnitude of the thrust acceleration. This is an original thrust model which is consistent with the transformation given in Reference [20], Equation (9.26), but here the thrust angle γ has been defined in the u coordinate system for simplification with no loss of generality. The relationship between the inertial Cartesian thrust angle, α , and the KS thrust angle, γ , is as follows:

$$\cos \gamma = r^{-1/2}(u_1 \cos \alpha + u_2 \sin \alpha) \quad (3.19)$$

$$\sin \gamma = r^{-1/2}(u_1 \sin \alpha - u_2 \cos \alpha) \quad (3.20)$$

At the initial time, $u_1 = 1$ and $u_2 = 0$, and $r = 1$. Therefore, $\gamma(0) = \alpha(0)$. Defining $v_i = u_i'$, the equations of motion and differential constraints may be expressed as five first-order differential equations:

$$t' = r \quad (3.21)$$

$$u_1' = v_1 \quad (3.22)$$

$$u_2' = v_2 \quad (3.23)$$

$$v'_1 = \left[\frac{2(\vec{v}^T \vec{v}) - \mu}{2r} \right] u_1 + \frac{1}{2} A r^{3/2} \cos \gamma \quad (3.24)$$

$$v'_2 = \left[\frac{2(\vec{v}^T \vec{v}) - \mu}{2r} \right] u_2 + \frac{1}{2} A r^{3/2} \sin \gamma \quad (3.25)$$

3.4 Summary

The equations of motion of a spacecraft under the influence of gravity and continuous thrust have been presented in four different coordinate frames. In three dimensions, inertial Cartesian coordinates are used. In two dimensions, inertial Cartesian or polar coordinates are used. Finally, the equations of motion are modified by the KS transformation. An original thrust model is presented that is simplified compared to the model given in Reference [20]. These sets of equations will be used in Chapter 4 to derive optimal control formulations for the minimum-time orbital transfer problem.

IV. Optimal Control Formulations and Solutions

This chapter begins with a standard development of the variational calculus approach to the minimum-time trajectory optimization problem [7]. Then, the resulting relationships are applied to the equations of motion for a spacecraft under continuous thrust in several coordinate systems, as derived in Chapter 3. Finally, the shooting method is presented as a means to solve the two-point boundary value problem of transferring from one orbit to another, using the optimal differential equations for the states and costates. There are two original presentations in this chapter: the application of Euler-Lagrange theory to the equations of motion under the KS transformation, and a dynamic step limiter which improves the convergence properties of the shooting method.

Optimization problems come in many forms, but the usual goal is to minimize (or maximize) the value of some desired quantity. Sometimes, the answer we seek is a function of time that will minimize this quantity. Suppose it is desired to get from one position to another in a minimum time. The solution to this problem is a path, or set of directions as a function of time. For example, a map with highlighted roads from an automobile club could be considered an optimal path to minimize travel time between cities. A better example might be a program for a road rally, in which the drivers are expected to arrive at intermediate checkpoints at specific times. In this case, the goal would be to maximize a score, rather than to minimize the time. Either way, the set of instructions specifies quantities like position, speed, and direction. To follow an optimal path as in these examples, a driver must control the vehicle by steering, accelerating, braking, and so on. These control actions must be done in exactly the right order at the right time for success. Thus, a set of control instructions or *control law* is the solution that we ultimately require.

Euler-Lagrange theory provides an analytical method to find the control law for a variety of path optimization problems through the calculus of variations [7]. To implement this theory, we need to define a quantity to be minimized (or maximized), and to determine any constraints that affect the optimal path. For a problem in spaceflight, the vehicle must move according to Newton's laws of motion under the influence of gravity and the propulsion system. We will not consider other perturbations or relativistic effects on the spacecraft. The equations of motion may be treated as constraints, since the vehicle has

no other choice than to obey them. These constraints may be written as a set of first order differential equations:

$$\dot{\vec{x}}(t) = \vec{f}(\vec{x}(t), \vec{u}(t), t) \quad (4.1)$$

If we wish to minimize or maximize a quantity \mathcal{J} , a cost functional is defined as:

$$\mathcal{J} = \int_0^{t_f} (\mathcal{L}) dt \quad (4.2)$$

where t_f is the final time. The integral form is chosen so that the integrand may be identified as the Lagrangian (\mathcal{L}), which will be used in the calculus of variations approach. The constraints may be added to the Lagrangian without changing the value of the cost function, if they are appended in the following way:

$$\mathcal{J} = \int_0^{t_f} (\mathcal{L} + \vec{\lambda}^T (\vec{f} - \dot{\vec{x}})) dt \quad (4.3)$$

Notice that the quantity $(\vec{f} - \dot{\vec{x}})$ is identically equal to zero if the state vector, \vec{x} , solves the differential equations, \vec{f} , by the definition of the equations of motion given above. Thus, we have added nothing to the cost function, as long as the constraints are obeyed. The variable $\vec{\lambda}$ is a vector of scalar valued functions known as Lagrange multipliers. Strictly speaking, the vector is a representation of linear functionals [14]. The Lagrange multipliers are also known as costates, since there will be one element of the Lagrange multiplier vector associated with each element of the state vector. The behavior of the costates turns out to be very important for defining the optimal control law, as will be shown.

The cost function is now dependent on the states, \vec{x} , and the controls, \vec{u} , which are contained in \vec{f} . An infinitesimal variation away from the minimum point will not increase the value of the cost, since the slope is zero there. The variation operation is similar to taking a derivative, but it provides information about the relationships of many variables at the same time. First, define a scalar valued function \mathcal{H} , the Hamiltonian:

$$\mathcal{H} = \mathcal{L} + \vec{\lambda}^T \vec{f} \quad (4.4)$$

The first, total variation of the cost function for either fixed or free final conditions and fixed initial conditions is given by [12]:

$$\delta \mathcal{J} = -\vec{\lambda}^T(t_f)\delta\vec{x}(t_f) + \mathcal{H}(t_f)\delta t_f + \int_0^{t_f} \left[\left(\frac{\partial \mathcal{H}}{\partial \vec{x}} + \dot{\vec{\lambda}}^T \right) \delta\vec{x} + \frac{\partial \mathcal{H}}{\partial \vec{u}} \delta\vec{u} \right] dt \quad (4.5)$$

We would like to be able to make small variations in the control and final time without changing the value of the cost function. For this to happen, the variation of \mathcal{J} must be zero for arbitrary δt_f and $\delta\vec{u}$. The states must be free to vary except at the endpoints, so $\delta\vec{x}$ is also arbitrary in the integrand. If some of our final conditions are not specified, such as the final radius, then the first term may have non-zero elements for $\delta\vec{x}(t_f)$. Since we assume the variation of the cost function to be identically zero, the final Lagrange multiplier vector would have as many zero components as necessary for the first term to vanish. As mentioned above, this reasoning will also apply if the initial states are free and the final states are specified [12, 7].

The second term in the variation requires that the final value of the Hamiltonian, $\mathcal{H}(t_f)$, is equal to zero if δt_f is free to vary. This is known as the transversality condition [7]. For minimum-time problems, the final time must be free to vary, so the final value of the Hamiltonian must be zero. This condition may be met through proper scaling of the Lagrange multipliers. Scaling may also be used to make the first term in the variation zero as well. The equations of motion for the states and costates in our problem will not be affected by scaling the Lagrange multipliers, which gives us some freedom to choose the scale factor. This is because the Lagrange multipliers appear in the equations of motion for the state variables as ratios of each other, as is shown in the following sections.

The integral term in the variation must also be zero for arbitrary values of $\delta\vec{x}$ and $\delta\vec{u}$. Thus, for the integrand to be zero, we have the Hamilton-Jacobi equations [11]:

$$\frac{\partial \mathcal{H}}{\partial \vec{u}} = \vec{0}^T \quad (4.6)$$

$$\frac{\partial \mathcal{H}}{\partial \vec{x}} = -\dot{\vec{\lambda}}^T \quad (4.7)$$

Equation (4.6) is the optimality condition, which states that the variation of the Hamiltonian with respect to the control should be zero on the optimal path. Equation (4.7) provides a set of first order differential equations that govern the behavior of the Lagrange multipliers. These are the costate equations, which may be integrated along with the state equations through the time interval.

In the calculus of variations, the Legendre-Clebsch condition is used to check if the control \vec{u} minimizes or maximizes the Hamiltonian. For minimization, we have [7]:

$$\frac{\partial^2 \mathcal{H}}{\partial \vec{u}^2} \geq 0 \quad (4.8)$$

which states that $\partial^2 \mathcal{H} / \partial \vec{u}^2$ is a positive semi-definite matrix throughout the time interval. For maximization, we have:

$$\frac{\partial^2 \mathcal{H}}{\partial \vec{u}^2} \leq 0 \quad (4.9)$$

which states that $\partial^2 \mathcal{H} / \partial \vec{u}^2$ is a negative semi-definite matrix throughout the time interval. Thus, we may check for either occurrence. If the second partial derivative of the Hamiltonian with respect to the control is equal to zero or a zero matrix, then we have a singular arc [12], and further investigation is necessary to determine the nature of the critical path. However, the partial derivatives of the Hamiltonian are functions of time, and numerical experience has shown that the second partial derivative is extremely unlikely to remain exactly equal to zero throughout a trajectory. This situation would amount to a case in which the optimal solution does not depend on the constraint equations in the Hamiltonian, as may be seen from control laws which are developed in the following sections. The Legendre-Clebsch condition provides the necessary conditions for a minimizing path [7]; however, to have both necessary and sufficient conditions for a minimum, one must make certain that there are no singular arcs encountered along the path. In the problem we are investigating, the second partial derivative is positive or negative semi-definite in all cases of interest.

The optimality condition and the costate equations are a very powerful result of Euler-Lagrange theory. This result may be used to determine the optimal control law for

a spacecraft under continuous thrust. However, there is a significant difficulty inherent in this formulation which is addressed in this research.

Although the costate equations may be derived from the above relationships, they must be initialized to begin a numerical integration procedure. We may choose the initial and final conditions for the physical states, but there is no guaranteed way to determine the correct, optimal boundary conditions for the costates. In addition, the costate equations tend to be very sensitive to initial conditions in practice. They are also just as sensitive when choosing final conditions for backwards integration, as in a forward/backward sweep approach [7]. The shooting method, which is described in a later section, depends on "reasonable" choices of initial Lagrange multiplier values. If they are too far away from the correct values, the shooting method will fail.

4.1 Optimal Control in Three Dimensions

Using the three-dimensional equations of motion derived in Chapter 3, Equations (3.3)-(3.5), we may form the following variational Hamiltonian:

$$\begin{aligned} \mathcal{H} = & 1 + \lambda_x \dot{x} + \lambda_y \dot{y} + \lambda_z \dot{z} + \lambda_x [-(\mu/r^3)x + A \cos \beta \cos \alpha] \\ & + \lambda_y [-(\mu/r^3)x + A \cos \beta \sin \alpha] + \lambda_z [-(\mu/r^3)x + A \sin \beta] \end{aligned} \quad (4.10)$$

The optimality condition leads to two control laws for the thrust vector angles α and β :

$$\tan \alpha = \frac{-\lambda_y}{-\lambda_x} \quad (4.11)$$

$$\tan \beta = \frac{-\lambda_z}{-(\lambda_x \cos \alpha + \lambda_y \sin \alpha)} \quad (4.12)$$

This choice of sign will guarantee the necessary conditions for a minimum with respect to each of the control angles, as is shown next using the Legendre-Clebsch condition. Since there are two control angles, the second partial derivative of the Hamiltonian will be a

2×2 matrix:

$$\frac{\partial^2 \mathcal{H}}{\partial \vec{u}} = \begin{bmatrix} \partial^2 \mathcal{H} / \partial \alpha^2 & \partial^2 \mathcal{H} / (\partial \beta \partial \alpha) \\ \partial^2 \mathcal{H} / (\partial \alpha \partial \beta) & \partial^2 \mathcal{H} / \partial \beta^2 \end{bmatrix} \quad (4.13)$$

Starting with the first diagonal term, we have:

$$\frac{\partial^2 \mathcal{H}}{\partial \alpha^2} = -\lambda_x A \cos \beta \cos \alpha - \lambda_y A \cos \beta \sin \alpha \quad (4.14)$$

Using Equations (4.11) and (4.12) to eliminate α and β from the right-hand side, it is possible to determine the sign of the second partial derivative of the Hamiltonian with respect to the control angle α :

$$\frac{\partial^2 \mathcal{H}}{\partial \alpha^2} = A \frac{\lambda_x^2 + \lambda_y^2}{\sqrt{\lambda_x^2 + \lambda_y^2 + \lambda_z^2}} \geq 0 \quad (4.15)$$

The second diagonal term is given by the second partial derivative of the Hamiltonian with respect to the control angle β :

$$\frac{\partial^2 \mathcal{H}}{\partial \beta^2} = \lambda_x A \cos \alpha (-\cos \beta) + \lambda_y A \sin \alpha (-\cos \beta) - \lambda_z A \sin \beta \quad (4.16)$$

As before, Equations (4.11) and (4.12) may be used to determine the sign of the second partial derivative with respect to β :

$$\frac{\partial^2 \mathcal{H}}{\partial \beta^2} = A \frac{\lambda_x^2 + \lambda_y^2 + \lambda_z^2}{\sqrt{\lambda_x^2 + \lambda_y^2 + \lambda_z^2}} \geq 0 \quad (4.17)$$

Lastly, the off-diagonal terms are necessary to complete the check for the Legendre-Clebsch condition:

$$\frac{\partial^2 \mathcal{H}}{\partial \alpha \partial \beta} = \frac{\partial^2 \mathcal{H}}{\partial \beta \partial \alpha} = \lambda_x A \sin \alpha \sin \beta - \lambda_y A \cos \alpha \sin \beta \quad (4.18)$$

Using Equations (4.11) and (4.12) to eliminate the control angles from the right-hand side yields the following:

$$\frac{\partial^2 \mathcal{H}}{\partial \alpha \partial \beta} = \frac{\partial^2 \mathcal{H}}{\partial \beta \partial \alpha} = \frac{A(\lambda_x \lambda_y \lambda_z - \lambda_x \lambda_y \lambda_z)}{\sqrt{\lambda_x^2 + \lambda_y^2} \sqrt{\lambda_x^2 + \lambda_y^2 + \lambda_z^2}} = 0 \quad (4.19)$$

Thus, the off-diagonal terms are identically equal to zero and the diagonal terms are both greater than or equal to zero. This makes the second partial derivative matrix positive semi-definite, which satisfies the Legendre-Clebsch condition. Thus, we have the necessary conditions to conclude that the control minimizes the path integral [7]. As mentioned before, there is no case of interest in which all three of the Lagrange multipliers λ_x , λ_y and λ_z are all identically equal to zero throughout the path integral over the transfer time. Since these costates premultiply the constraint equations in the Hamiltonian, the optimal path would be independent of the gravitation and thrust models if the velocity costates were all zero throughout the transfer.

The costate equations are found using Equation (4.7), and the results are as follows:

$$\dot{\lambda}_x = \frac{\mu}{r^5} [\lambda_x (y^2 + z^2 - 2x^2) - 3x (\lambda_y y + \lambda_z z)] \quad (4.20)$$

$$\dot{\lambda}_y = \frac{\mu}{r^5} [\lambda_y (x^2 + z^2 - 2y^2) - 3y (\lambda_x x + \lambda_z z)] \quad (4.21)$$

$$\dot{\lambda}_z = \frac{\mu}{r^5} [\lambda_z (x^2 + y^2 - 2z^2) - 3z (\lambda_x x + \lambda_y y)] \quad (4.22)$$

$$\dot{\lambda}_x = -\lambda_x \quad (4.23)$$

$$\dot{\lambda}_y = -\lambda_y \quad (4.24)$$

$$\dot{\lambda}_z = -\lambda_z \quad (4.25)$$

In the two-dimensional problem, the three final boundary conditions are the radial distance $r = R$, the radial velocity $u = 0$, and the tangential velocity $v = 1/\sqrt{R}$. This set of conditions may be used to define a circular orbit completely with a desired direction of rotation. In the three-dimensional problem, two more final conditions are necessary to correspond with the two out-of-plane initial costates, $\lambda_x(0)$ and $\lambda_z(0)$. If the three components of the angular momentum vector \vec{h} are used along with the radial and tangential velocities, a total of five scalar boundary conditions are established. These quantities will uniquely determine a circular orbit with a desired inclination and ascending node. Since

$\vec{h} = \vec{r} \times \dot{\vec{r}}$, the components of the angular momentum vector may be calculated as follows:

$$h_x = y\dot{z} - z\dot{y} \quad (4.26)$$

$$h_y = z\dot{x} - x\dot{z} \quad (4.27)$$

$$h_z = x\dot{y} - y\dot{x} \quad (4.28)$$

The above equations are useful for checking end conditions after integrating the Cartesian equations of motion in three dimensions. If the final orbit is circular with a given radius, inclination and ascending node, the components of the final angular momentum may be found from the circular velocity and angular information.

Now that the equations of the states and costates have been derived, they must be initialized prior to numerical integration. The initial values of the states are known, but the initial values of the Lagrange costates are unknown. However, the number of independent unknown initial costates may be reduced. Either $\lambda_x(0)$, $\lambda_y(0)$, or $\lambda_z(0)$ may be initially scaled to unity by dividing the initial value of the Hamiltonian by $\lambda_x(0)$, $\lambda_y(0)$ or $\lambda_z(0)$. Although there is no mathematical reason to prevent these initial costates from being zero at the same time, the resulting problem would not be of practical interest. This is because the resulting optimal trajectory would be independent of the initial velocity components, as can be seen from the Hamiltonian. Thus, it is assumed that $\lambda_x(0) \neq 0$, allowing it to be divided through the Hamiltonian. As a result of this scaling, $\lambda_x(0) = 1$, and the cost is also scaled since the Lagrangian becomes $1/\lambda_x(0)$, a new constant. This has no effect on the final optimal trajectory since the minimum of the scaled cost corresponds to the minimum time. If the scaling changes the sign of the terms in the Hamiltonian, then the optimization problem becomes one of maximizing the negative of the time. This is discussed in the section on optimization of the two-dimensional problem.

The Lagrange costates associated with the z position and velocity, $\lambda_z(0)$ and $\lambda_{\dot{z}}(0)$, are unknown at the initial time. However, they may be set equal to zero as a reasonable starting guess at the initial time. This is because λ_z and $\lambda_{\dot{z}}$ are both always equal to zero if the transfer is confined to the x, y plane. In Table 4.1, the initial values $\lambda_z(0)$ and $\lambda_{\dot{z}}(0)$

are indicated as unknowns, because zero will not be the optimal value in general. Finally, it will be shown in a later section that the initial values $\lambda_y(0)$ and $\lambda_x(0)$ are equal if the starting orbit is circular. The three-dimensional set of states and costates are initialized as given in Table 4.1:

Table 4.1 Initialization for 3D Problem

$x(0)$	$=$	1	$\lambda_x(0)$	$=$	1
$y(0)$	$=$	0	$\lambda_y(0)$	$=$	$?$
$z(0)$	$=$	0	$\lambda_z(0)$	$=$	$?$
$\dot{x}(0)$	$=$	0	$\lambda_{\dot{x}}(0)$	$=$	$\lambda_y(0)$
$\dot{y}(0)$	$=$	1	$\lambda_{\dot{y}}(0)$	$=$	$?$
$\dot{z}(0)$	$=$	0	$\lambda_{\dot{z}}(0)$	$=$	$?$

Table 4.1 shows a total of four unique scalar values to be found, and the optimal flight time makes five unknowns for the three-dimensional problem. Five scalar end conditions are required at the final time to produce a square Jacobian matrix, which will be described later in this chapter. To provide a total of five scalar end conditions, the three components of the final angular momentum vector are used in addition to the radial and tangential velocities. If angular momentum and velocity are matched correctly, their relationship guarantees the correct value of R . Thus, R becomes a redundant end condition, and does not need to appear explicitly. In fact, any one of the six scalar quantities r , u , v , h_x , h_y , h_z could be eliminated in this way.

4.2 Optimal Control in Two Dimensions

Using the two-dimensional equations of motion derived in Chapter 3, the Hamiltonian for this problem becomes:

$$\mathcal{H} = 1 + \lambda_x \dot{x} + \lambda_y \dot{y} + \lambda_{\dot{x}} \left(-\frac{\mu}{r^3} x + A \cos \alpha \right) + \lambda_{\dot{y}} \left(-\frac{\mu}{r^3} y + A \sin \alpha \right) \quad (4.29)$$

The control law which minimizes the flight time for a given end condition is found by setting $\partial \mathcal{H} / \partial \alpha = 0$, and leads to:

$$\tan \alpha = \left(\frac{-\lambda_{\dot{y}}}{-\lambda_{\dot{x}}} \right) \quad (4.30)$$

Using the control law given above, we obtain the following:

$$\cos \alpha = \frac{-\lambda_{\dot{x}}}{\sqrt{\lambda_{\dot{x}}^2 + \lambda_{\dot{y}}^2}} \quad (4.31)$$

$$\sin \alpha = \frac{-\lambda_{\dot{y}}}{\sqrt{\lambda_{\dot{x}}^2 + \lambda_{\dot{y}}^2}} \quad (4.32)$$

Substituting these results into the Legendre-Clebsch condition yields:

$$\frac{\partial^2 \mathcal{H}}{\partial \alpha^2} = A \frac{\lambda_{\dot{x}}^2 + \lambda_{\dot{y}}^2}{\sqrt{\lambda_{\dot{x}}^2 + \lambda_{\dot{y}}^2}} \geq 0 \quad (4.33)$$

Equation (4.33) provides the necessary conditions for a minimum. It is interesting to notice the similarity between the above result and the equivalent development in the three dimensions. In both cases, the velocity costates appear in the denominator. Equation (4.33) could be further reduced by division, but it is left in this form for comparison with the three-dimensional results.

In order to be consistent with the results of Bryson and Ho [7], the Hamiltonian may be multiplied by -1 without loss of generality. The Lagrangian and Lagrange multipliers will all change sign. This leads to an equivalent control law:

$$\tan \alpha = \left(\frac{\lambda_{\dot{y}}}{\lambda_{\dot{x}}} \right) \quad (4.34)$$

We then have the following:

$$\cos \alpha = \frac{\lambda_{\dot{x}}}{\sqrt{\lambda_{\dot{x}}^2 + \lambda_{\dot{y}}^2}} \quad (4.35)$$

$$\sin \alpha = \frac{\lambda_{\dot{y}}}{\sqrt{\lambda_{\dot{x}}^2 + \lambda_{\dot{y}}^2}} \quad (4.36)$$

When the Lagrangian is -1 , the optimization problem is one of maximizing the negative of the time of flight. The Legendre-Clebsch condition is still satisfied as follows:

$$\frac{\partial^2 \mathcal{H}}{\partial \alpha^2} = -A \frac{\lambda_x^2 + \lambda_y^2}{\sqrt{\lambda_x^2 + \lambda_y^2}} \leq 0 \quad (4.37)$$

which provides the necessary conditions for a maximum of the negative of the time of flight, or the minimum time to a given final boundary condition.

Using the control law in Equation (4.34), the differential equations for the states and costates are as follows:

$$\ddot{x} = -\frac{\mu}{r^3}x + A \left(\frac{\lambda_x}{\sqrt{\lambda_x^2 + \lambda_y^2}} \right) \quad (4.38)$$

$$\ddot{y} = -\frac{\mu}{r^3}y + A \left(\frac{\lambda_y}{\sqrt{\lambda_x^2 + \lambda_y^2}} \right) \quad (4.39)$$

$$\dot{\lambda}_x = -\frac{\mu}{r^3} \left[\left(\frac{3x^2}{r^2} - 1 \right) \lambda_x + \frac{3xy}{r^2} \lambda_y \right] \quad (4.40)$$

$$\dot{\lambda}_y = -\frac{\mu}{r^3} \left[\left(\frac{3y^2}{r^2} - 1 \right) \lambda_y + \frac{3xy}{r^2} \lambda_x \right] \quad (4.41)$$

$$\dot{\lambda}_x = -\lambda_x \quad (4.42)$$

$$\dot{\lambda}_y = -\lambda_y \quad (4.43)$$

Every solution of the differential equations for the state and costates is a minimum-time arc to some final end condition. The states and costates are initialized as follows:

Table 4.2 Initialization for 2D Problem

$x(0)$	$=$	1	$\lambda_x(0)$	$=$	1
$y(0)$	$=$	0	$\lambda_y(0)$	$=$	$?$
$\dot{x}(0)$	$=$	0	$\lambda_x(0)$	$=$	$\lambda_y(0)$
$\dot{y}(0)$	$=$	1	$\lambda_y(0)$	$=$	$?$

Table 4.2 shows the initialization of the states and costates in the two-dimensional problem. There are two unknown initial costates, and the unknown flight time makes a total of three scalars to be found. The end conditions for r , u , and v are an appropriate choice for matching via the shooting method, which is discussed later in this chapter.

Using the polar equations of motion from Chapter 3, Equations (3.8) - (3.10), the Hamiltonian is as follows:

$$\mathcal{H} = 1 + \lambda_r u + \lambda_u \left(\frac{v^2}{r} - \frac{\mu}{r^2} + A \sin \phi \right) + \lambda_v \left(-\frac{uv}{r} + A \cos \phi \right) \quad (4.44)$$

The optimality condition yields the following:

$$\frac{\partial \mathcal{H}}{\partial \phi} = A(\lambda_u \cos \phi - \lambda_v \sin \phi) = 0 \quad (4.45)$$

Solving for the polar thrust angle ϕ leads to:

$$\phi = \tan^{-1} \left(\frac{\lambda_u}{\lambda_v} \right) \quad (4.46)$$

Using the control law given above, we obtain the following:

$$\cos \phi = \frac{\lambda_v}{\sqrt{\lambda_u^2 + \lambda_v^2}} \quad (4.47)$$

$$\sin \phi = \frac{\lambda_u}{\sqrt{\lambda_u^2 + \lambda_v^2}} \quad (4.48)$$

To find the costates, we need the other result from Euler-Lagrange theory:

$$\dot{\lambda}_r = -\frac{\partial \mathcal{H}}{\partial r} = -\lambda_u \left(-\frac{v^2}{r^2} + \frac{2\mu}{r^3} \right) - \lambda_v \frac{uv}{r^2} \quad (4.49)$$

$$\dot{\lambda}_u = -\frac{\partial \mathcal{H}}{\partial u} = -\lambda_r + \lambda_v \frac{v}{r} \quad (4.50)$$

$$\dot{\lambda}_v = -\frac{\partial \mathcal{H}}{\partial v} = -\lambda_u \frac{2v}{r} + \lambda_v \frac{u}{r} \quad (4.51)$$

Table 4.3 Initialization for Polar Coordinate Problem

$r(0)$	$=$	1	$\lambda_r(0)$	$=$	1
$u(0)$	$=$	0	$\lambda_u(0)$	$=$	$?$
$v(0)$	$=$	1	$\lambda_v(0)$	$=$	$?$

which completes the set of optimal control equations in the polar case. The polar states and costates are initialized as shown in Table 4.3.

In the polar coordinate case, there are two unknown initial costates along with the unknown final time. These three quantities are used in discussion of the Jacobian matrix later in this chapter.

4.2.1 Comparison of Cartesian and Polar Hamiltonians. At the initial time only, the inertial thrust angle α may be used in the polar Hamiltonian since the polar and inertial angles sum to exactly $\pi/2$ at $t = 0$. At $t = 0$, the spacecraft is located at the point $(1,0)$ on the x -axis. The spacecraft local horizontal direction is along the positive y -axis. The inertial angle α is always measured to the thrust vector from the x -axis, and initially the polar angle $\phi(0)$ is measured to the thrust vector from the y -axis. Since the x and y axes are $\pi/2$ radians apart, the two angles must sum to $\pi/2$. This relationship may be expressed as follows:

$$\sin \phi(0) = \cos(\pi/2 - \phi(0)) = \cos \alpha(0) \quad (4.52)$$

$$\cos \phi(0) = \sin(\pi/2 - \phi(0)) = \sin \alpha(0) \quad (4.53)$$

The sine and cosine terms will then be reversed because of this relationship. This substitution allows for direct comparison of the terms in each Hamiltonian.

Here, the initial Hamiltonian is expressed in both sets of coordinates, with "p" denoting polar and "c" denoting Cartesian:

$$\mathcal{H}_p(0) = 1 + \lambda_r u + \lambda_u \left(\frac{v^2}{r} - \frac{\mu}{r^2} + A \cos \alpha \right) + \lambda_v \left(-\frac{uv}{r} + A \sin \alpha \right) \quad (4.54)$$

$$\mathcal{H}_c(0) = 1 + \lambda_x \dot{x} + \lambda_y \dot{y} + \lambda_{\dot{x}} \left(-\frac{\mu}{r^3} x + A \cos \alpha \right) + \lambda_{\dot{y}} \left(-\frac{\mu}{r^3} y + A \sin \alpha \right) \quad (4.55)$$

where all terms have their initial values. The initial conditions for the polar and Cartesian cases are:

$$\begin{aligned} r(0) &= 1 & x(0) &= 1 \\ u(0) &= 0 & \& & y(0) &= 0 \\ v(0) &= 1 & \dot{x}(0) &= 0 \\ & & \dot{y}(0) &= 1 \end{aligned}$$

Using these initial conditions and equating the resulting initial Hamiltonian expressions yields:

$$\lambda_u A \cos \alpha + \lambda_v A \sin \alpha = \lambda_y + \lambda_{\dot{x}} (-1 + A \cos \alpha) + \lambda_{\dot{y}} A \sin \alpha \quad (4.56)$$

where all terms have their initial values. By equating coefficients of $\sin \alpha(0)$ and $\cos \alpha(0)$, the following three relationships are obtained:

$$\lambda_y(0) = \lambda_{\dot{x}}(0) \quad (4.57)$$

$$\lambda_{\dot{x}}(0) = \lambda_u(0) \quad (4.58)$$

$$\lambda_{\dot{y}}(0) = \lambda_v(0) \quad (4.59)$$

The equality in Equation (4.57), $\lambda_y(0) = \lambda_{\dot{x}}(0)$, is the same relationship shown in the initialization Tables 4.1 and 4.2 for the three- and two-dimensional problems. The initial conditions used in each Hamiltonian are expressed in dimensionless, canonical units, which allow for great simplification by substitution of appropriate ones and zeros. If physical units were used instead, then $\lambda_y(0)$ and $\lambda_{\dot{x}}(0)$ would be related by some constant conversion factor based on the system of units. However, this constant may be found by simply equating the polar and Cartesian Hamiltonians as done here, only with the initial conditions expressed in the physical units.

This same relationship between $\lambda_y(0) = \lambda_{\dot{x}}(0)$ also arises in the minimum-fuel problem with impulsive thrust, and may be derived from Lawden's primer vector results for the impulsive orbital transfer case [13, 18]. In both the minimum-time and the minimum-fuel

formulations, a starting circular orbit of unit radius is required for the simple equality relationship to hold.

4.3 Optimal Control under the Kustaanheimo-Stiefel (KS) Transformation

Although it is possible to use the KS transformation for problems with three dimensions [21], only the two-dimensional problem will be addressed here for the purpose of comparison with the two-dimensional Cartesian case. In the next chapter, the initial values of the costates are presented graphically as functions of A and R for the two-dimensional case. The three-dimensional case requires two more parameters, so this type of graphical presentation is not possible. Thus, only the two-dimensional case under the KS transformation is necessary for the graphical comparison.

In the minimum-time problem [7], the cost functional is the real time. As shown in Chapter 3, the independent variable is changed to s under the KS transformation. Therefore, the cost functional becomes:

$$\mathcal{J} = t = \int_{s=0}^{s=s_f} r ds \quad (4.60)$$

Thus, the Lagrangian is r . The Hamiltonian for this problem is as follows:

$$\begin{aligned} H = & \lambda_{u_1} v_1 + \lambda_{u_2} v_2 + \lambda_{v_1} \left\{ \left[\frac{2(\vec{v}^T \vec{v}) - \mu}{2r} \right] u_1 + \frac{1}{2} A r^{3/2} \cos \gamma \right\} \\ & + \lambda_{v_2} \left\{ \left[\frac{2(\vec{v}^T \vec{v}) - \mu}{2r} \right] u_2 + \frac{1}{2} A r^{3/2} \sin \gamma \right\} + r + \tilde{\lambda}_t r \end{aligned} \quad (4.61)$$

Defining $\lambda_t = \tilde{\lambda}_t + 1$, the Hamiltonian becomes:

$$\begin{aligned} H = & \lambda_{u_1} v_1 + \lambda_{u_2} v_2 + \lambda_{v_1} \left\{ \left[\frac{2(\vec{v}^T \vec{v}) - \mu}{2r} \right] u_1 + \frac{1}{2} A r^{3/2} \cos \gamma \right\} \\ & + \lambda_{v_2} \left\{ \left[\frac{2(\vec{v}^T \vec{v}) - \mu}{2r} \right] u_2 + \frac{1}{2} A r^{3/2} \sin \gamma \right\} + \lambda_t r \end{aligned} \quad (4.62)$$

As before, the parameter A is a function of time, defined by $A = T/(m_0 + \dot{m}t)$. T is the thrust, m_0 is the initial spacecraft mass, and \dot{m} is the constant mass flow rate. The optimal control law is found by setting $\partial H/\partial \gamma$ equal to zero. For a minimum, the result is:

$$\tan \gamma = \frac{-\lambda_{v_2}}{-\lambda_{v_1}} \quad (4.63)$$

This choice of sign satisfies the Legendre-Clebsch condition for a minimum. From this control law, we have the following:

$$\cos \gamma = \frac{-\lambda_{v_1}}{\sqrt{\lambda_{v_1}^2 + \lambda_{v_2}^2}} \quad (4.64)$$

$$\sin \gamma = \frac{-\lambda_{v_2}}{\sqrt{\lambda_{v_1}^2 + \lambda_{v_2}^2}} \quad (4.65)$$

These relationships may be used to eliminate the $\sin \gamma$ and $\cos \gamma$ terms from the Hamiltonian. The costate equations are then found using the canonical relationship $\vec{\lambda}' = -\partial H/\partial \vec{q}$, in which $\vec{q} = (u_1, u_2, v_1, v_2, t)$. Recall that the primes indicate differentiation with respect to the fictional time, s . Using this relationship and taking the indicated partial derivatives produces the following five first-order differential equations:

$$\lambda'_t = \frac{-\dot{m}T r^{(3/2)}}{2(m_0 + \dot{m}t)^2} \sqrt{\lambda_{v_1}^2 + \lambda_{v_2}^2} \quad (4.66)$$

$$\begin{aligned} \lambda'_{u_1} &= \left[\frac{2(\vec{v}^T \vec{v}) - \mu}{2r} \right] \left[\frac{2u_1}{r} (\lambda_{v_1} u_1 + \lambda_{v_2} u_2) - \lambda_{v_1} \right] \\ &+ (3/2) A r^{(1/2)} u_1 \sqrt{\lambda_{v_1}^2 + \lambda_{v_2}^2} - 2u_1 \end{aligned} \quad (4.67)$$

$$\begin{aligned} \lambda'_{u_2} &= \left[\frac{2(\vec{v}^T \vec{v}) - \mu}{2r} \right] \left[\frac{2u_2}{r} (\lambda_{v_1} u_1 + \lambda_{v_2} u_2) - \lambda_{v_2} \right] \\ &+ (3/2) A r^{(1/2)} u_2 \sqrt{\lambda_{v_1}^2 + \lambda_{v_2}^2} - 2u_2 \end{aligned} \quad (4.68)$$

$$\lambda'_{v_1} = \left(\frac{-2v_1}{r} \right) (\lambda_{v_1} u_1 + \lambda_{v_2} u_2) - \lambda_{u_1} \quad (4.69)$$

$$\lambda'_{v_2} = \left(\frac{-2v_2}{r} \right) (\lambda_{v_1} u_1 + \lambda_{v_2} u_2) - \lambda_{u_2} \quad (4.70)$$

If $\dot{m} = 0$, then $\lambda_t' = 0$ as well. In this case, λ_t will be a constant. It would then be possible to divide the Hamiltonian through by λ_t which would scale the remaining costate variables, and eliminate λ_t from the problem. If $\dot{m} \neq 0$, λ_t must be retained because the real time will explicitly appear in the equations of motion. The Hamiltonian may be set equal to zero at the initial time by adding an arbitrary constant, since the constant will contribute nothing to the partial derivatives. Then, it is possible to solve for initial λ_t (or λ_{v_2}) as a function of the initial values of the remaining states and costates:

$$\lambda_t(0) = -\frac{1}{2}A_0\sqrt{\lambda_{v_1}^2(0) + \lambda_{v_2}^2(0)} \quad (4.71)$$

At the initial time, $\lambda_{v_1} = 2\lambda_{u_2}$. This may be shown by equating the KS Hamiltonian to another Hamiltonian in polar coordinates, but with fictitious time. This procedure is analogous to the derivation given earlier using the Cartesian and polar Hamiltonians. Also, the Hamiltonian may be scaled such that $\lambda_{u_1} = 1$. Thus, there are three remaining values that must be found to solve the boundary value problem of coplanar transfer between two circular orbits. As shown in Table 4.4, they are: s_f , $\lambda_{u_2}(0)$, and $\lambda_{v_2}(0)$. If λ_t is not used, then the three values that must be found are s_f , $\lambda_{u_1}(0)$, and $\lambda_{u_2}(0)$. The other two costates are found from $\lambda_{v_1} = 2\lambda_{u_2}$, and from solving $H(0) = 0$ for λ_{v_2} . Since the final circular orbit may be described using three scalar values, the number of unknowns is the same as the number of end conditions to be matched.

Table 4.4 Initialization for KS Problem

$u_1(0)$	$=$	1	$\lambda_{u_1}(0)$	$=$	1
$u_2(0)$	$=$	0	$\lambda_{u_2}(0)$	$=$	$?$
$v_1(0)$	$=$	0	$\lambda_{v_1}(0)$	$=$	$2\lambda_{u_2}(0)$
$v_2(0)$	$=$	$1/2$	$\lambda_{v_2}(0)$	$=$	$?$

4.4 Solution of the Optimal Control Problem

4.4.1 The Shooting Method. The shooting method [16] is an indirect technique for solving a two-point boundary value problem by numerically perturbing a reference trajectory. It is named after the classical method of aiming an artillery piece. The basic

idea is to fire one shell as a reference, then "bracket" the target by adjusting the angle up or down if the shot fell short or long, respectively. Inherent in this method is the need to guess the initial angle for the first shot, and the need for an effective means of selecting the next angle based on the results of the previous shot.

When applied to the continuous-thrust spacecraft problem, the differential equations governing the state and costate variables are numerically integrated to form the required reference trajectory. Since the initial values of the costate variables are usually unknown, they must be guessed. This normally results in failure to meet the desired end conditions for the state of the spacecraft, even though every trajectory satisfies the optimality condition. To correct this, additional trajectories are propagated with slight changes in the initial values of the costates. Then, a matrix of partial derivatives is formed to quantify the influence of initial costate values on final states. With this "secant" or Jacobian matrix, the optimal initial values of the costates may be found approximately. If the elements of the Jacobian matrix are found numerically with one-sided difference approximations, as is done in this implementation, the search is a *quasi*-Newton method. Also, the Jacobian matrix represents only a first order linear approximation for a typically highly nonlinear set of equations. Often, the nonlinearity results in a process that will not converge from poor initial guesses. The Jacobian matrix may also be found analytically, allowing for integration of the equations of variation and better convergence properties. This technique is a multi-variable application of Newton's method [14, 16] to a nonlinear problem, which is only guaranteed to converge within a "small" neighborhood of the solution point. The size of this neighborhood is determined by the extent over which the problem is approximately linear about the solution point. Since the exact equations for the states and costates do not have an analytical solution, the only way to approximate the size of the nearly linear region is through numerical methods. Appendix A contains a flowchart that outlines the shooting method algorithm. Appendix A also contains a description of the convergence criteria used for all of the numerical examples in this dissertation.

When attempting to solve a problem of this nature, the analyst has a choice of variables to use in forming the Jacobian matrix. It is generally a good idea to keep the partial derivative matrix square, since the inverse will be required to find the corrections

to the initial costates. If the Jacobian matrix is not square, other alternatives exist such as left and right inverses [22]. If the final time of a boundary value problem is unknown, but the final states are specified, then the final time may be chosen as an input to the Jacobian matrix. This way, the unknown final time may be refined from an initial guess along with the costates.

The first step in solving this boundary value problem is to guess the two unknown costates and a final time, then numerically integrate. Once the final time has been reached, the final state values are examined to see how close they came to the desired final conditions. Since they will undoubtedly be wrong, the initial costates and final time must be adjusted to try again. If this process is convergent, the final conditions will be met to a desired accuracy after several iterations. Time is the independent variable, so a final value of the time makes a reliable stopping condition for integrating the equations of motion. The stopping condition $r = R$ is not as useful, since the equations of motion apply equally to orbit-lowering and orbit-raising. Thus, some initial values of the costates lead to a decrease in r , so that $r = R$ may not occur at or before $t = t_f$. Therefore, refining the final time is the most practical approach to the problem.

To adjust the initial costate values and final time, we form the Jacobian matrix of partial derivatives numerically to see how the final state errors depend on initial guesses. We will now describe the formulation of the quasi-Newton step using the polar, two-dimensional case which results in a 3×3 Jacobian matrix since there are two initial costates and the time of flight to be determined. By comparison, the three-dimensional case will have a 5×5 Jacobian matrix corresponding to four unknown initial costates and the time of flight.

If the initial value of λ_r was not taken to be unity as explained before, a reasonable formulation for the quasi-Newton step in polar coordinates would be as follows:

$$\begin{bmatrix} \Delta\lambda_r(0) \\ \Delta\lambda_u(0) \\ \Delta\lambda_v(0) \end{bmatrix} = \begin{bmatrix} \partial r(t_f)/\partial\lambda_r(0) & \partial r(t_f)/\partial\lambda_u(0) & \partial r(t_f)/\partial\lambda_v(0) \\ \partial u(t_f)/\partial\lambda_r(0) & \partial u(t_f)/\partial\lambda_u(0) & \partial u(t_f)/\partial\lambda_v(0) \\ \partial v(t_f)/\partial\lambda_r(0) & \partial v(t_f)/\partial\lambda_u(0) & \partial v(t_f)/\partial\lambda_v(0) \end{bmatrix}^{-1} \begin{bmatrix} \Delta r(t_f) \\ \Delta u(t_f) \\ \Delta v(t_f) \end{bmatrix} \quad (4.72)$$

Each of the partial derivatives is formed by making small changes to the initial conditions of a reference trajectory, and noting the changes in the final conditions. As mentioned previously, the partial derivatives are approximated numerically, so this technique is a *quasi-Newton* method.

Since the initial value $\lambda_r(0)$ may be scaled to unity, there is no need to include it in the above formulation. However, the final time is also unknown in this problem. Rather than make manual changes in final time, it is possible to incorporate it directly into the quasi-Newton step formulation:

$$\begin{bmatrix} \Delta t_f \\ \Delta \lambda_u(0) \\ \Delta \lambda_v(0) \end{bmatrix} = \begin{bmatrix} \partial r(t_f)/\partial t_f & \partial r(t_f)/\partial \lambda_u(0) & \partial r(t_f)/\partial \lambda_v(0) \\ \partial u(t_f)/\partial t_f & \partial u(t_f)/\partial \lambda_u(0) & \partial u(t_f)/\partial \lambda_v(0) \\ \partial v(t_f)/\partial t_f & \partial v(t_f)/\partial \lambda_u(0) & \partial v(t_f)/\partial \lambda_v(0) \end{bmatrix}^{-1} \begin{bmatrix} \Delta r(t_f) \\ \Delta u(t_f) \\ \Delta v(t_f) \end{bmatrix} \quad (4.73)$$

This is an original formulation that saves computing time, since it completely automates the shooting technique. In this form, the boundary value problem may be imbedded in a larger programming loop that allows for parameter variations. This way, we can more easily study the effects of changing the thrust level, mass flow rate, final radius, and gravitational constant.

The above Jacobian matrix formulation automates the search over a range of fixed final time values. Each "shot" in the shooting method is still a minimum-time arc, but this technique allows us to match the desired end conditions *and* determine the correct final time simultaneously. In the three-dimensional case, the quasi-Newton step becomes:

$$\Delta \bar{P} = \begin{bmatrix} \Delta t_f \\ \Delta \lambda_y(0) \\ \Delta \lambda_x(0) \\ \Delta \lambda_y(0) \\ \Delta \lambda_z(0) \end{bmatrix} = J^{-1} \begin{bmatrix} \Delta u(t_f) \\ \Delta v(t_f) \\ \Delta h_x(t_f) \\ \Delta h_y(t_f) \\ \Delta h_z(t_f) \end{bmatrix} \quad (4.74)$$

The Jacobian matrix is denoted by J . This expression corresponds to the results given in Table 4.1. The partial derivatives in the 5×5 Jacobian matrix are similar to the two-dimensional case, using the variables given in the above equation.

4.4.2 Dynamic Step Limiter. To improve the convergence properties for these problems, an original modification is made to Newton's method by providing a variable scaling factor for the quasi-Newton step. Let \vec{P} be a vector of unknowns such as $\vec{P} = (t_f, \lambda_u(0), \lambda_v(0))$, and let $\Delta\vec{P}$ be the quasi-Newton step from Equation (4.73), where

$$\Delta\vec{P} = \begin{bmatrix} \Delta t_f \\ \Delta\lambda_u(0) \\ \Delta\lambda_v(0) \end{bmatrix} \quad (4.75)$$

Then, the following equation is used:

$$\vec{P}_{i+1} = \vec{P}_i + \frac{\Delta\vec{P}_i}{1 + \|\Delta\vec{P}_i\|} \quad (4.76)$$

This modification provides a dynamic scaling effect on the quasi-Newton step. If $\|\Delta\vec{P}_i\|$ is large, the scaling limits the individual component changes to less than unity, without changing the step direction. If $\|\Delta\vec{P}_i\|$ is small, the scaling does not affect the magnitudes of the individual component changes very much, so the quadratic convergence rate is nearly maintained in the neighborhood of the solution point. The scaling preserves the direction of the quasi-Newton step in the search space, but prevents the magnitude from becoming unreasonably large, as can happen with nonlinear problems.

A proof of convergence for Newton's method is given by Luenberger [14] for the multivariable, nonlinear case. To quote the source, "the theorem can be paraphrased roughly by simply saying that Newton's method converges provided that the initial approximation x_1 is sufficiently close to the solution x_0 ." Luenberger also states, "One device useful in these situations is to begin iterating with a slower but surer technique and then change over to Newton's method to gain the advantage of quadratic convergence near the end of the process." This is exactly the purpose of the dynamic scaling technique presented here.

From numerical experience, it has been found that an initial approximation that is just outside of the region of convergence will often result in a very large quasi-Newton step magnitude. By limiting the magnitude of the step, it is possible to exploit the directional information from the quasi-Newton step while potentially increasing the region of convergence. Due to the nonlinearity of the problem, this result has only been shown to hold true to varying degrees based on numerical experimentation. The one definite statement that can be made about this scaling technique is that it cannot make the region of convergence smaller. If the quasi-Newton step is denoted by $\Delta\vec{P}$ as before, the convergence proof [14] requires that:

$$\|\Delta\vec{P}_i\| \leq \eta \quad (4.77)$$

where η is some sufficiently small scalar quantity to provide convergence. Clearly, it may be seen that

$$\left\| \frac{\Delta\vec{P}_i}{1 + \|\Delta\vec{P}_i\|} \right\| \leq \|\Delta\vec{P}_i\| \leq \eta \quad (4.78)$$

The modified Newton step satisfies the proof, as long as the original Newton step does. The modified quasi-Newton method may take more iterations to achieve convergence, but it also increases the radius of convergence, based on numerical experience.

In this research, the modified quasi-Newton method is used for its simplicity. The initial costate approximations contain an entire control history in a compact form, since the thrust angle is produced automatically with numerical integration through the final time. Thus, by applying the modified quasi-Newton method to determine the initial costates and time of flight, it is possible to explore a large range of control functions. Further extensions of Newton's method are available [9], but they add more complication to the search technique. Most importantly, the purpose of this research is to provide approximate models with enough accuracy so that the modified quasi-Newton method converges without further modification. A convergence sensitivity study is presented in Chapter 5, which shows the number of iterations required for convergence for the entire practical range of R and A .

Figure 4.1 shows a comparison of the modified quasi-Newton method (MNM) with the unmodified quasi-Newton method (NM). This is a well-known Earth-to-Mars transfer

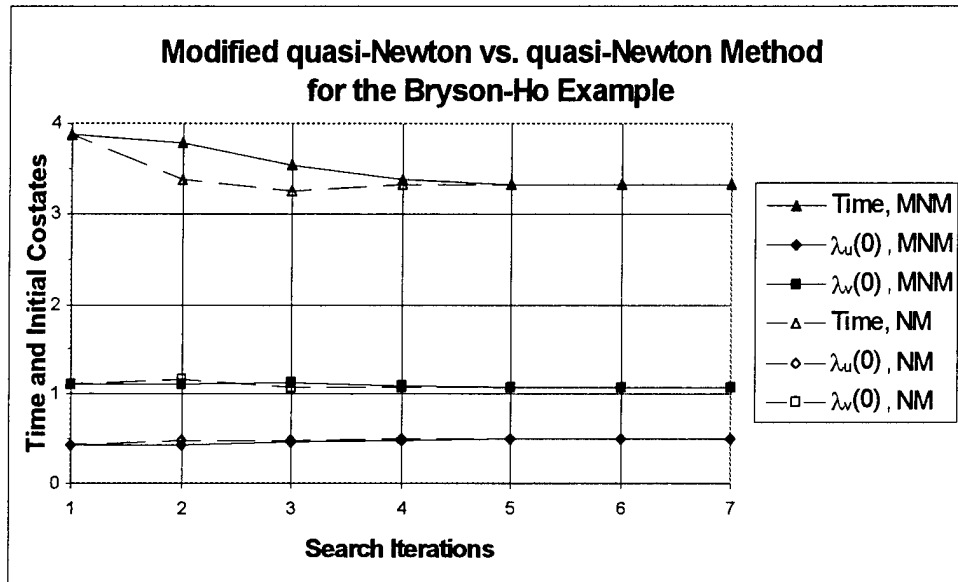


Figure 4.1 Iteration History for Modified vs. Unmodified Quasi-Newton Method

example developed by Bryson and Ho [7], which will be discussed in greater detail in Chapter 6. The iteration history shows seven modified quasi-Newton steps with solid lines, and six unmodified quasi-Newton steps with dashed lines. The solid line segments in Figure 4.1 are seen to have slope magnitudes less than or equal to the dashed line segments between iteration numbers 1 and 2. Since iterations 2 through 6 start from different values using the two methods, the modified quasi-Newton steps may have slopes that are larger, smaller or the same as the quasi-Newton steps. In this example, the modification caused an increase of one iteration over the quasi-Newton method to reach the same converged values. Appendix A describes the numerical criteria used in this and all other examples presented in this dissertation.

Table 4.5 shows a case with $R = 2.2$ and $A = 0.01$ in which the quasi-Newton method begins to diverge on the third iteration. The modified quasi-Newton method achieves convergence in 11 iterations.

4.5 Summary

This chapter presents the minimum-time optimal control formulation in several coordinate systems for the orbital transfer problem considering gravity and continuous thrust.

Table 4.5 Comparison of Search Methods for $R = 2.2$, $A = 0.01$

quasi-Newton Method			Modified quasi-Newton Method				
it.	$\lambda_u(0)$	$\lambda_v(0)$	time	it.	$\lambda_u(0)$	$\lambda_v(0)$	time
1	0	1	32.58001	1	0	1	32.58001
2	-0.01441	0.637370	32.44273	2	-0.00295	0.925693	32.55188
3	2.19319	0.912565	59.36023	3	-0.00138	0.825579	32.92815
4	-51.25330	95.665720	-54.05710	4	0.00441	0.823785	33.02219
		divergence		5	0.033265	0.816452	33.48742
				6	0.059477	0.817559	33.90471
				7	0.080149	0.823066	34.24611
				8	0.093224	0.829128	34.47590
				9	0.098446	0.832526	34.57503
				10	0.099224	0.833181	34.59116
				11	0.099240	0.833198	34.59154
					convergence achieved		

In an original presentation, the minimum-time formulation is also applied to the equations of motion under the KS transformation. Numerical initialization techniques are discussed for each set of optimal control equations. The shooting method is described as a means to solve the boundary value problem. Finally, an original dynamic scaling modification to the quasi-Newton method is provided which improves the convergence properties of the shooting method. An example is provided showing differences in the convergence properties of the quasi-Newton method and the modified quasi-Newton method. The modified quasi-Newton step satisfies the conditions for convergence, as long as the conditions are met by the unmodified quasi-Newton step, and often when the unmodified quasi-Newton step does not.

V. *Optimal Initial Costate Locus*

In this chapter, the optimal initial Lagrange multipliers are modeled as functions of the problem parameters which include $R = r(t_f)$, the final radius, and $A = A(0)$, the initial thrust acceleration. This is accomplished by first examining the functional form of the costates graphically, then dividing the resulting locus into three distinct regions for separate analysis. A combination of analytical and empirical techniques is used to model the regions of the costate locus. The models are then evaluated by measuring the convergence sensitivity for the entire practical range of A and R . Finally, the initial costate locus is presented under the KS transformation to provide a qualitative, graphical comparison to the Cartesian form. Appendix A contains a description of the numerical convergence criteria used to determine the “exact” solutions that appear in the figures and examples.

To illustrate the importance of developing the initial costate models, one may simply consider the alternatives. There are no models available in the literature that provide initial costate estimates for the minimum-time, continuous thrust orbit transfer problem as functions of the problem parameters. As mentioned previously, others [15, 18] have tried, with limited success, to use the Hohmann transfer to initialize the Lagrange costates for the minimum-fuel problem with coasting arcs. However, the minimum-fuel problem allows for throttling and has a Lagrangian based on fuel mass, neither of which appear in the minimum-time problem. Thus, the minimum-fuel results provide no reliable information to initialize the costates in the minimum-time problem.

The only way to solve the minimum-time boundary value problem is to guess some initial Lagrange costate values and hope for good fortune, resulting in a convergent case. However, good fortune is notoriously unreliable. Even if one happens upon a convergent case to the desired final radius, it is unlikely that the parameter value of the thrust acceleration will match the spacecraft design. Then, the task is to adjust the value of A until it matches the desired value. If A is too large, it may be reduced by some small percentage, and used with the initial costate values from the known case. If the reduction percentage is small enough, the problem may converge for the new value of A . This process may be repeated until the desired value of A is achieved. The drawback to this technique, known

as the continuation method [12], is that the step size for A to result in convergence is not constant, and one must therefore “hand-hold” the process by monitoring the convergence behavior through perhaps hundreds of small changes in A . Depending on the available computing power and sensitivity of the problem, this process could take days or weeks to complete. Again, one must also have found a “seed” case to begin the search.

Suppose $R = 2$, and we have a converged case for $A = 100$. A numerical description of convergence for this and all other examples is presented in Appendix A. If A is multiplied by 0.9, then convergence may be achieved using the last values of the initial costates as the new starting guess. If this procedure is repeated more than roughly 20 times, the shooting method will take more iterations to converge, and eventually will not converge at all. Then, the multiplication factor must be increased to perhaps 0.95, and higher still as A decreases. This phenomenon is due to the sensitivity of the system to initial conditions, which increases for the increased flight times associated with small thrust values at a given R . Although this process is difficult and time consuming, it does produce valuable information. After completing the process for a large range of A , it is instructive to make a plot of the converged initial values of the costates versus one another to examine their behavior. This is an original presentation technique [23, 24] which first appears in Figure 5.1. This choice of axes is motivated by the polar thrust angle ϕ as shown in Figure 3.2. The initial value of ϕ may be measured from the $\lambda_v(0)$ axis to a point on the locus with the vertex at the origin. Thus, the initial thrust angle may be seen relative to the spacecraft local horizon directly from the figure. For large values of A , the initial thrust angle $\phi(0)$ approaches 90 degrees, and for small values of A , $\phi(0)$ approaches zero degrees, in the spacecraft horizontal direction. The analysis of the initial costate locus is carried out using the two-dimensional Cartesian coordinate formulation, so it is important to remember that $\lambda_x(0) = \lambda_u(0)$ and $\lambda_y(0) = \lambda_v(0)$, as shown in Equations (4.58) and (4.59).

As the thrust acceleration decreases, the optimal trajectory will cover a larger transfer angle to reach the same final radius. There are particular values of A that result in integer values of orbital revolutions, and the points corresponding to one through twelve revolutions are indicated in Figure 5.2 for $R = 2$. The first point marked with a circle on the outermost curve of the spiral corresponds to a one-revolution transfer. The next indicated

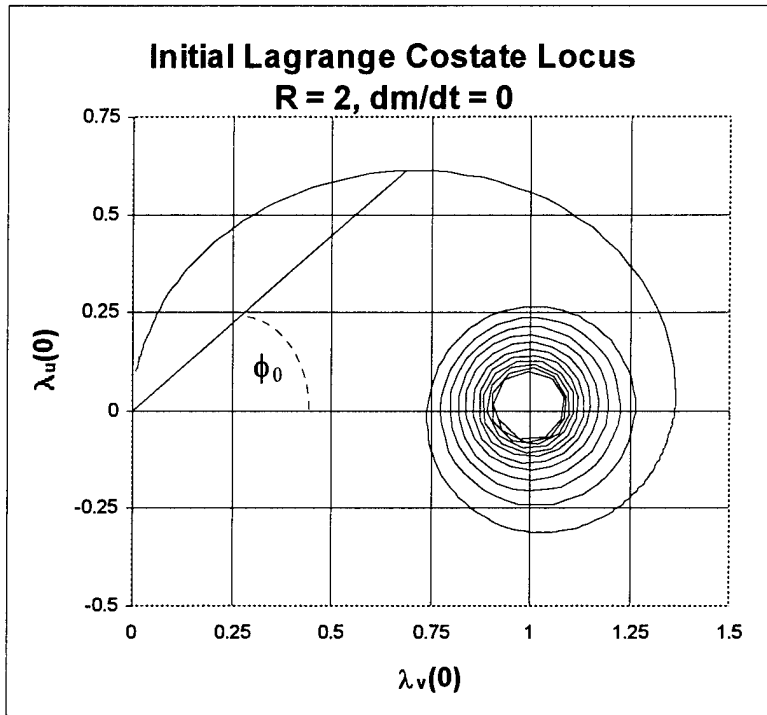


Figure 5.1 Optimal Initial Costate Locus for $R = 2, \dot{m} = 0$

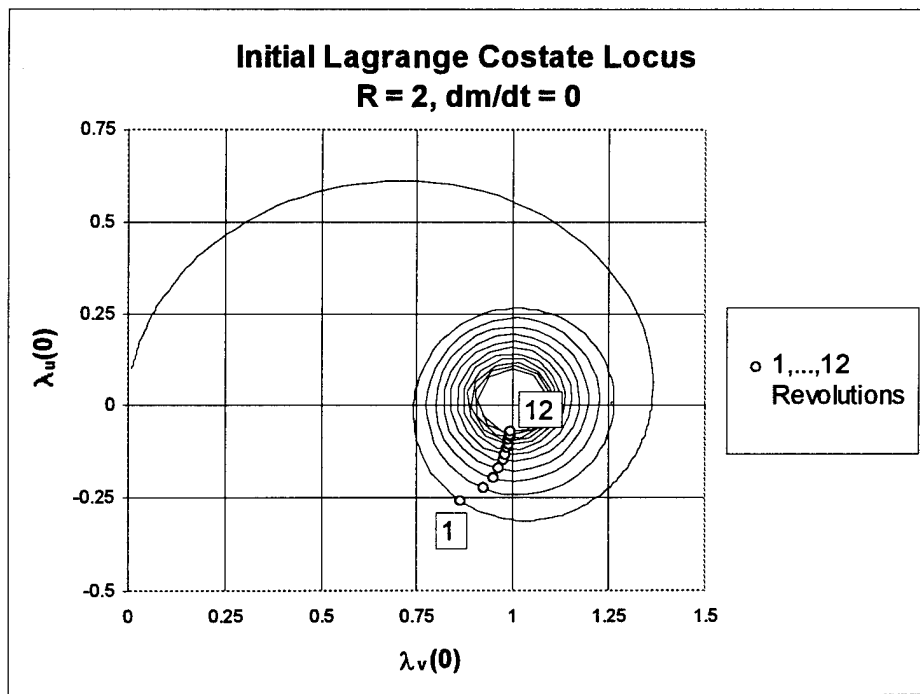


Figure 5.2 Optimal Initial Costate Locus for $R = 2, 1-12$ Revolutions

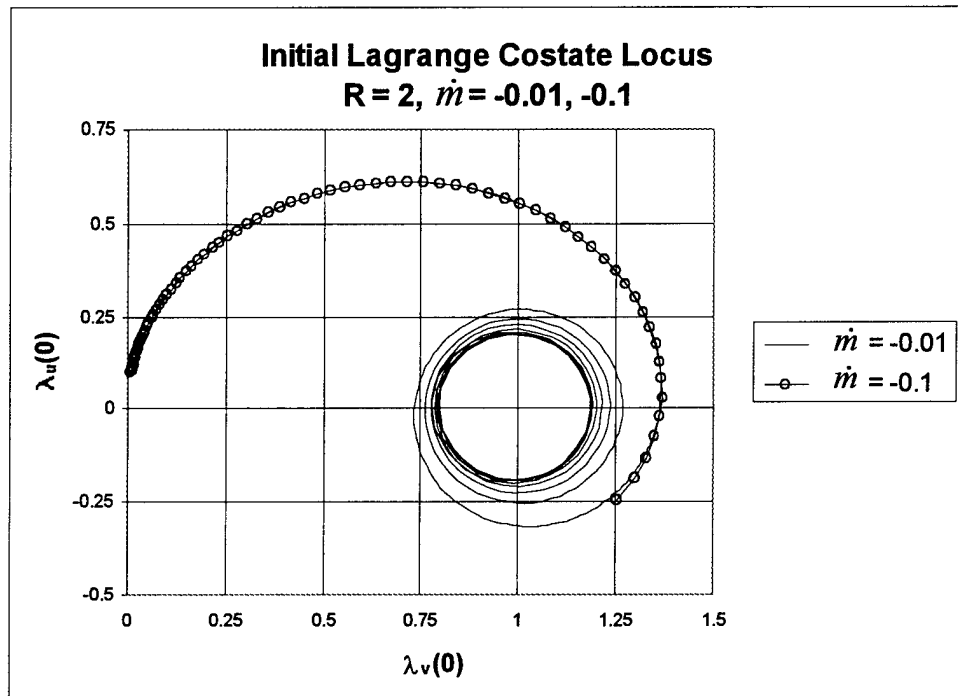


Figure 5.3 Optimal Initial Costate Locus for $R = 2$, $\dot{m} = -0.01, -0.1$

point inward towards the center of the spiral corresponds to a two-revolution transfer, and so on, until the last indicated point closest to the center of the spiral represents a twelve-revolution transfer. The number of revolutions will continue to increase as the thrust is reduced, but the flight time increases as well. This pattern continues indefinitely if the mass flow rate is equal to zero, because the spacecraft will never run out of propellant mass. The values of A that correspond to integer revolution transfers will change with R , but they have been found to give a negative value of $\phi(0)$ in all cases.

The process used to create the solid locus in Figure 5.1 is repeated for different values of the mass flow rate, and shown in Figure 5.3. When $\dot{m} = -0.1$ mass units per time unit, the final time cannot exceed 10 time units, since all of the spacecraft mass would be consumed. Similarly, the final time cannot exceed 100 time units for $\dot{m} = -0.01$. Thus, the locus spiral will stop for some minimum value of A , because small values of A correspond to long flight times. When \dot{m} is taken to be zero, there is no time limit for the powered trajectory, and any value of A may be used. Therefore, the $\dot{m} = 0$ locus may continue spiraling indefinitely as A is reduced. It is clear from Figure 5.3 that the

changes in \dot{m} have little effect on the location of the initial costates. A possible physical interpretation of this relative insensitivity to \dot{m} is that mass flow rate has no immediate effect at the initial time, since the spacecraft mass is normalized to unity at $t = 0$. Also, only small changes in the costates at the initial time are required for significant changes in the trajectory at the final time, due to the sensitivity of the problem. Based on observations from the numerically generated initial costate loci, the quantity \dot{m} is assumed to be zero in the development of the initial costate models, in order to simplify the analysis. However, the equations of motion always include \dot{m} , so the examples in Chapter 6 may be given realistic values of the mass flow rate.

The next step in the analysis is to take the numerical results of many converged cases with R and A as parameters, and plot the optimal initial costates as functions of R and A , forming the loci shown in Figure 5.4. In this way, the functional behavior of the costates is easily seen to be represented by three distinct regions. Near the origin of the $\lambda_v(0)$, $\lambda_u(0)$ plane, the optimal initial costates lie on a nearly parabolic arc. As A decreases or R increases, the locus moves away from the origin on a nearly elliptical path, and eventually spirals into the point $\lambda_v = 1$, $\lambda_u = 0$. This point represents the limiting case of purely tangential thrust [26]. The optimal initial costate loci show a common tendency to spiral towards the point $(1,0)$ with $\dot{m} = 0$. Two example points are shown in Figure 5.4, which correspond to an anti-satellite avoidance mission (ASAT) [10] and the well-known Earth-to-Mars transfer example given by Bryson and Ho [7]. These examples will be described in detail in Chapter 6. The parameter $S = \sqrt{(R-1)/A}$ is developed in the next section.

The parabolic, elliptic, and spiral regions of the costate locus will be addressed separately for modeling purposes. The parabolic region represents orbital transfers that take less than about one quarter revolution to complete, either due to high thrust or small radius change. This situation lends itself to an analytical approach, which is presented in the next section.

5.1 Parabolic Region

For orbital transfers with large A or small R , the optimal trajectory tends to be a nearly linear path which takes less than roughly one quarter revolution, based on numerical

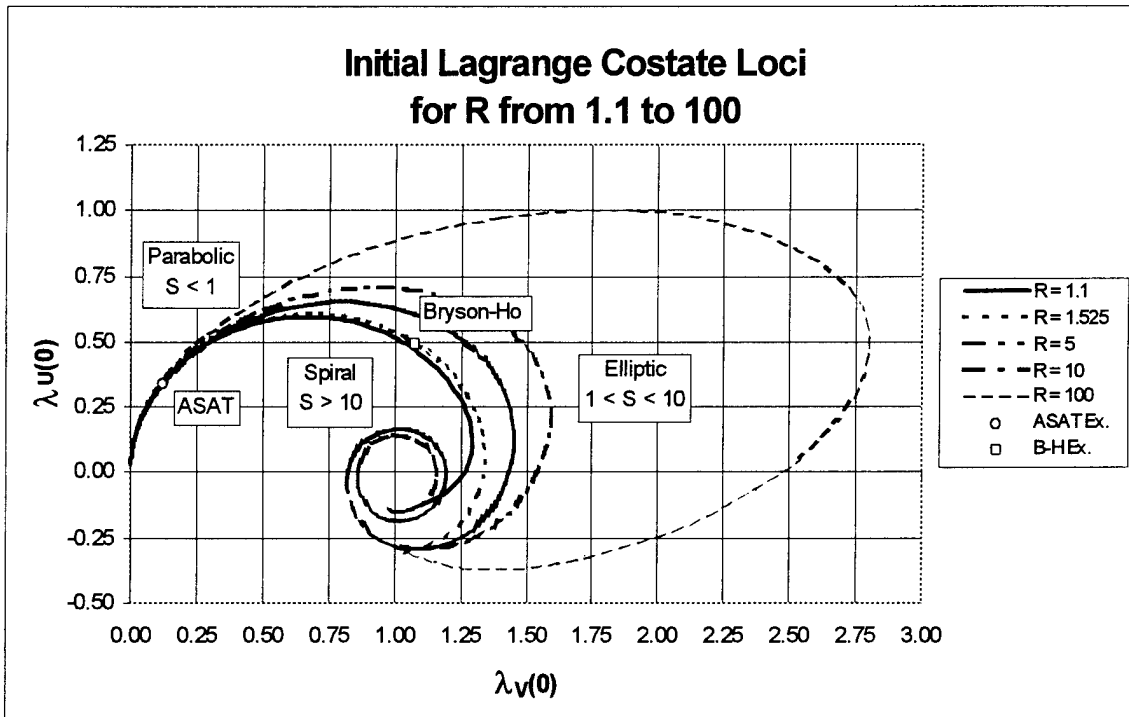


Figure 5.4 Optimal Initial Costate Loci

investigation. Under these conditions, the problem may be approximated with gravity-free space, since it is the influence of gravity that causes multiple revolution trajectories.

Large A and small R values correspond to the parabolic region of Figure 5.4, near the origin. If the equations of motion are approximated by setting $\mu = 0$ and $\dot{m} = 0$, the differential equations for the states and costates may be integrated in closed form. Although ignoring the gravity may not seem to be the most obvious choice for approximation, it does reduce the problem to a system of *algebraic* equations. Further, the boundary conditions are still chosen to be circular orbits. Thus, gravity still has an influence on the solution since the boundary conditions depend on the nominal gravitational constant value, $\mu = 1$.

Once these two approximations ($\mu = 0$, $\dot{m} = 0$) have been made, the equations of motion in Cartesian coordinates simplify enough to allow analytical integration. The result is a system of eight algebraic equations for the position and velocity components and their associated costates. These solutions are functions of A , R , time and eight constants of integration. Recall that the polar and Cartesian optimal initial costates are related by Equations (4.58) and (4.59).

5.1.1 *Equations of Motion with Zero Gravity.* Setting the gravitational constant to zero, the differential equations of motion simplify to:

$$\ddot{x} = A \left(\frac{\lambda_{\dot{x}}}{\sqrt{\lambda_x^2 + \lambda_y^2}} \right) \quad (5.1)$$

$$\ddot{y} = A \left(\frac{\lambda_{\dot{y}}}{\sqrt{\lambda_x^2 + \lambda_y^2}} \right) \quad (5.2)$$

$$\dot{\lambda}_x = 0 \quad (5.3)$$

$$\dot{\lambda}_y = 0 \quad (5.4)$$

$$\dot{\lambda}_{\dot{x}} = -\lambda_x \quad (5.5)$$

$$\dot{\lambda}_{\dot{y}} = -\lambda_y \quad (5.6)$$

The last four equations may be integrated immediately and substituted into the first four equations. Defining $\lambda_{pos} = \sqrt{\lambda_x^2 + \lambda_y^2}$, and $\lambda_{vel} = \sqrt{\lambda_{\dot{x}}^2 + \lambda_{\dot{y}}^2}$, the $\mu = 0$ solutions for the costate and state equations are:

$$\lambda_x = a \quad (5.7)$$

$$\lambda_y = b \quad (5.8)$$

$$\lambda_{\dot{x}} = -at + c \quad (5.9)$$

$$\lambda_{\dot{y}} = -bt + d \quad (5.10)$$

$$\begin{aligned} x = & A \left[\frac{\lambda_{vel}}{2\lambda_{pos}^4} (a^2c - 2b^2c + 3abd - a\lambda_{pos}^2 t) \right. \\ & + \frac{1}{2\lambda_{pos}^5} (-3ab^2c^2 + 4a^2bcd - 2b^3cd - a^3d^2 + 2ab^2d^2 + 2\lambda_{pos}^2 b(bc - ad)t) \\ & \left. \times \ln(-ac - bd + \lambda_{pos}^2 t + \lambda_{pos}\lambda_{vel}) \right] + k_1 t + k_3 \end{aligned} \quad (5.11)$$

$$\begin{aligned}
y &= A \left[\frac{\lambda_{vel}}{2\lambda_{pos}^4} (b^2d - 2a^2d + 3abc - b\lambda_{pos}^2 t) \right. \\
&\quad + \frac{1}{2\lambda_{pos}^5} (-3a^2bd^2 + 4ab^2cd - 2a^3cd - b^3c^2 + 2a^2bc^2 + 2\lambda_{pos}^2 a(ad - bc)t) \\
&\quad \left. \times \ln(-ac - bd + \lambda_{pos}^2 t + \lambda_{pos}\lambda_{vel}) \right] + k_2 t + k_4 \quad (5.12)
\end{aligned}$$

$$\dot{x} = \frac{A}{\lambda_{pos}^3} \left[-a\lambda_{pos}\lambda_{vel} + b(bc - ad) \ln(-ac - bd + \lambda_{pos}^2 t + \lambda_{pos}\lambda_{vel}) \right] + k_1 \quad (5.13)$$

$$\dot{y} = \frac{A}{\lambda_{pos}^3} \left[-b\lambda_{pos}\lambda_{vel} + a(ad - bc) \ln(-ac - bd + \lambda_{pos}^2 t + \lambda_{pos}\lambda_{vel}) \right] + k_2 \quad (5.14)$$

The terms a , b , c , d , k_1 , k_2 , k_3 and k_4 are constants of integration. Because the Lagrange multipliers appear in the Hamiltonian as linear terms, the initial value of one of them may be scaled to unity. For this system, we choose $\lambda_x(0) = 1$, thus $a = 1$. Also, if the initial state is on a circular orbit, we have $b = c$, as shown in Chapter 4 by equating the system Hamiltonian expressed in polar and Cartesian coordinates.

The constants k_1 and k_2 may be eliminated from Equations (5.13) and (5.14) by using the velocity component end conditions, $\dot{x}(0)$, $\dot{x}(t_f)$, $\dot{y}(0)$, $\dot{y}(t_f)$ and the final time, t_f . The final velocity components come from the desired final orbit. It should be noted that λ_{pos} does not have a time argument since it is a constant in the zero-gravity case where $\lambda_{pos} = \sqrt{1 + b^2}$, using the definition given previously. Performing these operations yields:

$$\frac{(\dot{x}(t_f) - \dot{x}(0))\lambda_{pos}^3}{A} = \lambda_{pos}(\lambda_{vel}(0) - \lambda_{vel}(t_f)) + b(d - b^2)L \quad (5.15)$$

$$\frac{(\dot{y}(t_f) - \dot{y}(0))\lambda_{pos}^3}{Ab} = \lambda_{pos}(\lambda_{vel}(0) - \lambda_{vel}(t_f)) + \left(\frac{b^2 - d}{b}\right)L \quad (5.16)$$

$$L = \ln \left(\frac{-b - bd + \lambda_{pos}\lambda_{vel}(0)}{-b - bd + \lambda_{pos}\lambda_{vel}(0) + \lambda_{pos}^2 t_f} \right) \quad (5.17)$$

5.1.2 Rectilinear Case. In the special case in which the initial and final velocity components are all equal to zero, the optimal trajectory is a straight line. This rectilinear

case allows for a simplification of the above equations. They take the form:

$$0 = \lambda_{pos} (\lambda_{vel}(0) - \lambda_{vel}(t_f)) + b (d - b^2) L \quad (5.18)$$

$$0 = \lambda_{pos} (\lambda_{vel}(0) - \lambda_{vel}(t_f)) + \left(\frac{b^2 - d}{b} \right) L \quad (5.19)$$

The only difference in the above two equations is the coefficient of the logarithmic term, so these coefficients must be equal. The logarithmic term is not zero unless the final time is zero, but this is a degenerate case since there would be no transfer at all. Also, the term λ_{pos} is greater than or equal to one, since $\lambda_{pos} = \sqrt{1 + b^2}$. The equality between coefficients leads to the following relationship:

$$(b^2 + 1) (d - b^2) = 0 \quad (5.20)$$

Clearly, the real solution is $d = b^2$. If this result is substituted back into Equation (5.18) or (5.19), the logarithmic term vanishes. Since $\lambda_{pos} \geq 1$ by definition, we have:

$$\lambda_{vel}(0) = \lambda_{vel}(t_f) \quad (5.21)$$

Using the definition $\lambda_{vel} = \sqrt{\lambda_x^2 + \lambda_y^2}$ and the solutions for λ_x and λ_y given in Equations (5.9) and (5.10), this becomes:

$$\sqrt{b^2 + d^2} = \sqrt{(b - t_f)^2 + (d - bt_f)^2} \quad (5.22)$$

Squaring both sides, expanding, collecting terms and using $d = b^2$ leads to:

$$0 = -2b^3 + t_f b^2 - 2b + t_f \quad (5.23)$$

$$0 = (b^2 + 1) (b - t_f/2) \quad (5.24)$$

Again taking the real solution, the result is $b = t_f/2$. As mentioned previously, Euler-Lagrange theory does not provide enough information to solve the orbital transfer boundary value problem. This situation does not change by approximating gravity to be zero. Thus,

additional information is required to solve the algebraic equations. Newton's law may be used to approximate the optimal time of flight, allowing for a solution. Having assumed $\dot{m} = 0$, the thrust will switch directions midway through the trajectory to decelerate to a stop, and the time of flight is $t_f = 2\sqrt{(R-1)/A}$. We now define an original parameter, S , as follows:

$$S = \sqrt{(R-1)/A} \quad (5.25)$$

The parameter S has the canonical units of time, and is equal to one-half of the flight time on a straight-line (rectilinear) trajectory in field free space with stationary end conditions. Since it includes both R and A , the S parameter provides a convenient way to quantify the regions of the costate locus, as shown in Figure 5.4. Since $\lambda_{\dot{x}}(0) = b$ and $\lambda_{\dot{y}}(0) = d$, we have an original solution for the rectilinear case:

$$\lambda_{\dot{x}}(0) = S \quad (5.26)$$

$$\lambda_{\dot{y}}(0) = S^2 \quad (5.27)$$

$$t_f = 2S \quad (5.28)$$

These solutions are for the simplest case of no gravity, no mass-flow rate, and zero velocity end conditions. Note that $\lambda_{\dot{x}} = b_0$ and $\lambda_{\dot{y}} = d_0$ define a parabola in the $\lambda_{\dot{y}}, \lambda_{\dot{x}}$ plane, or equivalently in the λ_u, λ_v plane as shown by Equations (4.58) and (4.59).

Equations (5.26), (5.27), and (5.28) along with $b = c$ and $a = 1$ provide an approximate analytical solution for the initial values of the Lagrange costates and the final time. These approximations can be used to start sub-optimal transfers, or as starting points for solving the two-point boundary value problem. Further refinement is possible by scaling these results, as will be shown next.

In Figure 5.5, the exact initial costates, obtained numerically as described in Appendix A, are shown on the solid line for the zero-gravity case. These are obtained by numerically solving the $\mu = 0 = \dot{m}$ two point boundary value problem with circular end conditions corresponding to an Earth-Mars transfer ($R=1.525$). The \circ symbols correspond to A values of 1000, 100, 10 and 1.6, with the largest values near the origin. The locus data

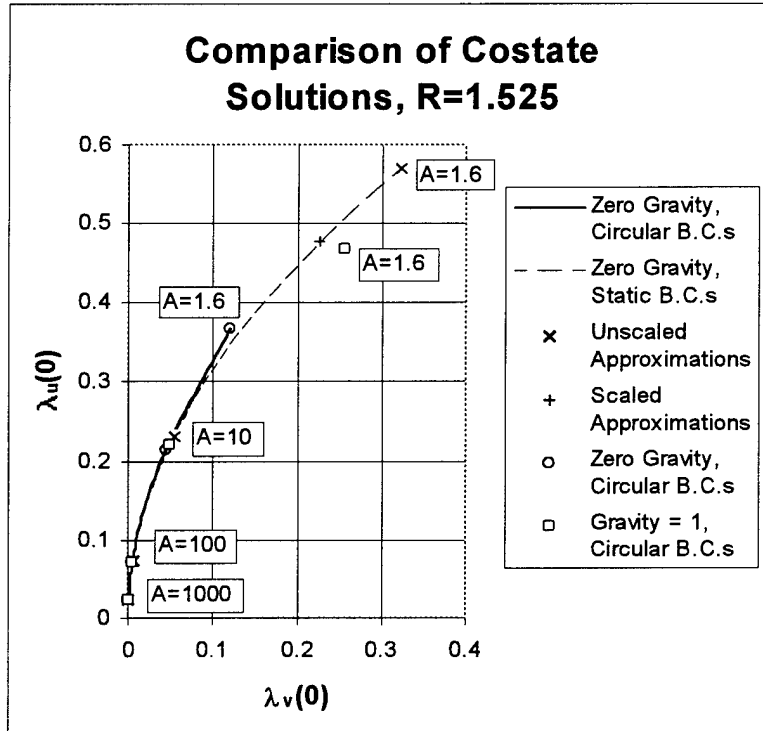


Figure 5.5 Comparison Costate Solutions to Exact Cases

is stopped at $A = 1.6$, because it has been numerically determined that the $R = 1.525$, $\mu = 0$ locus no longer resembles the $\mu = 1$ locus for $A < 1.6$. The dashed line is a parabola defined by Equations (5.26) and (5.27) for $b_0 = \lambda_x(0)$ and $d_0 = \lambda_y(0)$. The \times symbols correspond to the same values of A as the o symbols. Note the excellent agreement for large A , as expected.

In Figure 5.5, the initial costate approximations based on Equations (5.26) and (5.27) lie on nearly the same parabolic arc as the exact values for $\mu = 0$, except that they appear to be shifted upwards along the arc. This makes them too large for the values of A , so if they are scaled down along the parabolic arc, they will more closely match the correct values. An original scaling approach leads to improved agreement for the lower values of A . The scaled points are shown with the $+$ symbols, and the scaling factor q is defined as follows:

$$b \approx qS \quad (5.29)$$

$$d \approx q^2 S^2 \quad (5.30)$$

It is interesting to observe that the scaled approximation for $A = 1.6$ is very close to the exact case with $\mu = 1$. Physically, the scaling factor increases the initial thrust angle, as seen in Figure 5.5 since the initial thrust angle ϕ is measured up from the horizontal $\lambda_v(0)$ axis. In the case with circular velocity boundary conditions, the initial velocity must be greater than the final velocity on a larger circular orbit. By raising the initial thrust angle, the scaling factor decreases the initial acceleration in the tangential direction, reducing the amount of velocity to be removed by the final time. In the case with $\mu = 1$ instead of $\mu = 0$, a larger initial thrust angle is needed to counter the gravity while raising the orbital altitude.

If the two velocity components, Equations (5.18) and (5.19), are used to eliminate their common logarithmic term, the following relationship is obtained:

$$\left(\frac{\dot{x}(t_f) - \dot{x}(0)}{A} \right) + b \left(\frac{\dot{y}(t_f) - \dot{y}(0)}{A} \right) + \sqrt{(b - t_f)^2 + (d - bt_f)^2} - \sqrt{b^2 + d^2} = 0 \quad (5.31)$$

The initial velocity components are $\dot{x}(0) = 0$ and $\dot{y}(0) = 1$ on the starting circular orbit. The final Cartesian velocity components are not known individually at t_f , and they may be set equal to zero as an approximation which results in the simplest form of the solution. This has been found to be the most useful approximation, but others have been tried such as $\dot{x}(t_f) = 0$ and $\dot{y}(t_f) = 1$. With both final velocity components set equal to zero, the scaling factor may be introduced to produce an equation in a single variable with two parameters, R and A . Then, Equation (5.31) becomes:

$$-\frac{qS}{A} + \sqrt{(q-2)^2 S^2 + (q^2 S^2 - 2qS^2)^2} - \sqrt{q^2 S^2 + q^4 S^4} = 0 \quad (5.32)$$

The scaling factor q may be expressed as an infinite series in the quantity $(1/A)$. After solving for the coefficients, the first three terms in this series solution are:

$$q \approx 1 - \frac{1}{2A} + \frac{R}{4A^2} \quad (5.33)$$

Numerically, it has been found that truncation after the third term is adequate in this approximation because there are greater sources of error from the other assumptions, such as zero gravity. Using this result, the initial costates are given by:

$$b \approx \left(1 - \frac{1}{2A} + \frac{R}{4A^2}\right) S \quad (= \lambda_x(0)) \quad (5.34)$$

$$d \approx \left(1 - \frac{1}{2A} + \frac{R}{4A^2}\right)^2 S^2 \quad (= \lambda_y(0)) \quad (5.35)$$

Since the expansion for q involves the quantity $(1/A)$, it should not be used if $A < 1$. If $A < 1$, the approximate initial costates may be obtained from Equations (5.26) and (5.27), which do not include the scaling factor q . The time of flight, t_f , is not as sensitive to the presence of the gravity term, so the formula for t_f does not require additional scaling.

To summarize, Equations (5.26) and (5.27) give the approximate initial costate values, and Equation (5.28) is the approximate time of flight. If $A > 1$, the scaled Equations (5.34) and (5.35) should be used to improve the approximate initial costate values. These relationships were derived using the assumptions of zero gravity, zero mass-flow rate, and zero final velocity components. Even using these assumptions, the results lead to a good initial guess for the associated boundary value problem over the parabolic region of the costate locus, where the parameter S is less than or equal to one. The convergence sensitivity of this model will be discussed at the end of the chapter, along with the elliptic and spiral region models.

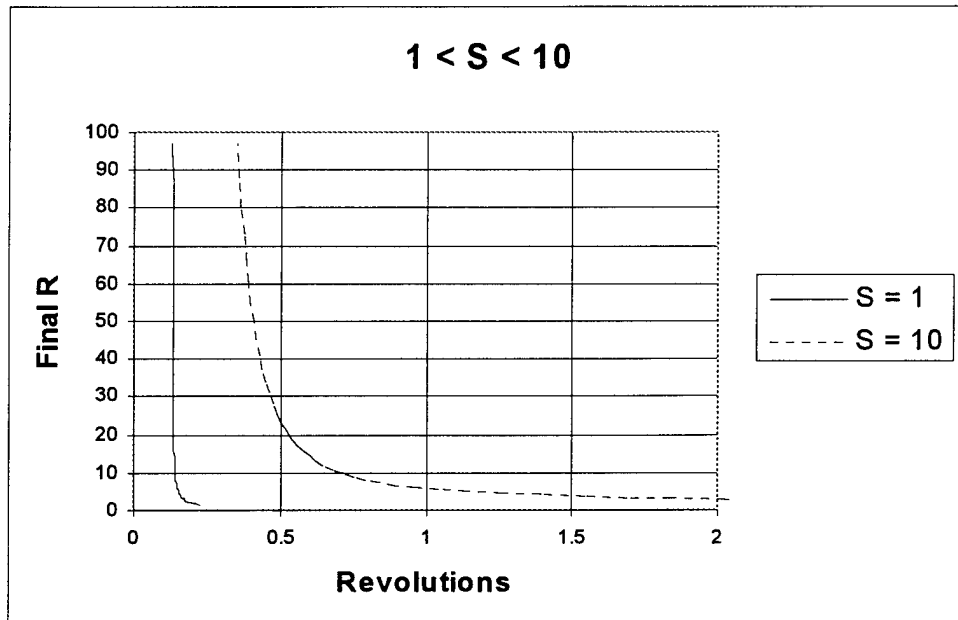


Figure 5.6 Final R vs. Orbital Revolutions

5.2 Elliptic and Spiral Regions

If the transfer occurs in the neighborhood of one-quarter to one-half revolution, the initial costates do not lie near the parabolic arc or the point $(1,0)$. In this case, the locus has a nearly elliptical shape as seen in Figure 5.4, and the range of S is roughly $1 < S < 10$. If $R = 2$, for example, $S = 1$ corresponds to a transfer over about 0.2 of a revolution, and $S = 10$ corresponds to a transfer over about 3 revolutions. As R increases, the range of orbital revolutions narrows between lines of constant $S = 1$ and $S = 10$, as shown in Figure 5.6. The well known Earth-Mars transfer example given in Bryson and Ho [7] with $R = 1.525$ lies in this region with $S = 1.933$, and has roughly 0.3 revolutions. This example will be presented in Chapter 6.

It is difficult to provide a physical explanation for the elliptical form of the locus in this region, but the appearance naturally leads one to try the equation of an ellipse as a model. In the parabolic region, the thrust term in the equations of motion is dominant over the gravity term. In the spiral region, the gravity dominates the thrust. Thus, the gravity or thrust may be taken to be zero as a limiting case, allowing for closed-form solutions of the equations for the states and costates. The zero-gravity development is presented

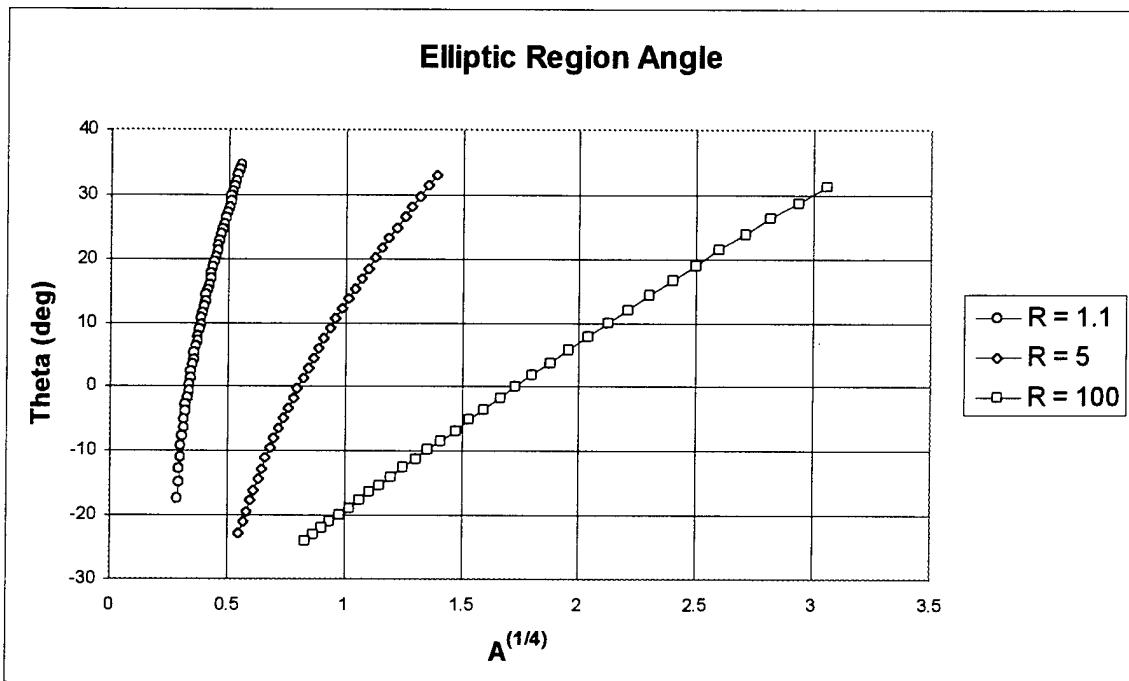


Figure 5.7 Elliptic Region Angles for $R = 1.1, 5, 100$

in the previous section, and the zero-thrust development is in the literature [26], with the results described later in this section. However, the thrust and gravity terms are typically within an order of magnitude of each other in the elliptic region. Therefore, neither term may be considered small relative to the other. Several attempts were made to develop a perturbation solution for this region, but because both the gravity and thrust terms must be retained, the attempts were unsuccessful. Since there is no closed form solution of the full equations for the states and costates, we approximate the initial costates in the elliptic region with the equations of ellipses through curve fitting of the numerical results, using the parameters R and A .

An empirical relationship between the polar angle and the fourth root of thrust acceleration A may be obtained from the data shown in Figure 5.7. This relationship is used in a linear approximation for the polar angle of the elliptic region to construct the complete parametric fit. The quarter power relationship is a result of simple trial and error to produce a fairly linear graph. Because of the form of the elliptic model, it is necessary to relate the parameter A to an angle along the elliptic curve. An example of the parametric fit is shown in Figure 5.8 for $R = 1.525$, the distance to Mars, and for $R = 100$. The model

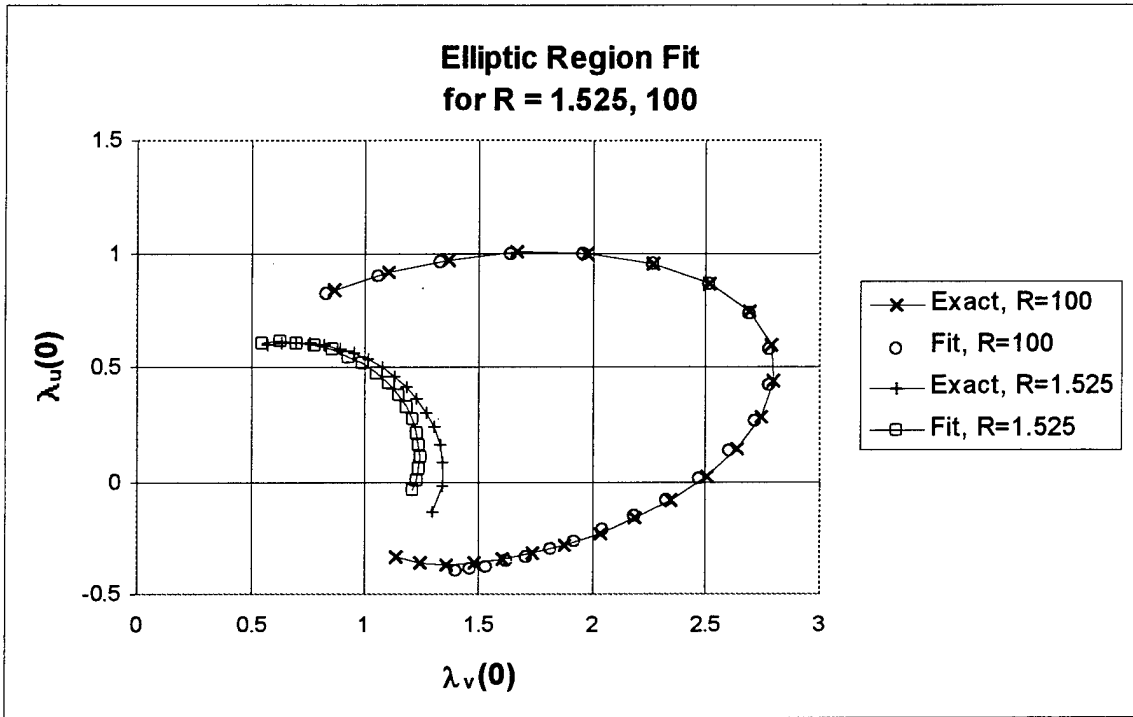


Figure 5.8 Elliptic Fit for $R = 1.525, 100$

accuracy decreases with decreasing R and A , but is still within the numerically determined radius of convergence using the modified quasi-Newton method described in Chapter 4. The elliptic models are as follows:

$$\theta_{ell} = \frac{1.0}{(0.498719 - 0.811477R^{(0.25)})} A^{(0.25)} + \frac{1.0}{(0.279574 - 0.050554R^{(-0.25)})} \quad (5.36)$$

$$r_{ell} = \frac{-0.00091R + 0.4114}{1.0 + (0.00264R + 0.616) \cos(\theta_{ell} + 0.0008124R + 0.11876)} \quad (5.37)$$

$$\lambda_u(0) = r_{ell} \sin \theta_{ell} + 0.03588 \quad (5.38)$$

$$\lambda_v(0) = 0.165989 - r_{ell} \cos \theta_{ell} \quad (5.39)$$

The spiral point on the costate locus corresponds to problems with more than 10 revolutions, and it is well known [26] that the optimal thrust direction is nearly tangential to the path through most of the transfer. For such cases, a good starting guess is $\lambda_u(0) = 0$, and $\lambda_v(0) = 1$. The time of flight for a many-revolution transfer is approximately given

by [26]:

$$t_f = \frac{1}{A} \left(1 - \frac{1}{\sqrt{R}} \right) \quad (5.40)$$

To solve the boundary value problem using the previous results, the parameter S is first calculated from Equation (5.25). If $S \leq 1$, then Equations (5.26), (5.27) and (5.28) should be used to initialize the problem. If $1 < S < 12$, then Equations (5.28) and (5.38)-(5.39) provide a reasonable set of initial values for the problem. The parameter value of $S = 12$ is used to extend the elliptic costate model further into the spiral region. If $S > 12$, the initial values of the costates will be close to $\lambda_u(0) = 0$, and $\lambda_v(0) = 1$. The approximate time of flight for this case is given by Equation (5.40).

5.3 Convergence Sensitivity

To measure the convergence sensitivity of the shooting method for various values of S and R , a plot of modified quasi-Newton method iterations is presented in Figure 5.9. The number of iterations for a given R and A is a good measure of the success of the approximate models, since closer initial values require fewer iterations for convergence to a desired error tolerance (as defined in Appendix A). Generally, the sensitivity of the system increases with decreasing A and thus increasing S , because the flight times become much longer for a given R value. In other words, the “shots” become much longer in the shooting method. The initial values of the Lagrange costates tend to stay within the neighborhood of unity, as seen in Figure 5.4. However, the flight time may become large for small A , so errors in the time models tend to be magnified for large values of S corresponding to multiple revolution transfers. This explains the increased system sensitivity for large S , but the modified quasi-Newton method will still converge using the models for the time and initial costates over the specified ranges of A and R . In Figure 5.9, the S parameter is plotted on the horizontal axis using a logarithmic scale, and the three decades shown correspond to the three regions of the costate loci in Figure 5.4. There are peaks in the sensitivity near $S = 1$ and $S = 12$, which occur in the transition regions between the parabolic, elliptic, and spiral point models for the approximate initial costates. Some of the curves do not span the entire range of S , because of the relationship $R = S^2 A + 1$.

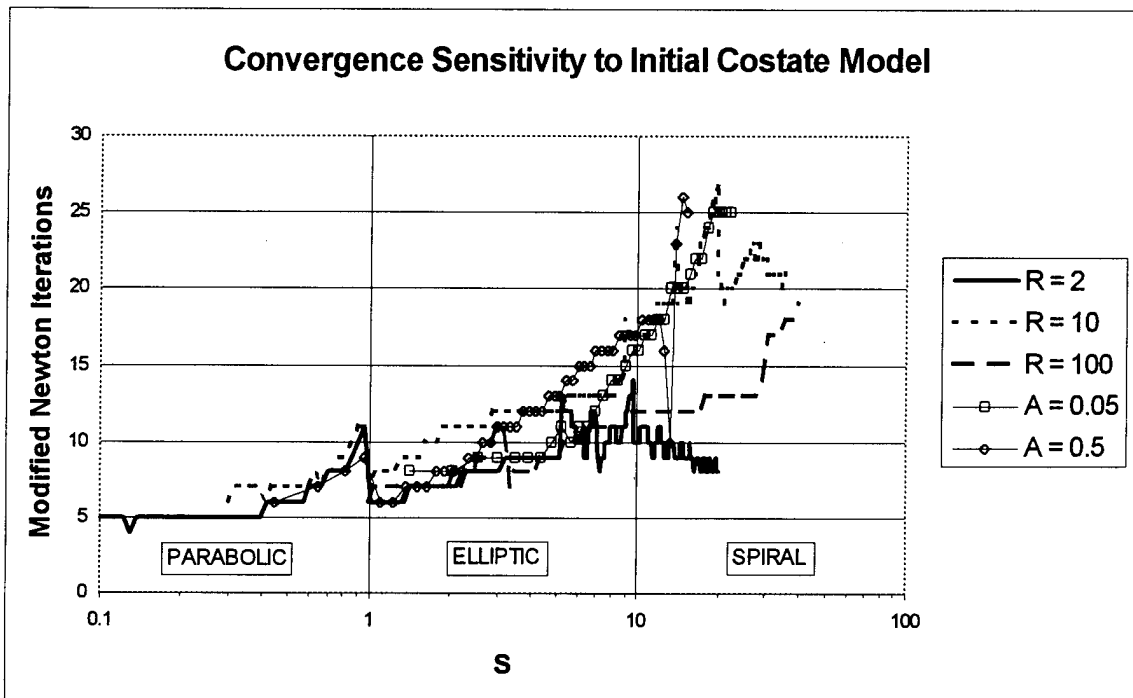


Figure 5.9 Convergence Sensitivity to Initial Costate Model

For instance, on the curve of constant $A = 0.5$, $R = 201$ when $S = 20$. Since this value of R is larger than the range of the models, the data is stopped when R reaches a value of 100. The value of $R = 100$ is used as an upper limit because of physical considerations. In an Earth-centered system, the lunar orbit is at roughly 60 DU, based on the radius of the Earth. In a Sun-centered system, the planet Pluto is at roughly 40 DU, based on the radius of the Earth's orbit about the Sun. Thus, $R = 100$ DU is more than adequate to cover the range of currently practical missions.

It is important to recognize that the iteration numbers shown in Figure 5.9 are based on the *approximate* costate models. If the boundary value problems represented by each point on the curves had been solved by slowly varying the thrust as described at the beginning of this chapter, the step size could be kept small enough such that each case could be done in about 5 iterations. However, that technique requires a slow approach from some elusive known case to the case of interest. Using the approximate costate models provided here along with the modified quasi-Newton method, any case of interest may be solved directly with *no prior knowledge*. Thus, one may proceed immediately with any

values of R and A to Figure 5.9 and obtain a rough idea of how many iterations to expect using the modified quasi-Newton method. Without the initial costate approximations, it would be unreasonable to expect convergence *at all* for arbitrary values of R and A , unless one is very fortunate.

The extreme sensitivity of the minimum-time continuous thrust problem to the initial costate values is well documented [7, 10]. As mentioned earlier regarding the continuation method [12], the step size in the problem parameter A must be constantly decreased to maintain convergence in a fixed number of iterations as the locus moves toward the center of the spiral region, where A approaches zero. This decreasing step size phenomenon is a direct measurement of the convergence sensitivity, but this also depends on the robustness of the search technique. Because of the interdependence of the model accuracy and the capabilities of search method, both the model and the modified quasi-Newton method are used to produce the iteration data shown in Figure 5.9 instead of the continuation method. Clearly, a different initial costate model and search method will produce different iteration data. Thus, the convergence sensitivity shown in Figure 5.9 is only intended to represent the behavior of the models and techniques presented in this dissertation.

5.4 *Optimal Initial Costate Locus under the KS Transformation*

Figure 5.10 shows the optimal initial costate locus under the KS transformation for $R = 2$ with $\dot{m} = 0$. The behavior of the locus is similar to the Cartesian case in that the spiral region corresponds to small A , many revolution transfers. Also, the “top” of the curve extends upward with increasing R . The entire initial costate locus is stretched horizontally compared to the Cartesian case. The focus of the spiral is at the point $(2,0)$, which may be found by letting $A = 0$ and equating the KS Hamiltonian to the polar Hamiltonian with fictitious time. As a result, the initial costate $\lambda_{v_2}(0)$ should be taken as $2\lambda_v(0)$ for the purpose of initial approximation. Because of the similarity to Figure 5.1, one might be tempted to conclude that the approximate initial costate models may be used to initialize the problem under the KS transformation in all cases. However, the horizontal stretching phenomenon is not linear, since the first horizontal axis crossing in Figure 5.1 is not exactly twice that of Figure 5.10, even though the spiral point is located at $(2,0)$.

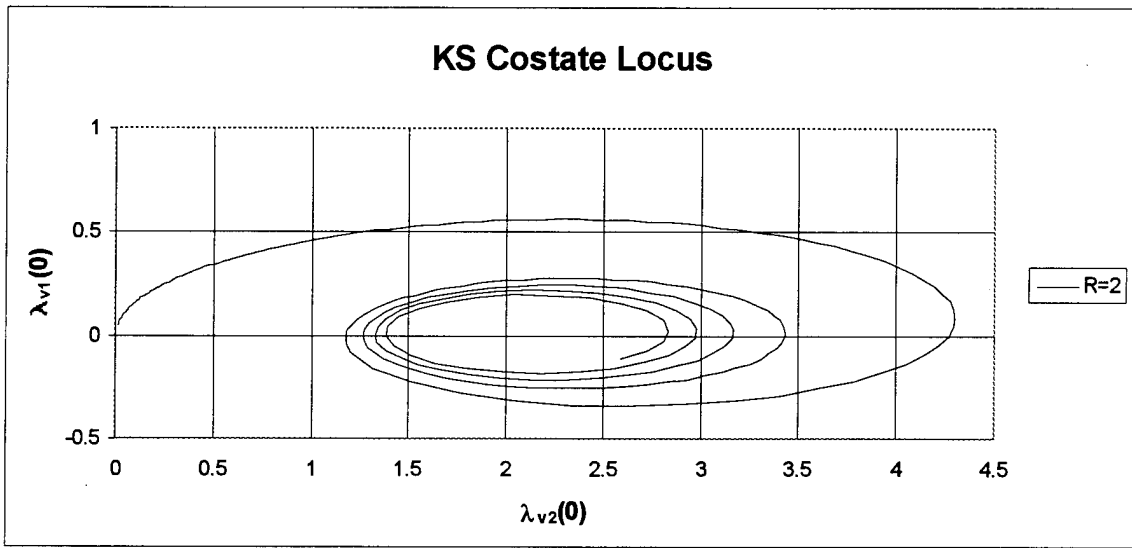


Figure 5.10 Optimal Initial Costate Locus under the KS Transformation

Thus, the approximate initial costate models provide only a rough estimate to initialize the problem under the KS transformation. Convergence may still be achieved in some cases, and an example of this is given in Chapter 6.

5.5 Summary

This chapter presents an original approach to solving the minimum-time orbital transfer problem under continuous thrust by modeling the initial values of the Lagrange costates. To accomplish this, numerical results from many cases are used to depict graphically the functional relationship between the initial costates and the parameters R and A . Then, analytical and empirical means are used to provide approximate expressions for the initial costates and time of flight. The success of the approximate models is examined by presenting the number of modified quasi-Newton steps required for convergence over the complete range of R and A . Again, convergence would not be expected at all for arbitrary parameter values without the approximate models, since there is no other information available for initialization. With the approximate models, one may quickly produce a minimum-time orbital transfer example based on any practical spacecraft design and mission requirement. Finally, a locus of the initial costates under the KS transformation is included for comparison.

VI. Numerical Examples

This chapter presents a series of numerical examples which correspond to each of the earlier theoretical developments. The boundary value problems are solved using the shooting method, and the quasi-Newton step is modified with the dynamic scaling technique described in Chapter 4. The trajectories are propagated with an integration tolerance of 10^{-8} , and an error tolerance in the final state values of 10^{-7} in canonical units. A discussion of convergence criteria is presented in Appendix A.

The approximate initial costate models developed in Chapter 5 are for the circle-to-circle, coplanar problem. Therefore, we first present two examples of coplanar, circle-to-circle problems, to demonstrate the parabolic and elliptic models. The first example is a military application with very low thrust [10], and the second is the well-known Earth-to-Mars example given by Bryson and Ho [7]. The reader should note that the approximate initial costate models developed in Chapter 5 lead to convergence for all values of A and R in the domain of intent ($0 < A < \infty, 1 < R \leq 100$). The KS transformation is used on the Bryson and Ho example for comparison, and is also used on a many-revolution circle-to-circle problem, which uses the spiral point model. This last example may be used as a sample truth model for a perturbation technique in which A is treated as a small perturbation.

The approximate initial costate models may also be used on problems with noncircular end conditions that are elliptical or hyperbolic. Thus, an example of a coplanar transfer to a non-circular end condition is presented. The final orbit is hyperbolic, but the initial costates still provide reasonable starting values, and convergence is achieved. An elliptical end condition case is presented later with the three-dimensional examples.

Continuing away from the coplanar, circle-to-circle case, the next example shows a trajectory from one circular orbit to another with a change in inclination. Thus, the trajectory occupies three dimensions. Convergence is still achieved using the initial costate models. An example with the largest departure from the coplanar, circle-to-circle case is then presented with an inclination change combined with non-circular end conditions. The final orbit in this example is both polar and elliptical.

Two additional examples are given that result from the solution of multiple boundary value problems with varying parameters. In the first example, after completing many coplanar, circle-to-circle cases, curves of time per revolution are plotted for a large range of A , with different values of R . In this way, it is possible to observe the behavior of the transfer angle as a function of R and A . In the final example, a plot is provided that shows the existence of a minimum-time ascending node value associated with R , A , and inclination in the noncoplanar, circle-to-circle case.

6.1 Two-Dimensional Problems

6.1.1 Circle-to-Circle. The first example involves a spacecraft design that has been investigated by past researchers [10]. A 2400 kg spacecraft is at geosynchronous altitude with a thrust of 1.3 N and a mass-flow rate of -0.000069 kg/s. In canonical units, the problem parameters are $A = 0.002425$ and $\dot{m} = -0.000395$. Suppose it is desired to make a small increase in altitude in minimum time to avoid a ballistic anti-satellite weapon. If $R = 1.000336$, the new orbit radius will increase by roughly 15 km. In this case, the quantity $S = \sqrt{(R-1)/A} = 0.3722$, which is less than unity. Thus, the optimal initial costates should lie near the parabolic region of the costate locus, and the approximate initial values are given by Equations (5.26) and (5.27). The approximate time of flight is given by Equation (5.28). Using the above problem parameters, the results in canonical units are given in Table 6.1.

Table 6.1 ASAT Avoidance Example

iteration	t_f	$\lambda_u(0)$	$\lambda_v(0)$
1	0.7441893	0.3720947	0.1384544
4	0.7366198	0.3395791	0.1201369

The first line in Table 6.1 is the set of initial approximations for the ASAT avoidance example. The first iteration is considered to be the evaluation of the approximate models for the initial costates and time of flight. The second line shows the final, converged values after 4 iterations of the shooting method. The converged initial costate values are plotted in Figure 5.4 as a point on the costate locus which is identified with the label "ASAT."

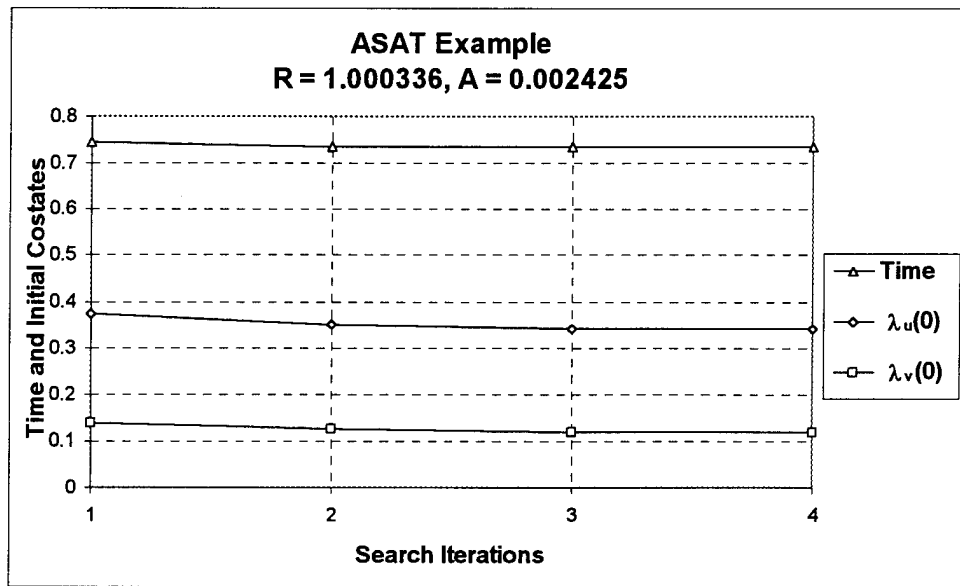


Figure 6.1 Iterative Search History for ASAT Avoidance Example

The initial costate approximations are obtained from Equations (5.26) and (5.27), and the approximate time of flight is given by Equation (5.28). The total thrusting time is roughly 2.8 hours in physical units. In this case, the initial approximations for the costates and flight time are very close to the converged values, allowing for quick convergence. Figure 6.1 shows the iterative search history for the flight time and initial costates from the initial guess to the converged values.

Figure 6.2 compares the exact control angle history from the converged case with the approximate history generated by the initial estimates. Both curves pass through the zero angle, showing the switch in thrust direction. The differences between the initial estimates and the converged values are most evident here, since the costate histories are very sensitive to the initial conditions.

Figure 6.3 shows a comparison of flight path trajectories using the control law from the initial estimates and the converged values. In this case, the paths are almost identical in spite of the differences in the control angle histories. Thus, approximate initial costates obtained assuming zero gravity, zero mass flow rate and zero final velocity are sufficient to achieve an almost optimal trajectory.

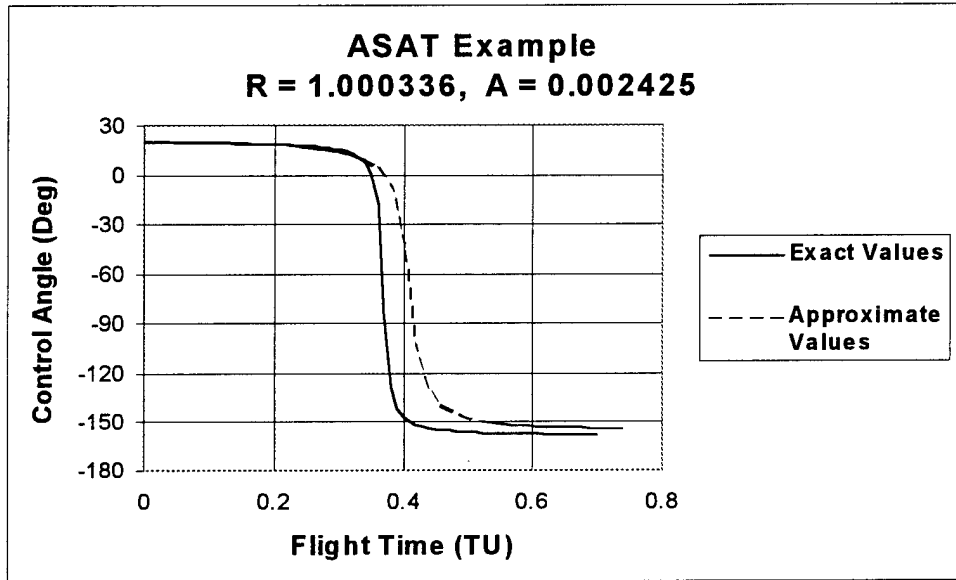


Figure 6.2 Control Angle History for ASAT Avoidance Example

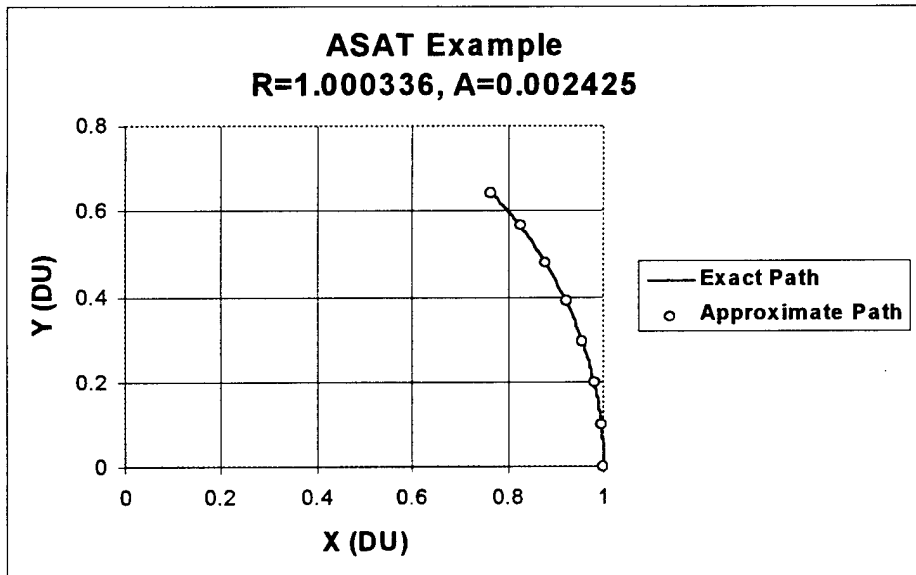


Figure 6.3 Optimal Trajectory for ASAT Avoidance Example

The next example will be the well known Earth-to-Mars orbital transfer case given in Bryson and Ho [7], page 66, where $R = 1.525$, $A = 0.1405$, and $\dot{m} = -0.07488$ mass units per TU. The initial costate values are not given in the reference. In this case, the quantity $S = 1.933$, so $1 < S < 10$. Thus, the optimal initial costates should lie in the elliptic region of the costate locus, and the approximate initial values are given by Equations (5.38) and (5.39). Using these problem parameters, the results in canonical units are given in Table 6.2.

Table 6.2 Bryson and Ho Example

iteration	t_f	$\lambda_u(0)$	$\lambda_v(0)$
1	3.8660858	0.4221273	1.1093899
7	3.3192600	0.4949228	1.0785465

The first line in Table 6.2 is the set of initial approximations for the Bryson and Ho example. The second line shows the final, converged values after 7 iterations of the shooting method. The converged initial costate values are plotted in Figure 5.4 as a point on the costate locus which is identified with the label "Bryson-Ho." The approximate time of flight is given by Equation (5.28). The initial approximations for the costates and time of flight are still close to the converged values, but this example takes more iterations for convergence than the ASAT example. This is because the convergence sensitivity is greater in the elliptic region than in the parabolic region, and the initial approximations are not as close as in the ASAT example. However, the initial approximations are all within roughly 15% of the converged values, which is certainly better than no information at all.

Figure 6.4 shows the iterative search history for the flight time and initial costates in the Bryson and Ho example from the initial guess to the converged values. Figure 6.5 compares the exact control angle history from the converged case with the approximate history generated by the first and third iterations of the initial estimates. All curves pass through 180 deg, showing the switch in thrust direction. As the search progresses, the control angle history approaches the optimal control angle solution. Again, the differences between the initial estimates and the converged values are most evident here, since the costate histories are very sensitive to the initial conditions.

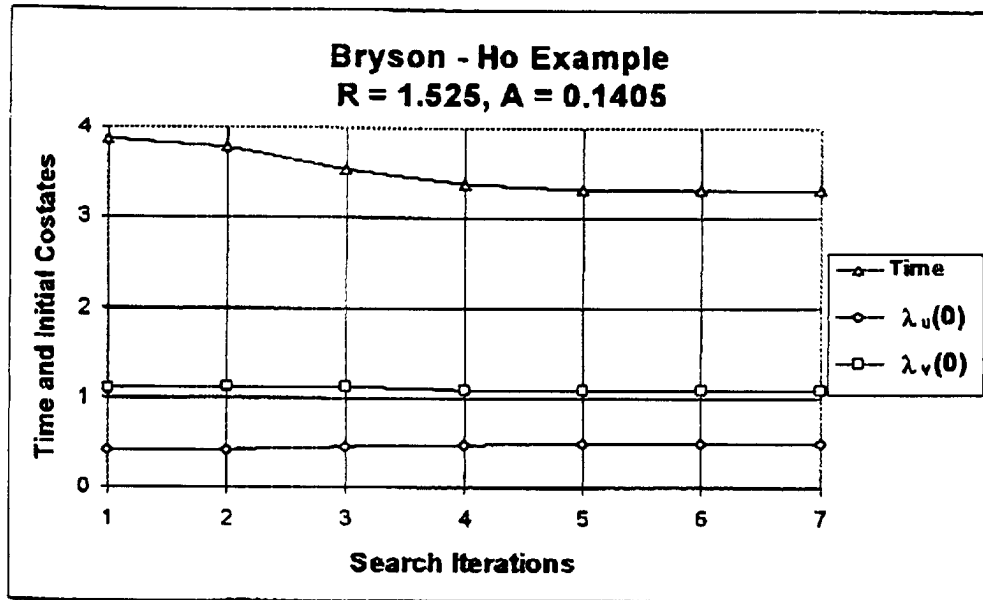


Figure 6.4 Iterative Search History for Bryson and Ho Example

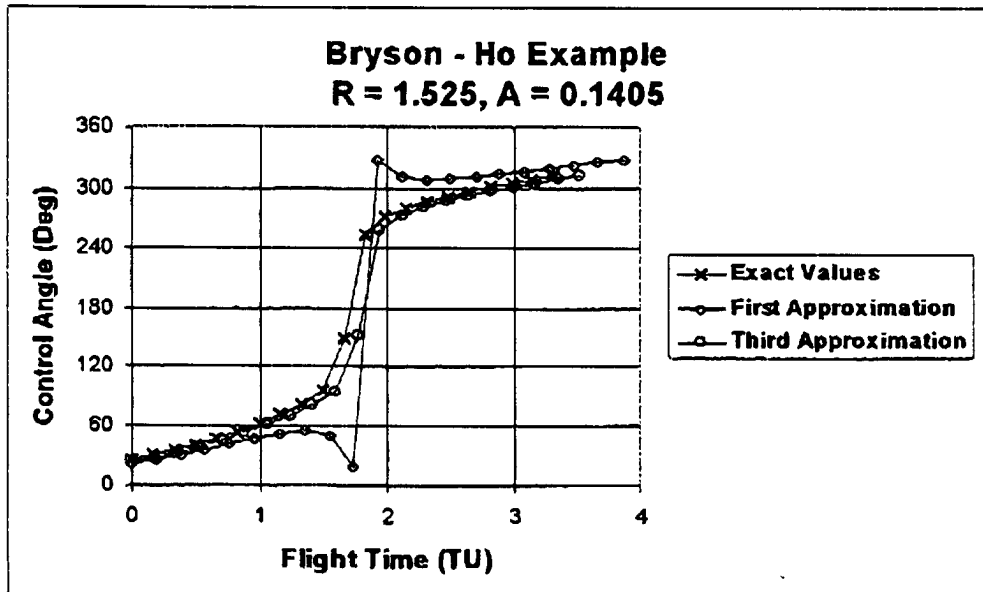


Figure 6.5 Control Angle History for Bryson and Ho Example

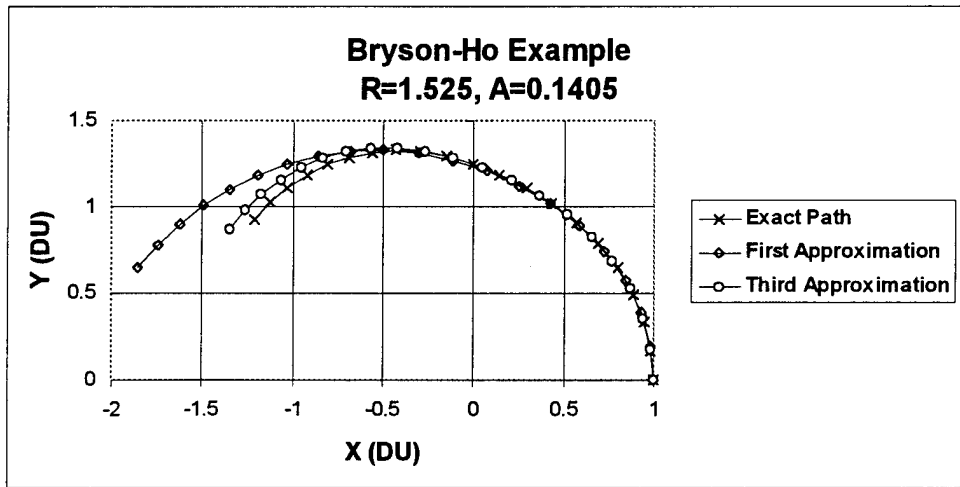


Figure 6.6 Optimal Trajectory for Bryson and Ho Example

Figure 6.6 shows three trajectories corresponding to the first, third, and seventh iterations in the shooting method to solve the Bryson and Ho example. The seventh iteration is considered the exact solution for this example, as described in Appendix A. The trajectory from the first iteration overshoots the desired final radius by roughly 0.5 DU, and the third is much closer. The “in track” error along the spacecraft velocity direction is dominant, and is sensitive to changes in the final flight time. This example shows typical behavior in which the final flight time is directly related to the final radius, assuming the errors are small. By this, we mean that a small increase in final time over that of the minimizing path will result in a small increase in R . Conversely, a small decrease from the optimal flight time will result in a small decrease in R . It is the observation of this direct relationship behavior that motivates the Jacobian formulation given in Chapter 4, Equation (4.73), in which the final time is used instead of the initial value of λ_r .

6.1.2 KS Transformation. The Bryson and Ho example will now be examined under the KS transformation, for comparison with the previous results using polar coordinates and real time. Before proceeding with the full example, the mass will be held constant to allow a comparison of two approaches, with and without a separate time costate λ_t .

Let $R = 1.525$, $A = 0.1405$, and $\dot{m} = 0$. Given these parameter values, the optimal fictitious time is $s_f = 2.864381149$. If λ_t is not used in the constant-mass case, the initial values of the costates are as follows: (Notice $\lambda_{v_1} = 2\lambda_{u_2}$, and λ_{v_2} is from $H(0)$)

$$\begin{aligned}\lambda_{u_1}(0) &= -5.506657441 \\ \lambda_{u_2}(0) &= -2.957059105 \\ \lambda_{v_1}(0) &= -5.914118211 \\ \lambda_{v_2}(0) &= -12.948161442\end{aligned}$$

If λ_t is used in the constant-mass case and $\lambda_{u_1}(0)$ is chosen to be unity, then the initial values of the costates are as follows, and s_f is unchanged:

$$\begin{aligned}\lambda_{u_1}(0) &= 1.000000000 \\ \lambda_{u_2}(0) &= 0.536997105 \\ \lambda_{v_1}(0) &= 1.073994210 \\ \lambda_{v_2}(0) &= 2.351364974 \\ \lambda_t(0) &= -0.181598367\end{aligned}$$

These values may be obtained by dividing the first four numbers by -5.506657441 , and also $\lambda_t = (-1/5.506657441)$, which is the coefficient of the Lagrangian r term. Here, the magnitude of the largest costate has been reduced by roughly a factor of 6, making the numerical search easier, since all of the numbers are closer to unity.

Next, the complete Bryson and Ho example is presented with $\dot{m} = -0.07488$. The first line in Table 6.3 is the set of initial approximations. These initial values are obtained from the approximate models of Chapter 5, and are the same values that are used in the previous presentation of this example. The second line shows the final, converged values under the KS transformation. Figure 6.7 shows the iterative search history for the flight

Table 6.3 Bryson and Ho Example under KS Transformation

iteration	s_f	$\lambda_{u_2}(0)$	$\lambda_{v_2}(0)$
1	3.8660858	0.4221273	2.2187798
18	2.7090520	0.5371110	2.3409681

time and initial costates in the Bryson and Ho example under the KS transformation,

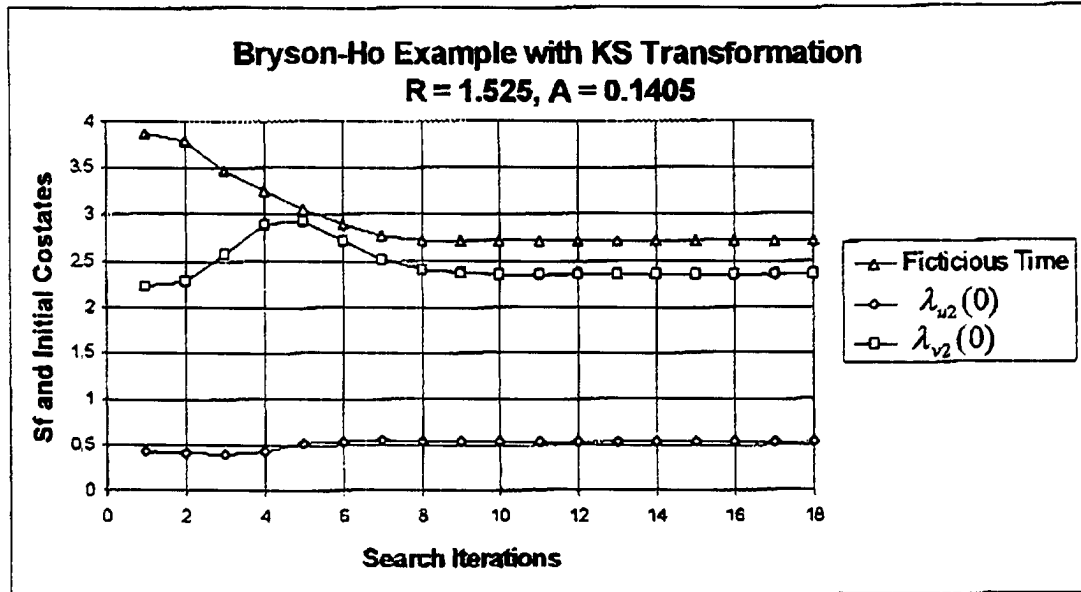


Figure 6.7 Iterative Search History for Bryson and Ho KS Example

from the initial approximations to the converged values. In this case, convergence took 18 iterations of the shooting method. The number of iterations is larger in this case than in the previous presentation of this example, mostly driven by the large difference in the fictitious time and the real time. However, the approximate initial costate and flight time models were not derived for the KS transformation. This example demonstrates the utility of the approximate models and the modified quasi-Newton method in solving problems under the KS transformation. It is important to recognize that the difference between t_f and s_f will increase with increasing R , so convergence may not be achieved for large values of R . The exact control angle history and flight path are the same as shown previously.

As a final example using the KS transformation, the initial costate values and fictitious time s_f for a many-revolution circle-to-circle transfer are presented as a possible test case for a perturbation technique. If the thrust is taken to be a small perturbation, the resulting minimum-time trajectory will typically be a many-revolution spiral. Thus, the results of a perturbation analysis may be checked for accuracy against this example for the particular values of R and A .

The following results are for a low thrust transfer with $A = 0.001$, $R = 2$, and $\dot{m} = 0$. The resulting fictitious time is $s_f = 215.5980372$. Again, $\lambda_{v_1}(0) = 2\lambda_{u_2}(0)$, and $\lambda_{v_2}(0)$ is from $H(0)$.

$$\begin{aligned}\lambda_{u_1}(0) &= -945.557353841 \\ \lambda_{u_2}(0) &= 17.418466660 \\ \lambda_{v_1}(0) &= 34.836933320 \\ \lambda_{v_2}(0) &= -1999.696574002\end{aligned}$$

This trajectory takes roughly 30 revolutions to complete, and resembles a simple spiral. The thrust angle never exceeds 5 degrees above or below the local spacecraft horizontal. The initial values of the costates are not scaled very well, as the largest magnitude is nearly 2000. By including the λ_t costate, all four of the above values could be divided through by -945.557353841 , which will bring them all nearer to the interval of $(-1, 1)$. After scaling in this way, $\lambda_{v_1}(0) = -0.0368$, and $\lambda_{v_2}(0) = 2.1148$, which is close the spiral point model of $\lambda_{v_1}(0) = 0$, and $\lambda_{v_2}(0) = 2$. However, for simplicity, it may not be desired to include λ_t in a perturbation technique. The reason the initial costates are shown with the large magnitudes is to demonstrate the inherent difficulty brought on by the elimination of λ_t . The poorly scaled numbers are nowhere near the interval $(-1, 1)$, so the search becomes more difficult to initialize. If it is required to eliminate λ_t to simplify a perturbation technique, the poor scaling shown above must be retained to satisfy $H(0) = 0$, as explained in Chapter 4.

6.1.3 Circle-to-Hyperbola. In order to demonstrate how the initial costate approximations may be used for a problem without circular end conditions, we present a case in which the final conditions are hyperbolic. The approximations may also be used if the final conditions are elliptical, which is demonstrated later in a three-dimensional example. In this example, a spacecraft starts with a circular orbit of unit radius, and arrives at $R = 5$ with a large tangential velocity. The final orbit is hyperbolic since the escape speed is 0.6325 DU/TU, and the spacecraft has a much larger tangential velocity of 2.0 DU/TU. The final radial velocity is zero, so the spacecraft arrives at the periapsis point of the hyperbola.

Table 6.4 Hyperbolic Example

iteration	t_f	$\lambda_u(0)$	$\lambda_v(0)$
1	10.7	-0.039250	1.226865
10	11.1	-0.109450	1.388047
circ:	8.1	-0.130130	1.388460

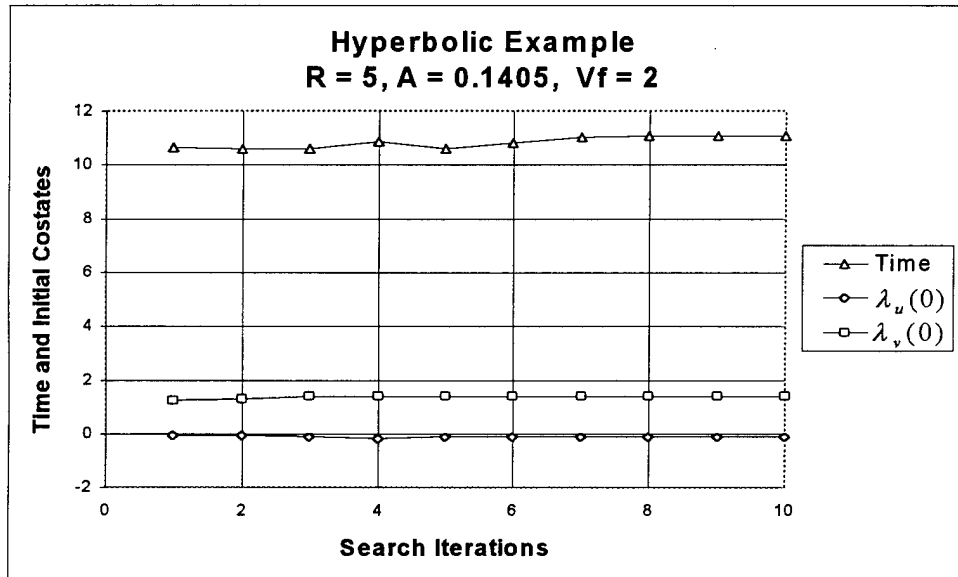


Figure 6.8 Iterative Search History for Hyperbolic Example

The first line in Table 6.4 is the set of initial approximations for the hyperbolic example. The second line shows the final, converged values after 10 iterations of the shooting method. Table 6.4 also shows the relationship between the initial costates for the circle-to-circle case and the hyperbolic case. The third line shows what the converged initial costates and flight time would be if the final conditions were circular at $R = 5$. The biggest difference is in the time of flight, which takes longer in the hyperbolic case to reach the final desired end conditions.

Figure 6.8 shows the iterative search history for the flight time and initial costates in the hyperbolic example from the initial guess to the converged values. In this case, convergence took 10 iterations of the shooting method.

Figure 6.9 shows the control angle history for the hyperbolic example. In this case, the initial thrust angle is below the spacecraft local horizon. Figure 6.10 shows the exact

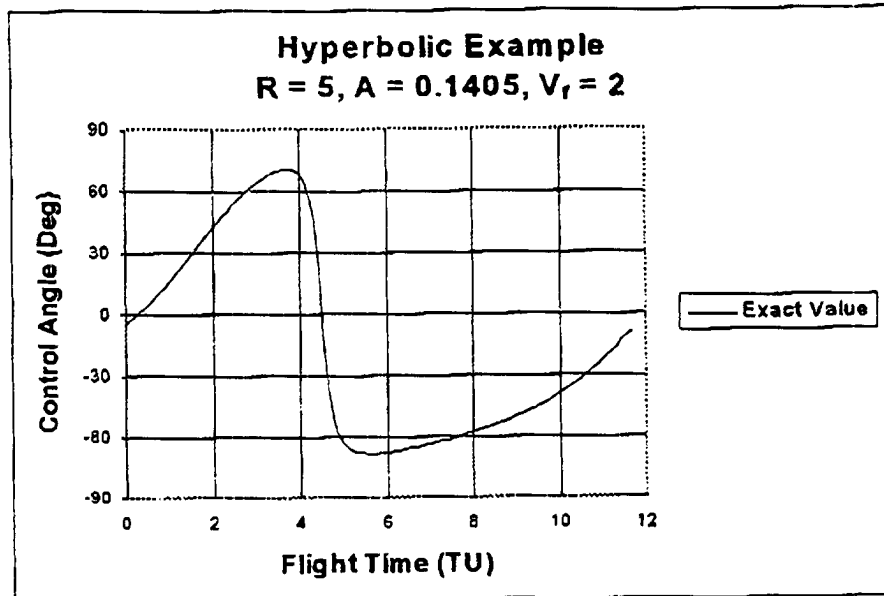


Figure 6.9 Control Angle History for Hyperbolic Example

trajectory for the hyperbolic example. It is interesting to notice that the optimal solution takes the trajectory beyond $R = 5$ in order to give the spacecraft "room" in terms of both space and time to accelerate to the final desired velocity. The initial and final thrusting times are indicated on the trajectory, to show that the final hyperbolic orbit continues on past $R = 5$.

This example illustrates the idea that the solution trajectory is a minimum-time path to a complete set of final states, not just a maximum radius. Otherwise, the problem would have been solved as the spacecraft first reached $R = 5$. However, the velocity components were not yet correct at that time, so the final path is the minimum-time arc to the final set of r , u , and v .

In spite of the highly noncircular final conditions, the initial costates are still similar to the circle-to-circle case, as shown in Table 6.4. For this example, convergence is achieved in ten iterations of the shooting method using the approximate initial costate model based on an empirical fit to the circle-to-circle case. If the final desired end conditions are for an elliptical path, the final velocity magnitude would lie between the circular and hyperbolic cases. Thus, the approximate initial costates may be used as initial guesses for elliptical end conditions as well as for the circular and hyperbolic end conditions.

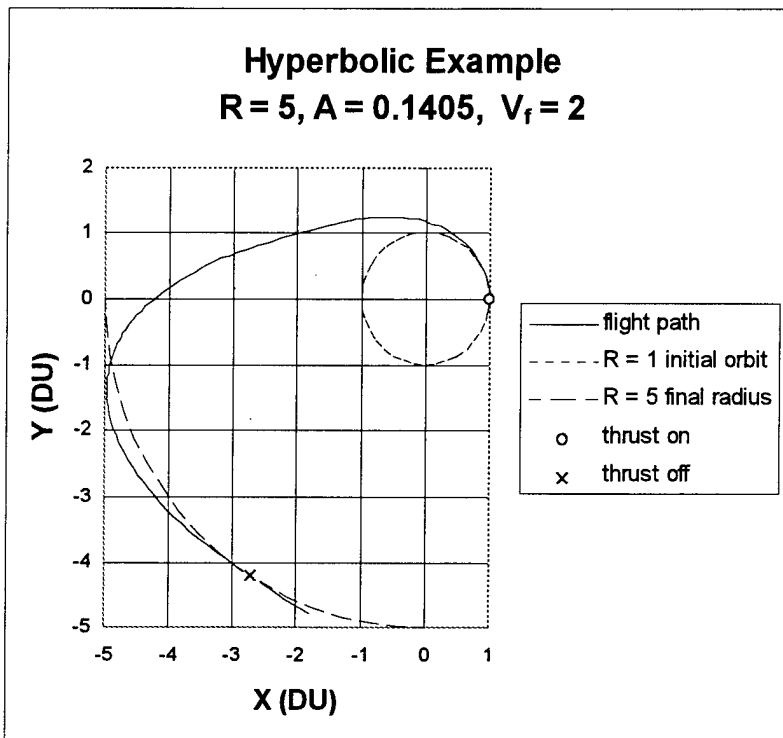


Figure 6.10 Optimal Trajectory for Hyperbolic Example

6.2 Three-Dimensional Problems

To show the relationships between the two- and three-dimensional cases, a two-dimensional example is first presented, then modified to include an inclination change. A third example is presented with a polar, elliptical end condition. This example uses the converged initial costates and flight time from the second example as initial values. All other parameters are held the same.

In Figure 6.11, an optimal transfer is shown where $R = 5$, $A = 0.1$, and $\dot{m} = -0.05$. In this case, the parameter S takes the value of 6.3246. Accordingly, the initial costates lie in the elliptic region of Figure 5.4. To solve this problem, the parameterized elliptic curve fits are used to provide the approximate initial costate values.

The second case is shown in Figure 6.12. The problem parameters are the same as in the first case, but the desired final inclination is 45 degrees, and the desired ascending node is zero degrees on the x axis. The approximate initial values for λ_u and λ_v are the same

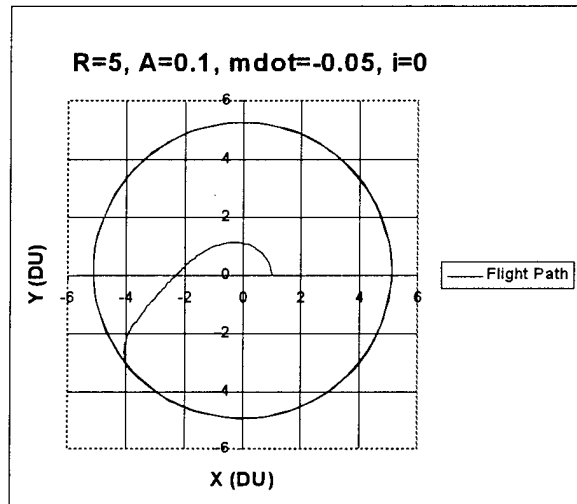


Figure 6.11 Flight Path for Two-Dimensional Example

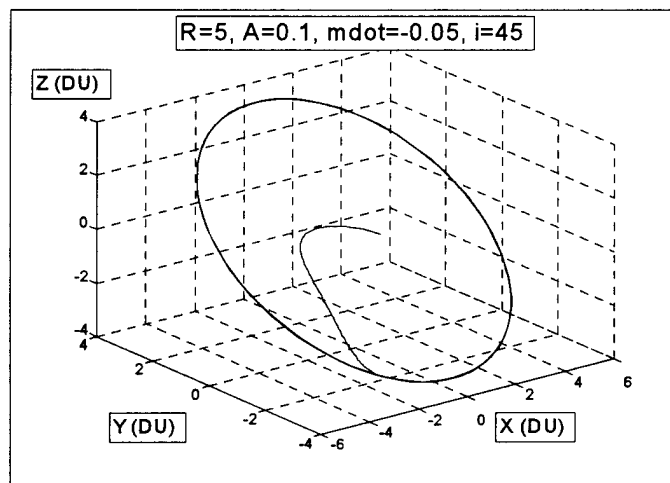


Figure 6.12 Flight Path for Three-Dimensional Example

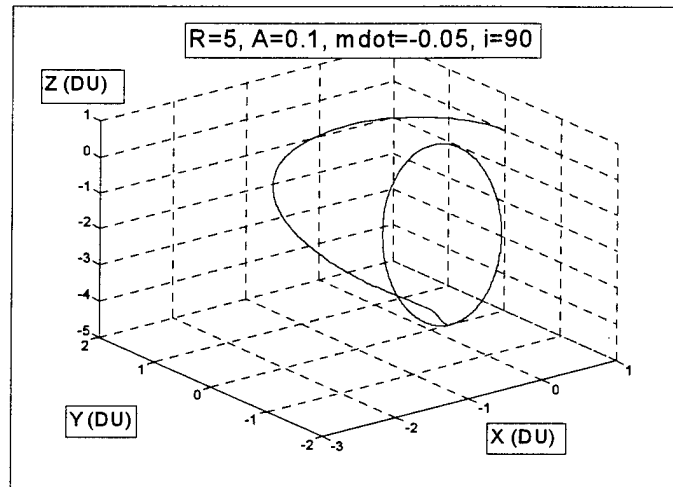


Figure 6.13 Flight Path for Polar-Elliptical Example

as in the two dimensional case, and $\lambda_z(0)$ and $\lambda_w(0)$ are taken to be zero. Convergence is achieved in 14 iterations, even with the change in final inclination.

In the third case, the goal is to reach a polar, elliptical orbit at apoapse where the tangential velocity is 0.4 DU/TU, which is less than the circular velocity of 0.447 DU/TU. Convergence is achieved in 18 iterations using the three-dimensional initial values from the fourth column of Table 6.4 with no further modification. Taking large steps in this way by using continuation combined with the approximate initial costate models can allow for the solution of a wide variety of orbit transfer problems in a short time. In this case, the steps involve inclination changes of 45 degrees each time. The converged trajectory is shown in Figure 6.13.

Both the first and second cases are solved using the two-dimensional approximations as initial values. The third case uses the results of the second case as initial values. The largest difference between the second and third cases is in the flight time. Some of the initial costates in the third case are actually closer to the approximate two-dimensional models than those in the second case. However, the difference in final time is apparently large enough to prevent convergence from the approximate models directly. For comparison, the final, converged values are shown in Table 6.5 for each case.

Figures 6.14, 6.15 and 6.16 show the iterative search histories for the flight time and initial costates in the two-dimensional, three-dimensional, and polar-elliptical examples

Table 6.5 Planar vs. Non-Coplanar Example

	<i>model</i>	2D	3D, <i>i</i> = 45	3D, <i>i</i> = 90
$\lambda_x(0)$	1	1	1	1
$\lambda_y(0)$	-0.1092950	-0.239259	-0.190287	-0.161830
$\lambda_z(0)$	0	0	0.565053	0.353082
$\lambda_{\hat{x}}(0)$	-0.1092950	-0.239259	-0.190287	-0.161830
$\lambda_{\hat{y}}(0)$	1.1923589	1.278794	1.281757	1.550567
$\lambda_{\hat{z}}(0)$	0	0	0.443959	0.827519
t_f	12.6491106	10.045897	10.985076	14.437969
<i>iterations</i> :	1	12	14	18

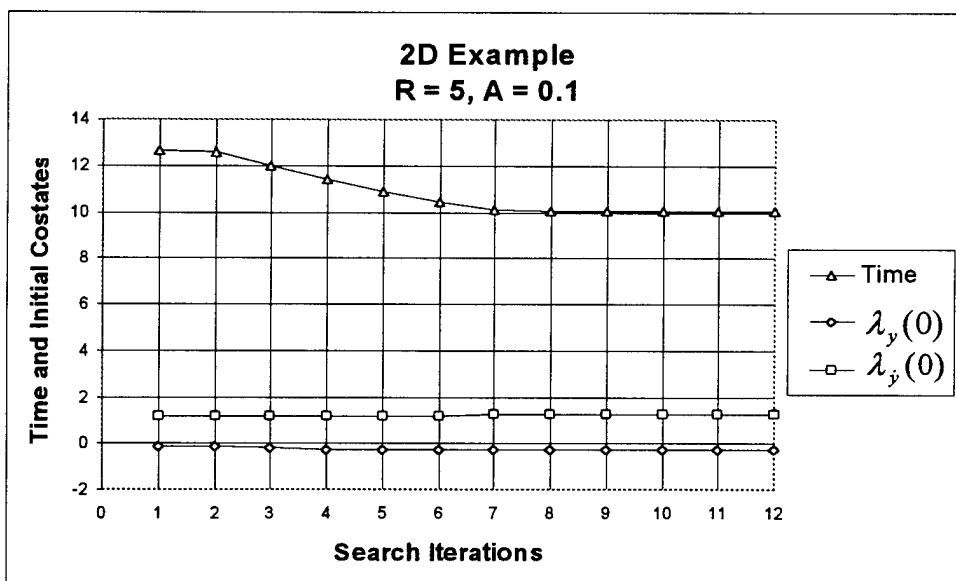


Figure 6.14 Iterative Search History for Two-Dimensional Example

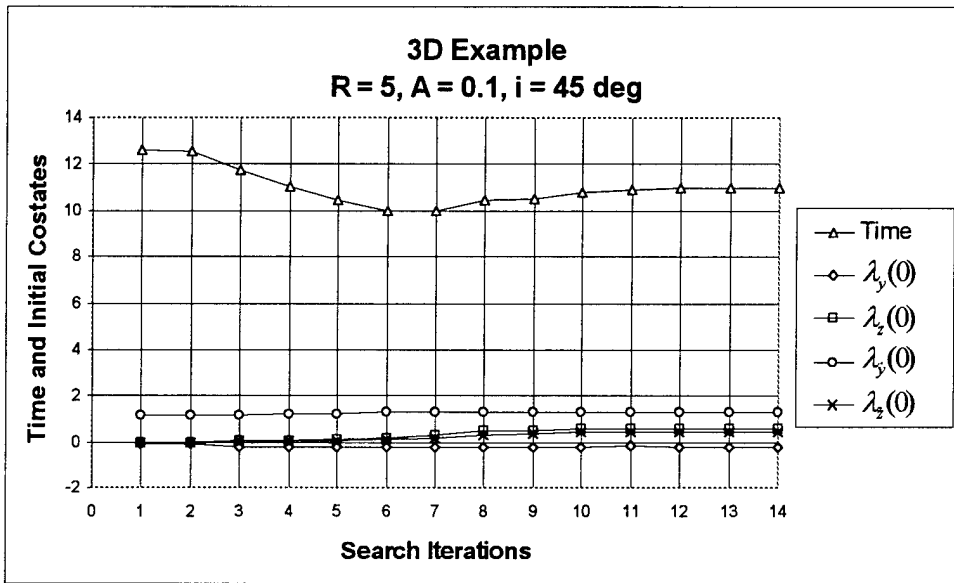


Figure 6.15 Iterative Search History for Three-Dimensional Example

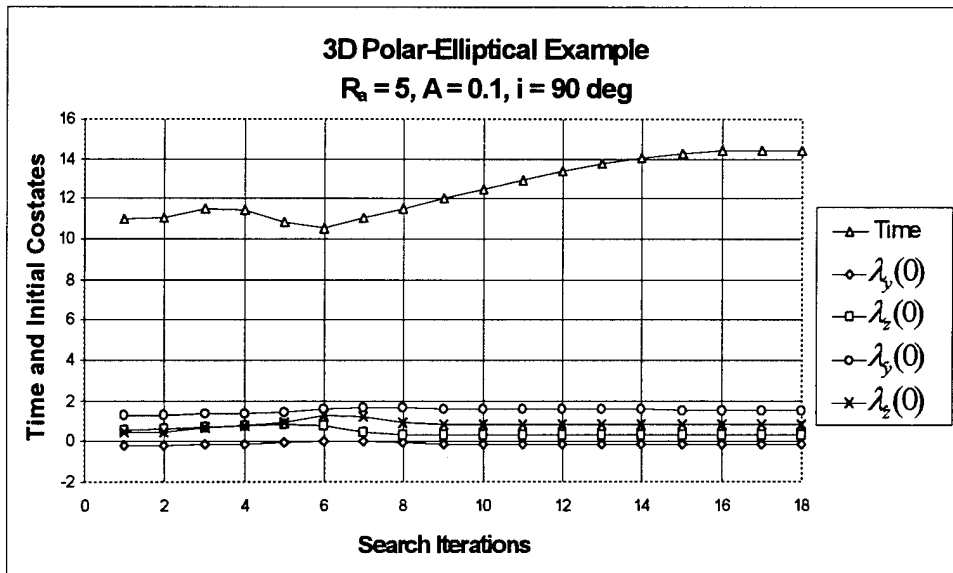


Figure 6.16 Iterative Search History for Polar-Elliptical Example

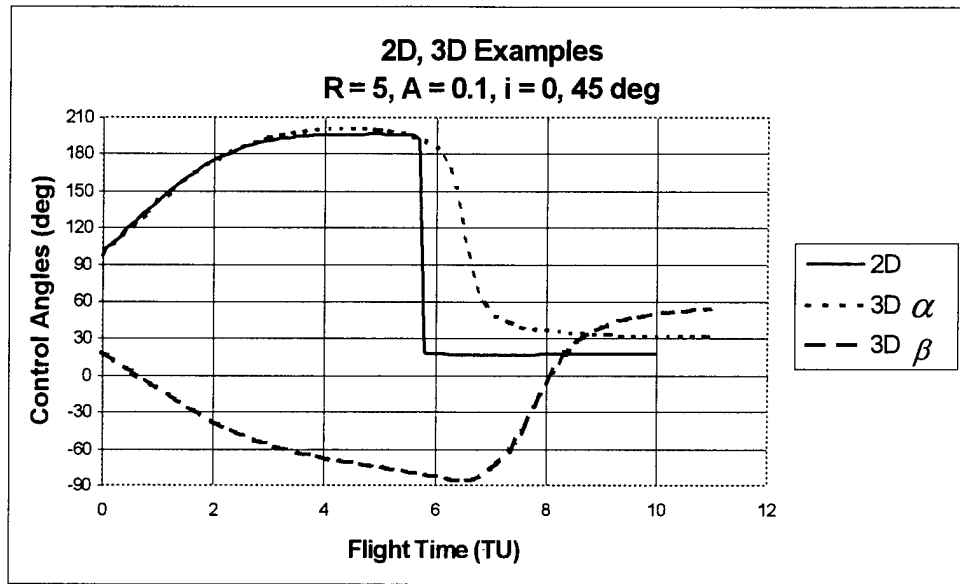


Figure 6.17 Control Angle Histories for 2D and 3D Examples

from the initial approximations to the converged values. In these cases, convergence took 12, 14, and 18 iterations of the shooting method, respectively.

Figure 6.17 shows that the behavior of the thrust angle α is similar between the two-dimensional and three-dimensional cases, although the three-dimensional case has smoother “corners,” which may be because it is not constrained to two dimensions. The thrust angle β starts off with similar behavior between the three-dimensional $i = 45^\circ$ case and the polar-elliptical example, and arrives at nearly the same final values for both cases. Figure 6.18 shows the control angle histories for α and β in the polar-elliptical example. The flattening of both curves at the end of the trajectory indicate the braking maneuver needed to arrive at apoapse.

In the two-dimensional case, the costates related to the z direction are zero throughout the transfer. In the three-dimensional case, all of the costates vary with time. The ascending node was zero for this example, but choosing other angles will result in different values for the optimal initial costates and final time. The best agreement between the two cases is for $\lambda_y(0)$ and $\lambda_{\dot{y}}(0)$, which may be approximated with Equations (5.26) and (5.27), Equations (5.34) and (5.35), or the point (0,1) as appropriate. Convergence is achieved in

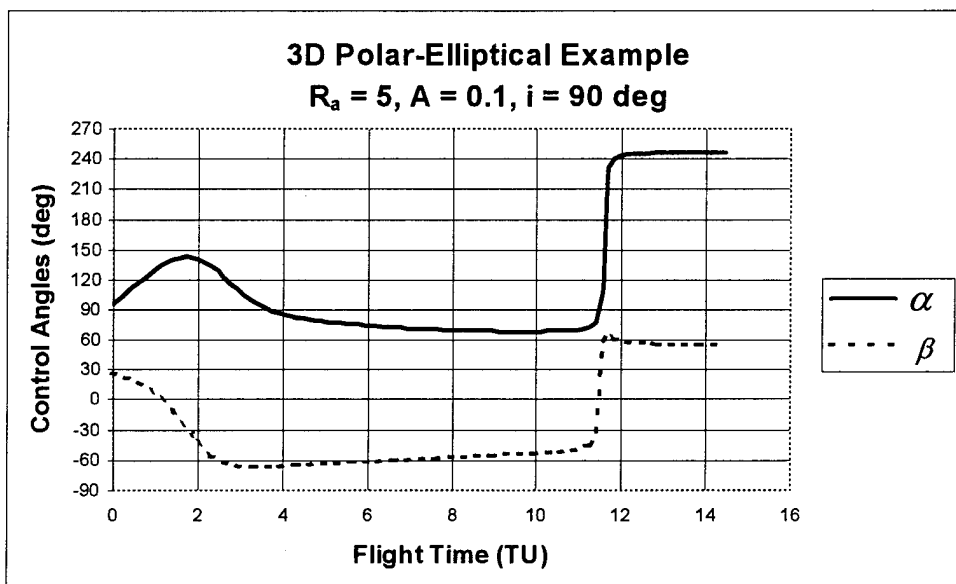


Figure 6.18 Control Angle Histories for Polar-Elliptical Example

12 iterations of the shooting method for the first case, 14 iterations for the second case, and 18 iterations in the third case.

6.2.1 Time per Revolution. Certain trends in the behavior of the optimal trajectories become evident after plotting the results for many numerical cases [2]. As the parameters R and A change, the time of flight per revolution changes as well. This relationship is difficult to model in general without performing numerical integration. However, the maximum value may be modeled as a function of R with a fairly simple expression.

Figure 6.19 shows the relationship between time of flight and transfer angle for a range of values of A and R . The maximum time per revolution occurs near a one-revolution transfer for each value of R . An empirical fit for the one-revolution case is as follows:

$$t_{f_1} \approx \sqrt{(R - 0.6551)/0.01231} \quad (6.1)$$

A plot of final radius against the time of flight for one revolution shows a roughly parabolic shape, as seen in Figure 6.20.

It is difficult to identify a physical explanation for the parabolic relationship, because the path is a powered trajectory, and Keplerian relationships do not apply directly to

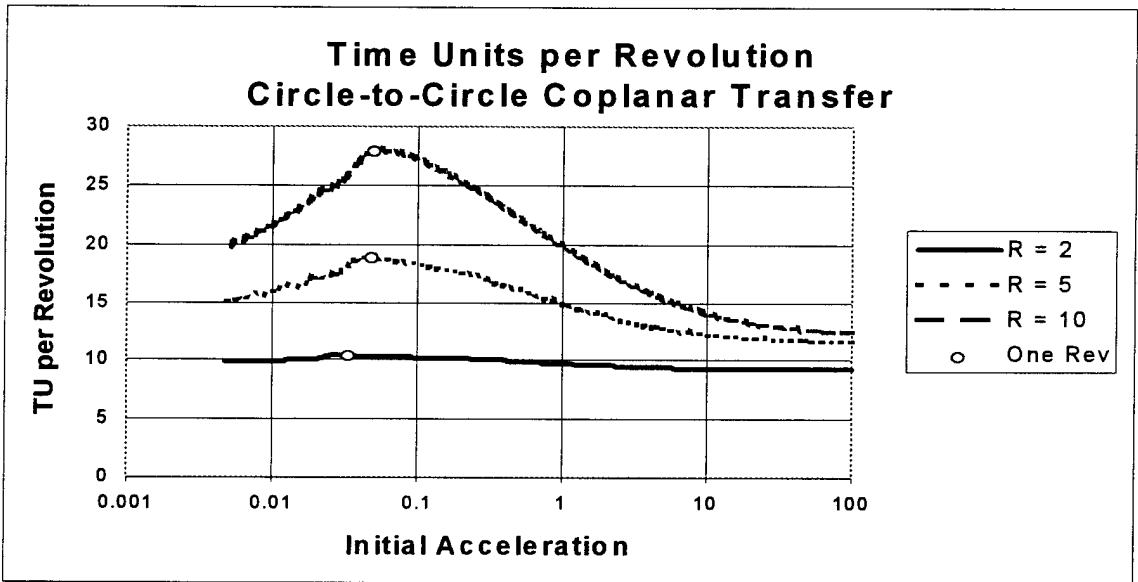


Figure 6.19 Time Per Revolution, Circle-to-Circle

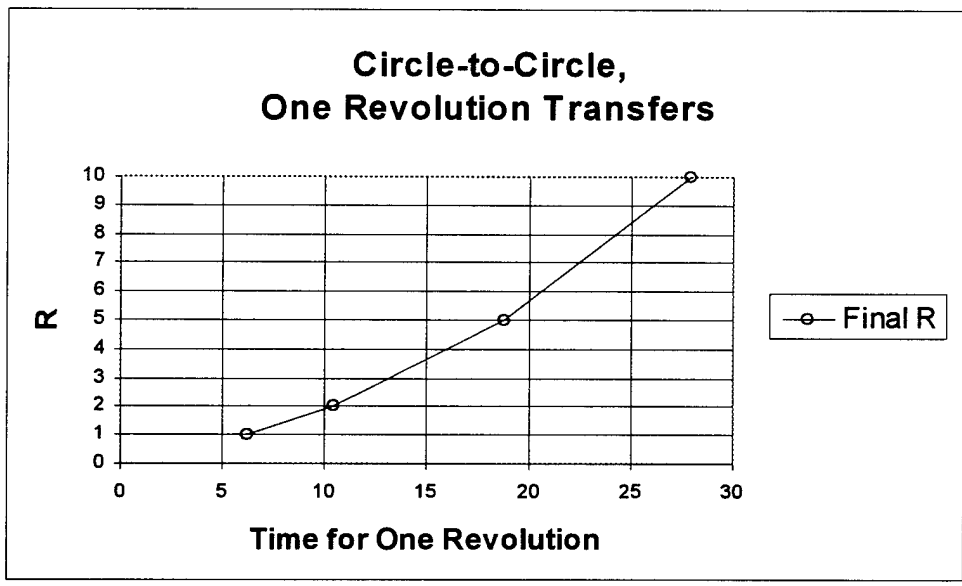


Figure 6.20 Time for One Revolution, Circle-to-Circle

these orbit transfers. The empirical relationship in Equation (6.1) is found by assuming $R = c_1 t_{f_1}^2 + c_2$, and solving for the unknown coefficients c_1 and c_2 . This functional form is the simplest available to model the parabolic shape adequately. A numerical example is given below to demonstrate the accuracy and utility of this simple model. It should be noted that the coefficients in Equation (6.1) are found using a small number of data points, so this is at best a rough approximation. The data points are found manually to match the requirement of exactly one revolution. It would be possible to modify the shooting method to include the unit revolution as an end condition, and allow the thrust magnitude to vary as an input. However, the purpose of the approximation in Equation (6.1) is only to provide a general idea of the relationship between the time of flight and the transfer angle in the neighborhood of one revolution.

A mission planner could use Equation (6.1) to find the approximate time of flight for one revolution to the final radius, and then decide whether more or less time would meet requirements. An estimate of the required thrust may be obtained by using this time value in Equation (5.28), and solving for the parameter A . Similar information about the relationship between time of flight and orbital revolutions is presented graphically in Reference [2]. As a numerical example, suppose that $R = 7$ and $\dot{m} = 0$. Using Equation (6.1) and Equation (5.28), we have $t_{f_1} \approx 22.7$, and $A \approx 0.0466$, each in canonical units. The exact values are $t_{f_1} = 22.9$ and $A = 0.0494$ to the same number of significant figures. Even as a rough approximation, Equation (6.1) gives a reasonable value of the optimal flight time for a one-revolution transfer.

6.2.2 Minimum Time vs. Ascending Node. Figure 6.21 shows the variation of time of flight to orbits with the same inclination but different ascending nodes. As the final inclination changes, the ascending node for the minimum time remains relatively constant. The two minima of each locus shown in Figure 6.21 are of equal values, and they represent trajectories that are reflected about the x, y plane. The values of the ascending node associated with these minima are normally spaced at π radians apart. This is because the intersection of the final orbit with the x, y plane is a line segment, and the two minimum-time paths typically arrive at locations on opposite sides from the origin as projected onto

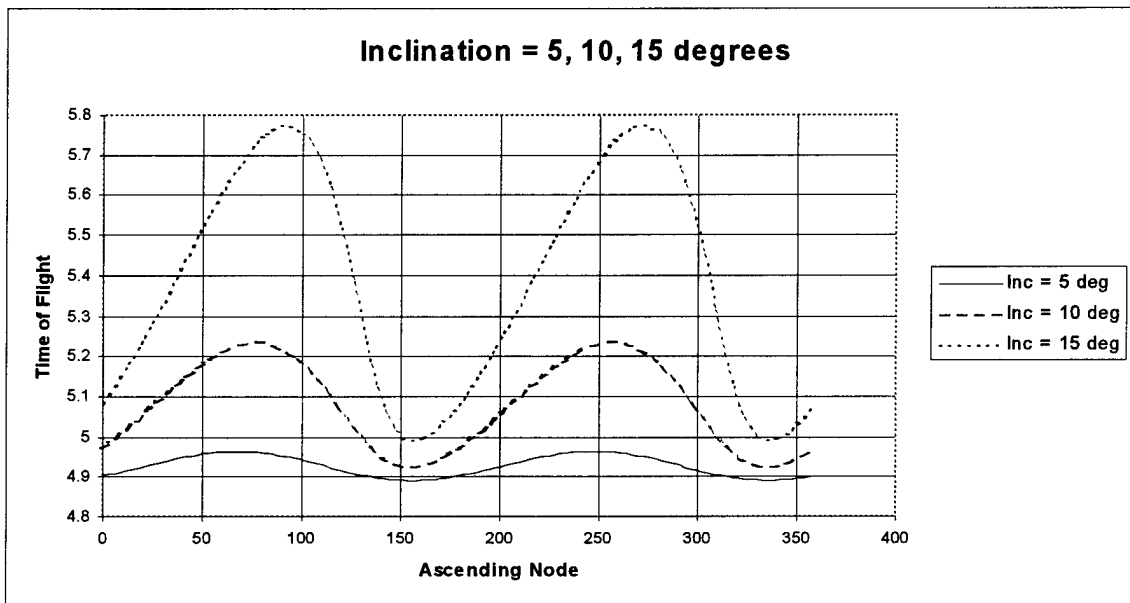


Figure 6.21 Time of Flight to Various Ascending Nodes

the line segment. It is difficult to model the minimum-time node as a function of R and A , due to extreme sensitivity. This example is provided to show a qualitative illustration of a typical relationship between the ascending node and the minimum-time path to a final orbit with a given inclination.

6.3 Summary

This chapter presents a series of numerical examples of minimum-time orbit transfers under continuous thrust for two- and three-dimensional end conditions, and also a two-dimensional problem under the KS transformation. The purpose of these examples is to demonstrate the wide range of applicability of the approximate initial costate models and the modified quasi-Newton method developed in Chapter 5. In addition, numerical results from many converged cases are presented concerning the time of flight for one revolution in the coplanar circle-to-circle case, and for the minimum-time path to a given final inclination. In all cases, the approximate initial costate relationships result in convergence directly or by continuation with a large step, as in the polar-elliptical example.

VII. Summary and Conclusions

7.1 Summary

The equations of motion for a spacecraft under the influence of gravity and continuous thrust are developed using several coordinate systems. Euler-Lagrange theory is then used to derive the optimal control law and differential equations for the states and costates in each of the coordinate systems. Expressions are developed for the approximate optimal initial costates as functions of R and A for the minimum-time, circle-to-circle continuous-thrust orbit transfer problem. The shooting method is described and used to solve the boundary value problem, and the approximate optimal initial costate expressions are used for the initial values. A dynamic step limiter is presented which improves convergence in the shooting method. The minimum-time continuous-thrust orbital transfer problem is also developed under the Kustaanheimo-Stiefel (KS) transformation, and the optimal initial costates are presented for comparison. Examples are provided for coplanar and non-coplanar orbital transfers, showing the utility of the two-dimensional approximations for three-dimensional problems and non-circular end conditions.

7.2 Conclusions

The prime motivation for this work is that there are no models available in the literature that provide initial costate estimates for the minimum-time, continuous-thrust orbit transfer problem as functions of the problem parameters. The inherent difficulty in classical optimization methods is the need to guess the initial values of the Lagrange multipliers. The expressions and techniques developed in this research lead to convergence in the shooting method for the indicated range of problem parameters. The greatest advantage to this approach is that the resulting trajectories satisfy the Euler-Lagrange equations, so optimality is guaranteed. This research has proven successful, in that it provides a reliable means to determine the optimal thrust angle history from the shooting method for arbitrary values of the problem parameters. It was not possible to do this before with any reliability, because the only other option is to rely on pure guesswork and good fortune.

In the literature, there are many attempts to solve approximations of the optimal control problem by making simplifications of the dynamics equations or assumptions about the control law. However, there are very few instances where researchers provide analysis for the problem of determining the initial costates [1, 13, 15, 18]. The references cited here each analyze the issue, but they assume impulsive thrust maneuvers or non-optimal constant tangential thrust. There is no information from these sources that provides any useful information to solve the minimum-time, continuous-thrust problem for arbitrary values of the parameters R and A . Thus, the research presented here is unique in that it directly addresses the optimal, minimum-time continuous-thrust case for the purpose of modeling the optimal initial costates based on the problem parameters.

A mission planner could use the results of this research to simplify the job of mission design for continuous-thrust spacecraft. Without the approximate initial costates, it is very difficult to find an optimal solution to match desired end conditions. If low-thrust devices are used on military spacecraft, there may not be much time available to design a tactical orbital maneuver. This adds importance to achieving convergence to the optimal trajectory as quickly as possible.

When tracking a maneuvering spacecraft, it is usually necessary to wait for the maneuver to be completed before estimating the new orbit. Under continuous thrust, however, the maneuver may go on indefinitely. In order to track such a spacecraft, the estimation process must include some sort of dynamics model that takes the thrust into account. If the trajectory of the thrusting spacecraft is assumed to be time optimal, the results of this research could be used to provide a reference trajectory for the estimation process.

A natural extension of this research is to examine the optimal initial costates for the minimum-fuel problem, which would involve throttling and coasting arcs. Also, the behavior of the optimal initial costates might be modeled for continuous-thrust Earth-Moon trajectories, where the Moon's gravity is included in the equations of motion [21]. The variational Hamiltonian would be much more complex in the restricted three body problem. Another extension of the research would be to include the effects of uncertainty in the values of the states, and to examine the effect on the costates for in-flight computations.

There are many possibilities for future research in the area of initial costate determination for continuous-thrust optimization. Simplified gravity models could yield closed form solutions for the equations of motion, or the costate equations. Any such solution might provide an analytical approximation for the initial costates when the accelerations due to gravity and thrust are of nearly the same magnitude. Also, the KS transformation development and examples could be used to verify perturbation analysis for low-thrust problems.

Appendix A. Numerical Solution and the Shooting Method

To solve the boundary value problems presented in the text, the differential equations of the states and costates must be numerically integrated from the initial time to the final time. The final conditions will depend on the choices for the initial conditions. If the final conditions are incorrect, then the initial conditions must be adjusted according to Equation (4.73). The partial derivatives in the Jacobian matrix may be found numerically, through the shooting method. First, a reference trajectory is propagated by numerically integrating the differential equations from the initial time to the final time. Then, small perturbations are made in each of the unknown initial conditions, and the trajectory is propagated again individually for each of the perturbations. The relative errors at the end time are collected and used with the perturbation magnitudes to calculate one-sided approximations of the partial derivatives in the Jacobian matrix. The corrections to the initial conditions are then given by Equation (4.73).

Because of the nonlinearities in the differential equations, the errors in the final conditions may grow, shrink or stay the same as the shooting process is repeated. With good initial costate models, and the modified Newton step described in Chapter 4, the final errors will normally get smaller with each iteration of the shooting method. Figure A.1 is a flowchart for the shooting method. Many sources of computer code are available to accomplish the tasks shown in this flowchart [16]. The code is available in the form of subroutines in various computer languages. The coding for this research was done in Borland Turbo Pascal for Windows, version 7.0, and the computations were performed on a Pentium-90 based personal computer.

The trajectories in all of the examples in this dissertation are propagated with an integration tolerance of 10^{-8} , and an error tolerance in the final state values of 10^{-7} in canonical units. This defines the “exact” solutions referenced in the text, regardless of which iteration in the shooting method results in the required error tolerance. Borland Turbo Pascal can support “extended” precision, which gives a floating point variable an accuracy of 19 digits past the decimal point. This is much more precision than 10^{-8} , but it is not necessary to exercise the full capability of the machine and programming language. Based on numerical experience, convergence always occurs, once the final errors

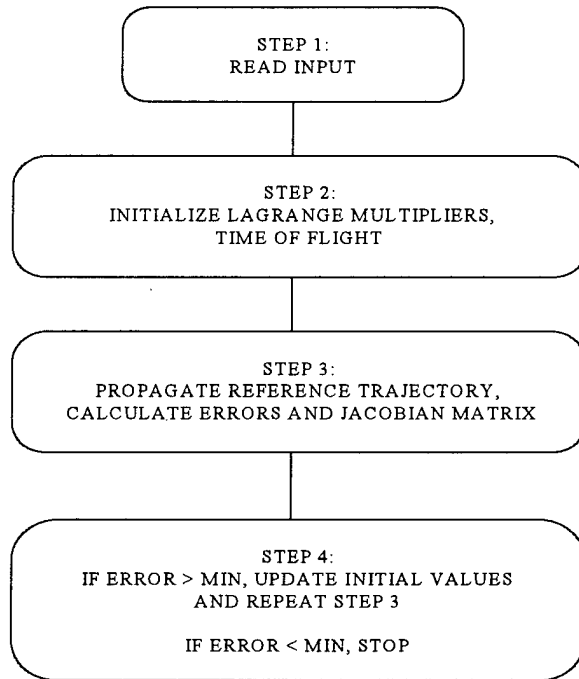


Figure A.1 Flowchart for the Shooting Method

are reduced to the order of 10^{-3} or 10^{-4} in canonical units. The error tolerance of 10^{-7} is three or four orders of magnitude more precise than necessary to indicate convergence, and thus provides confidence that the minimizing path has been found for the particular problem. If all 19 digits are used, the integration time becomes much larger per trajectory. Since the shooting method requires many trajectories to be calculated during an iterative search, the increase in computing time is multiplied, with no great benefit.

Bibliography

1. Alfano, S. *Low Thrust Orbit Transfer*. MS thesis, AFIT/GA/AA/82D-2. School of Engineering, Air Force Institute of Technology (AU), Wright-Patterson AFB OH, December 1982 (No DTIC entry).
2. Alfano, S. and J. D. Thorne. "Constant-Thrust Orbit-Raising," *The Journal of the Astronautical Sciences*, 42(1):35-45 (1994).
3. Bate, R., D. Mueller and J. White. *Fundamentals of Astrodynamics*. New York: Dover Publications Inc., 1971.
4. Battin, R. H. *An Introduction to the Mathematics and Methods of Astrodynamics*. New York: American Institute of Aeronautics and Astronautics, Inc., 1987.
5. Bell, D. J. "Optimal Space Trajectories - A Review of Published Work," *Aeronautical Journal of The Royal Aeronautical Society*, 72(686):141-146 (1968).
6. Broucke, R. A. "Low-Thrust Trajectory Optimization in an Inverse Square Force Field," *AAS/AIAA Spaceflight Mechanics Meeting* (Feb 1991).
7. Bryson, A. E. and Y. C. Ho. *Applied Optimal Control*. Washington, D.C.: Hemisphere Publishing Co., 1975.
8. Coverstone-Carroll, V. and S. N. Williams. "Optimal Low-Thrust Trajectories Using Differential Inclusion Concepts," *The Journal of the Astronautical Sciences*, 42(4):379-393 (1994).
9. Dennis, J. E. and R. B. Schnabel. *Numerical Methods for Unconstrained Optimization and Nonlinear Equations*. Englewood Cliffs, New Jersey: Prentice-Hall, Inc., 1983.
10. Eide, S. A. *Optimal Thrust Vector Control of Coplanar Orbital Evasive Maneuvers*. MS thesis, AFIT/GA/AA/87D-2. School of Engineering, Air Force Institute of Technology (AU), Wright-Patterson AFB OH, December 1987 (AD-A189544).
11. Gregory, J. and C. Lin. *Constrained Optimization in the Calculus of Variations and Optimal Control Theory*. New York: Van Nostrand Reinhold, 1992.
12. Kirk, D. E. *Optimal Control Theory - An Introduction*. Englewood Cliffs, New Jersey: Prentice-Hall Inc., 1970.
13. Lawden, D. F. *Optimal Trajectories for Space Navigation*. London: Butterworths, 1963.
14. Luenberger, D. G. *Optimization by Vector Space Methods*. New York: John Wiley and Sons, Inc., 1969.
15. Pines, S. "Constants of the Motion for Optimal Thrust Trajectories in a Central Force Field," *AIAA Journal*, 2(11):2010-2014 (1964).
16. Press, W. H., B. P. Flannery, S. A. Teukolsky and W. T. Vetterling. *Numerical Recipes in C-The Art of Scientific Computing*. Cambridge: Cambridge University Press, 1988.
17. Prussing, J. E. "Equation for Optimal Power-Limited Spacecraft Trajectories," *Journal of Guidance, Control and Dynamics*, 16(2):391-393 (1993).

18. Redding, D. C. and J. V. Breakwell. "Optimal Low-Thrust Transfers to Synchronous Orbit," *Journal of Guidance, Control and Dynamics*, 7(2):148-155 (1984).
19. Seywald, H. "Trajectory Optimization Based on Differential Inclusion," *AAS/AIAA Spaceflight Mechanics Meeting* (Feb 1993).
20. Stiefel, E. L. and G. Scheifele. *Linear and Regular Celestial Mechanics*. New York: Springer-Verlag, 1971.
21. Szebehely, V. *Theory of Orbits*. New York-London: Academic Press, 1967.
22. Takahashi, Y., M. J. Rabins, and D. M. Auslander. *Control and Dynamic Systems*. Reading, Massachusetts: Addison-Wesley, 1970.
23. Thorne, J. D. and C. D. Hall. "Approximate Initial Lagrange Costates for Continuous-Thrust Spacecraft," *Journal of Guidance, Control and Dynamics*, 19(2):283-288 (1996).
24. Thorne, J. D. and C. D. Hall. "Optimal Continuous Thrust Orbit Transfers," *AAS/AIAA Spaceflight Mechanics Meeting* (Feb 1996).
25. Wiesel, W. E. *Spaceflight Dynamics*. New York: McGraw-Hill, Inc., 1989.
26. Wiesel, W. E. and S. Alfano. "Optimal Many-Revolution Orbit Transfer," *Journal of Guidance, Control and Dynamics*, 8(1):155-157 (1985).
27. Zondervan, K. P. "Optimal Low-Thrust, Three-Burn Orbit Transfers with Large Plane Changes," *The Journal of the Astronautical Sciences*, 32(2):407-427 (1984).

Vita

Major James Dana Thorne was born on 15 February 1962, in Fairbanks, Alaska. He graduated from Grove City High School, Grove City, Pennsylvania, in 1980, and enrolled at Purdue University. After completing a Bachelor of Science degree in Aeronautical and Astronautical Engineering, he was commissioned as a Second Lieutenant into the USAF in May, 1984. Major Thorne began active duty in June 1984 as satellite systems integration officer at the Air Force Satellite Control Facility, Sunnyvale, California. While living in California, he met and married Andrea Dovidio, a computer scientist originally from Walton, New York.

In May, 1988, Major Thorne entered a masters degree program at the Air Force Institute of Technology (AFIT) Graduate School of Engineering, Department of Aeronautics and Astronautics, where he majored in astronautical engineering. He completed an analytical thesis in the area of astrodynamics, which determined a series solution of the Lambert (or Gauss) problem, and graduated in December, 1989. Based on his thesis work, Major Thorne was presented with the AFIT Department of Aeronautics and Astronautics Research Award in Dynamics and Controls for 1989.

Following the first AFIT tour, Major Thorne was assigned to the Space Technology Center, Kirtland Air Force Base, New Mexico. When the Phillips Laboratory was formed in December 1990, he proposed and formed an astrodynamics division within the Laboratory which later became PL/VTA. This division produced analytical studies and algorithm developments to support DoD space operations, as well as many internal Laboratory projects.

In July 1993, Major Thorne entered a doctoral program in the AFIT Graduate School of Engineering, Department of Aeronautics and Astronautics, where he majored in astronautical engineering. After graduation in June 1996, Major Thorne's follow-on assignment was to the Defense Support Program SPO at Los Angeles Air Force Base, California.

Permanent address: 8399-E SW 90th Street
Ocala, FL 34481

REPORT DOCUMENTATION PAGE

Form Approved
OMB No. 0704-0188

Public reporting burden for this collection of information is estimated to average 1 hour per response, including the time for reviewing instructions, searching existing data sources, gathering and maintaining the data needed, and completing and reviewing the collection of information. Send comments regarding this burden estimate or any other aspect of this collection of information, including suggestions for reducing this burden, to Washington Headquarters Services, Directorate for Information Operations and Reports, 1215 Jefferson Davis Highway, Suite 1204, Arlington, VA 22202-4302, and to the Office of Management and Budget, Paperwork Reduction Project (0704-0188), Washington, DC 20503.

1. AGENCY USE ONLY (Leave blank)	2. REPORT DATE June 1996	3. REPORT TYPE AND DATES COVERED Dissertation	
4. TITLE AND SUBTITLE OPTIMAL CONTINUOUS-THRUST ORBIT TRANSFERS		5. FUNDING NUMBERS	
6. AUTHOR(S) James D. Thorne			
7. PERFORMING ORGANIZATION NAME(S) AND ADDRESS(ES) Air Force Institute of Technology, WPAFB OH 45433-6583		8. PERFORMING ORGANIZATION REPORT NUMBER AFIT/DS/ENY/96-7	
9. SPONSORING / MONITORING AGENCY NAME(S) AND ADDRESS(ES) LtCol Salvatore Alfano PL/VTA, Kirtland AFB, NM 87117		10. SPONSORING / MONITORING AGENCY REPORT NUMBER	
11. SUPPLEMENTARY NOTES			
12a. DISTRIBUTION / AVAILABILITY STATEMENT Distribution Unlimited		12b. DISTRIBUTION CODE	
13. ABSTRACT (Maximum 200 words) The minimum time orbital transfer problem for spacecraft with steerable, continuous thrust of constant magnitude may be solved using Euler-Lagrange theory, which leads to the optimal control law in terms of Lagrange multipliers. However, the initial values of the Lagrange multipliers are not known from the orbital boundary conditions. Using analytical and empirical results, the optimal initial costates are modeled as functions of the problem parameters which are the initial thrust acceleration, A, and the final orbit radius, R, in canonical units. For circle-to-circle, coplanar orbit transfers, these approximate initial costate models lead to convergence in the shooting method for all practical values of A and R. The models also lead to convergence for a wide range of other problems, including circle-to-hyperbola transfers and non-coplanar transfers. To counter the extreme sensitivity to small changes in the initial costate conditions, a dynamic step limiter is introduced which improves the convergence properties.			
14. SUBJECT TERMS optimal, continuous, thrust, orbit, transfers, Lagrange			15. NUMBER OF PAGES 101
			16. PRICE CODE
17. SECURITY CLASSIFICATION OF REPORT UNCLASSIFIED	18. SECURITY CLASSIFICATION OF THIS PAGE UNCLASSIFIED	19. SECURITY CLASSIFICATION OF ABSTRACT UNCLASSIFIED	20. LIMITATION OF ABSTRACT UL